Mathematical Modeling and Analysis for Multiple Myeloma Treatment

by

Kenton D. Watt

A thesis submitted to the Faculty of Graduate and Postdoctoral Studies of
The University of Manitoba
in partial fulfillment of the requirements of the degree of

Master of Science

Department of Mathematics
University of Manitoba
Winnipeg

Copyright © 2026 by Kenton D. Watt

Abstract

Multiple myeloma (MM) is a cancer of plasma cells in the bone marrow, where abnormal plasma cells overproduce a harmful antibody, M protein, leading to conditions such as bone lesions, renal dysfunction, and hypercalcemia. Although incurable, controlling M protein levels can reduce complications and extend patients' lives. A previous ODE model examined M protein, CTLs, NK cells, and regulatory T cells in the MM microenvironment to analyze steady states (SS), time to steady state (TTSS), and parameter sensitivity. However, that model lacked experimental data and realistic calibration. To address these limitations, we incorporated new clinical datasets showing patients' initial conditions and longitudinal M protein levels after CAR-T cell treatment. We developed a reduced ODE model with the same four variables but included effects of anti-PD-1, elotuzumab, and daratumumab therapies. Our model reproduced similar SS and TTSS distributions as the previous one, while mathematical and bifurcation analyses identified four non-negative equilibria and showed that varying regulatory T cell and CTL homeostasis rates can shift dynamics from a single stable state to oscillations. After calibrating both models to clinical M protein data (Group I: remission; Group II: relapse), Akaike Information Criterion indicated that our model better fits both datasets. Parameter distributions from calibration revealed potential biomarkers for predicting patient outcomes, and sensitivity analysis suggested possible therapeutic targets to lower M protein levels. Combination therapy simulations showed that daratumumab benefits all relapse patients, whereas anti-PD-1 is only effective for specific cases. The general model instead predicted benefit from elotuzumab or anti-PD-1 at higher doses or longer durations. Finally, identifiability analysis by using profile likelihood found that key parameters are structurally identifiable but practically non-identifiable with current

data, emphasizing the need for additional experimental measurements to improve parameter estimation.

Acknowledgements

This work was carried out under the supervision of Dr. Kang-Ling Liao and was supported by a Discovery Grant from the Natural Sciences and Engineering Research Council of Canada (NSERC). [grant number RGPIN-2020-07097 for Kang-Ling Liao].

This work is dedicated to my dad, Doug, who inspired me to explore this topic after his courageous battle with multiple myeloma. My hope for this work is to help others in battling this disease and live life to its fullest. I thank my supervisor, Dr. Kang-Ling Liao, for her commentary, advice, patience and guidance throughout this project. I thank my mom, Sherry, for being there as I talked about this project and asked for her advice on writing. I thank Dr. Wenrui Hao for introducing me to the idea of model identifiability. I thank the other math graduate students in the office, as they kept me sane near the end of the working of the first draft. I thank the committee members of my defense, Dr. Julien Arino and Dr. Stephanie Portet, for providing insightful comments to fix this manuscript.

Contents

List of Figures

List of Tables

1

Introduction

1.1 Multiple Myeloma

Multiple myeloma (MM) is a cancer of plasma cells. Plasma cells are commonly found in the bone marrow. (25; 39). Plasma cells produce antibodies called immunoglobulin, including Immunoglobulin (Ig) G, IgA, IgM, IgD, and IgE, which have different functions in various parts of the human body to protect from antigens via binding to the antigen (48). Moreover, plasma cells can also produce another type of antibody called light chain proteins, either lambda (LAM) or kappa (KAP), where the light chain proteins are used to aid in the binding to antigens by immunoglobulins (53).

Disease progression toward MM begins when plasma cells mutate, creating abnormal plasma cells called myeloma cells (25; 39). These cells divide uncontrollably to take over the bone marrow and lead to the precancerous state called monoclonal gammopathy of undetermined significance (MGUS), resulting in an overproduction in an abnormal immunoglobulin or light chain protein in the bloodstream called monoclonal protein or M protein (21; 25; 28; 39). When at least 10% of the plasma cells in the bone marrow are myeloma cells, the disease progresses to an asymptotic state called smoldering multiple myeloma (SMM) (21; 25; 39). When patients with SMM

become symptomatic, the disease progresses to MM (21; 25; 39). These symptoms are known as CRAB conditions, with CRAB standing for: (C) hypercalcemia or an increased blood calcium concentration, (R) renal impairment or impaired kidney functions caused by M protein, (A) anemia or a decrease in the number of red blood cells, and (B) bone lesions called plasmacytomas (39). The M protein produced by myeloma cells can have different immunoglobulin types: IgG, IgA, IgM, or rarely IgE or IgD (21; 25; 34; 39) and alternatively, M protein can also be a light chain protein, either KAP or LAM (39). The M protein stands for the total amount of these immunoglobulin and light chain protein types. Since M protein is positively correlated with the amount of myeloma cells in the bone marrow (12), M protein can be an alternative way of measuring tumour burden in MM. Moreover, M protein is a more convenient and less invasive way to measure tumour burden, as it can be measured via blood collection and/or urine samples (21; 39). The disease progression from MGUS to MM is shown in Fig. 1.1. The disease progression of MM can be summarized in different stages, going from stage 1 to stage 3, shown in Table 1.1. There are several different stage systems for disease progression; however as the stage increases, worse symptoms appear (21; 25; 34; 39). The rate of progression differs for MM, compared to other cancers, as the rate of development to MM is 1% per year (21; 25; 39). Additionally, the Mayo Clinic observed, in 241 referral patients, that the range of time between MGUS recognition and MM diagnosis was 1 to 32 years, with a median of about 10 years (29). Thus, it is important to study the long-term dynamics in the MM microenvironment.

MM has many ways to be diagnosed. Blood collection is one way, as red blood cell, calcium and M protein levels can be checked (21; 39). Another way is through urine tests (21; 39), as M protein may appear in urine when symptoms have presented (21). Bone marrow biopsy is a critical test which can be done to test for the number of myeloma cells in the bone marrow (21; 34; 39). Imaging techniques (34), such as

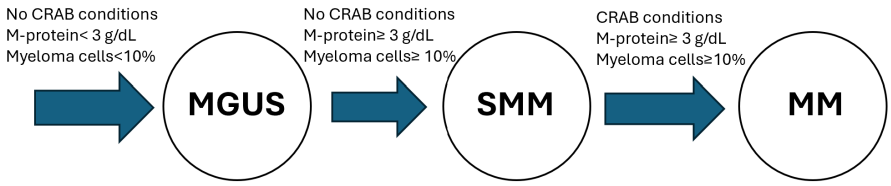

Figure 1.1: **Disease progression.** Disease progression of MGUS to MM, adapted from Table 1 in (21).

Table 1.1: **Definitions of stages 1-3 MM, as shown from column 2 of Table 4 in (39).**

Stage	Criteria
1	Hemoglobin $> 10\ g/dL$ Serum Calcium $\leqslant 12\ mg/dL$ Absence of bone disease or solitary plasmacytomas Serum paraprotein $< 3\ g/dL$ (IgA type) or $< 5\ g/dL$ (IgG type) Urinary light chain excretion $< 4\ g/24\ hours$
2	Not stage 1 or stage 3
3	Hemoglobin $< 8.5\ g/dL$ Serum Calcium $> 12\ mg/dL$ At least 2 lytic lesions Serum paraprotein $> 5\ g/dL$ (IgA type) or $> 7\ g/dL$ (IgG type) Urinary light chain excretion $> 12\ g/24\ hours$

X-ray, magnetic resonance imaging (MRI), computed tomography (CT) scans, can be used to detect bone problems, such as plasmacytomas.

1.2 Treatment Options

Due to the nature of the mutation from plasma cells to myeloma cells in the bone marrow, MM is ultimately incurable (21; 28) and thus, treatment efforts are instead focused on reducing the number of myeloma cells in the bone marrow and/or reducing the M protein amount in patients so that patients can be in a controlled disease state. A challenge for MM is choosing if a patient with SMM needs immediate treatment, which can be determined through assessing a patient's risk level for MM (namely, Box 5 in (28)). Thus, one of our goals is to identify biomarkers to predict a patient's

M protein level and to select an optimal treatment, by using mathematical models. Additionally, another challenge for MM is determining scheduling and dosage for treatment of patients with relapsed/refractory MM, as patient factors are necessary to consider for the timing and type of treatment (21; 25; 28). Thus, another goal of our work is to indicate potential treatment combinations, along with dosage and schedule, that could be effective for a patient in relapse.

There are several treatment options for MM including immunotherapy. Immunotherapy regulates the immune responses and reactivates the immune cells. There are several methods in immunotherapy, including immune checkpoint inhibitors, cytokines, oncolytic virus (OV), and chimeric antigen receptor (CAR)-T cells (56; 57). Cytokines are proteins, and can be categorized as pro-inflammatory which activates anti-tumour reactions and anti-inflammatory which activates pro-tumour reactions. Cytokine treatment involves the use of cytokines to either boost pro-inflammatory reactions or reduce anti-inflammatory reactions (7). OV infects tumour cells and this infection triggers the innate immunity that brings in macrophages to eat the infected tumour cells, and hence provide an additional killing of tumour cells beyond the adaptive immunity by T cells (26). In CAR-T cell treatment, T cells are taken from the patient and are genetically engineered to express chimeric antigen receptors that allows the T cells to specifically recognize the target tumour cells and hence increases the killing rate of tumour cells. Then, these engineered T cells are cultured and expanded in a large population and then are infused back into the patient (36). CAR-T cell therapy has shown great success in hematological tumours (36; 52). In (37), the authors applied BM38 CAR-T cell therapy to patients with MM at different dosage levels. They found that the treatment induced several anti-myeloma activities, increased the median progression-free survival, and reduced the number of relapsed cases. Moreover, even one year after the treatment was withdrawn, a high percentage of patients still exhibited detectable BM38 CAR-T

cells.

Immune checkpoints are molecules expressed on the cell membrane, and they can inhibit the target cells. For example, Programmed Death-Ligand 1 (PD-L1), which is the immune checkpoint, is mostly expressed on activated T cells and some is expressed on cancer cells. Its receptor, Programmed Death 1 (PD-1), is mainly expressed on activated T cells (33). When PD-1 and PD-L1 bind to form the PD-1-PD-L1 complex, it generates negative signals to deactivate the target immune cells (33). For the PD-1-PD-L1 complex, the immune checkpoint inhibitor treatment is to block the complex formation by occupying either the receptor (PD-1) or ligand (PD-L1) through the antibody, anti-PD-1 or anti-PD-L1, respectively. This method also enhances the adaptive immunity, as it keeps more activated T cells present and thus enhances the killing of tumour cells (33).

There are two additional treatment methods for MM that target certain membrane protein on myeloma cells. CD38 is a transmembrane protein expressed on myeloma cells, lymphoid cells, myeloid cells, and regulatory T cells (42). CD38 is involved in triggering the activation of certain cytokine production, such as Interleukin-6 (IL-6) and Interleukin-10 (IL-10) (42). These cytokines are involved in anti-inflammatory activites in the tumour microenvironment and thus result in the reduction in the immune response (42). The high expression level of CD38 makes the monoclonal antibody, **daratumumab**, targeting CD38, as a potential treatment option for MM (42). Experimental results suggest that daratumumab induces cell death of myeloma cells through multiple mechanisms and reduces the activities of CD38 (42). Moreover, daratumumab could act as an immunomodulator to deplete the number of CD38+ regulatory T cells and to enhance T cell expansion (42).

SLAMF7 is another cell membrane protein that is expressed on myeloma/plasma cells and natural killer cells (NK cells). SLAMF7 is part of the signaling lymphocytic activation molecule (SLAM) family of cell membrane receptors (54). For NK

cells, the role of SLAMF7 depends on the presence of EWSFli1-activated transcript-2 (EAT-2). If EAT-2 is present and it binds to SLAMF7 on NK cells, then SLAMF7 promotes the functions of NK cells. Otherwise, SLAMF7 inhibits the functions of NK cells (54). SLAMF7 is important for the adhesion between myeloma cells and bone marrow stromal cells (BMSC) and for the activation of certain cell pathways that promote survival of myeloma cells (54). The monoclonal antibody, **elotuzumab**, binds to SLAMF7 on myeloma cells to activate NK cells, and hence mediates the antibody-dependent cell-mediated cytotoxicity (ADCC) to inhibit myeloma cells (Figure 1 in (54)). Thus, targeting SLAMF7 via elotuzumab promotes and activates the functions of NK cells in the treatment of MM (54).

1.3 Previous Mathematical Modeling Results

There are a few modelling works related to MM. In (19), the authors created an ODE model, including variables M protein, NK cells, cytotoxic T lymphocytes (CTLs), and regulatory T cells, without any treatments, to investigate how the parameter values affect the steady states of the model and model calibration. Because the level of M protein can be used to determine the disease state, namely, patients are in MGUS when M protein is lower than 3 g/dl and are in SMM or MM when M protein is higher than 3 g/dl, the authors used 3 g/dl as a threshold of M protein to distinguish patients into two groups: the patient is under control when M protein is lower than 3 g/dl, whereas the patient is in a severe case when M protein is higher than 3 g/dl. Then, the authors mainly studied the properties of their model in these two groups. Due to the lack of data, they randomly generated parameter sets and used numerical computation to find the corresponding steady states evaluated from random initial condition, then studied the distributions of these steady states (SS) and time to steady state (TTSS) to predict the disease onset time. They also applied

global sensitivity analysis to identify significant parameters to the model outcome, then performed identifiability analysis on these significant parameters to investigate the uniqueness of parameter values from data fitting.

Next, in (18), the authors performed mathematical analysis on the model created in (19). The populations of NK cells and regulatory T cells do not vary heavily among patients in different disease states, so the authors assumed that the populations of NK cells and regulatory T cells are constants and then reduced their model to two variables, M protein and CTLs. The authors found that the reduced model had two types of non-negative equilibria, $E_1^* := (M^*, 0)$ and $E_2^* := (M^*, T_C^*)$ and established conditions for their existence and local stability. First, for the trivial equilibrium E_1^*, the model either has a unique equilibrium which is locally asymptotically stable, or three equilibria: a stable one with a low level of M protein, a stable one with a high level of M protein, and an unstable one with an intermediate level of M protein. Second, for the positive equilibrium E_2^*, their numerical test identifies a potential bifurcation parameter could induce bistability. As the parameter value increases, the model dynamics shifts from a unique stable E_2^* with a high level of M protein to three E_2^* that only the equilibrium with medium level of M protein is unstable, then to a unique stable E_2^* with a low level of M protein. Therefore, a treatment that targets this parameter could efficiently change the disease severity.

1.4 Summary of This Work

In this work, we modify the ODE model presented in (19) into two versions, a general model and a simplified model, that incorporate the effects of anti-PD-1, elotuzumab, and daratumumab treatments to investigate how these three therapies influence model dynamics and disease progression. Both models still include the variables: M protein (M), CTLs (T_C), NK cells (N), and regulatory T cells (T_R).

Because the disease progression of MM is much slower than that of most other cancer types, the steady state of the model serves as an ideal target for investigating the onset of MM. Therefore, most of our analysis focuses on the steady states. Similar to (19), we use 3 g/dl as the threshold of M protein to classify cases into two groups: a low M protein group with levels below 3 g/dl and a high M protein group with levels above 3 g/dl. For these two models, we first generate numerical solutions using random parameter values and initial conditions, then collect the steady states and record the convergence time to each steady state. This information is used to investigate how the treatment effects of anti-PD-1, elotuzumab, and daratumumab influence the distributions of steady states and convergence times for the low and high M protein groups. We then compare our findings with those reported in (19). Notice that, different to (19), our initial conditions of M protein are based on clinical data in (30).

We next analyze the basic dynamics of the simplified model without any treatments to determine its positive invariant set, establish the existence of nonnegative solutions, and derive the conditions that guarantee the existence and local stability of four types of nonnegative equilibria: $X_1^* = (M^*, 0, N^*, 0)$, $X_2^* := (M^*, 0, N^*, T_R^*)$, $X_3^* := (M^*, T_C^*, N^*, 0)$, and $X_4^* := (M^*, T_C^*, N^*, T_R^*)$. Based on these conditions, we examine the distributions of parameter values that lead to locally asymptotically stable equilibria with low or high M protein levels. These distributions help identify potential biomarkers for predicting patient outcomes. Note that X_2^* and X_3^* represent the worst and best patient cases, respectively, while X_1^* and X_4^* correspond to the second best patient state and an uncertain patient state, respectively. Therefore, we also perform global sensitivity analysis to explore the correlations between parameter values and the magnitudes of these four equilibria, aiming to identify strategies that reduce the M protein level at steady state and thereby mitigate disease progression. For instance, whether a patient in the X_4^* state develops MM depends on

the M protein level; thus, analyzing parameter correlations can help determine effective ways to lower M protein levels even under the X_4^* condition. Furthermore, our analysis indicates that the homeostasis rates of CTLs and regulatory T cells act as potential bifurcation parameters. Accordingly, we present two bifurcation examples to investigate how variations in these homeostasis rates influence the dynamics of the simplified model.

Finally, we investigate the treatment outcomes of combining CAR-T cell therapy with one of the treatments, anti-PD-1, elotuzumab, or daratumumab, using the CAR-T cell treatment data provided in (37). In (37), all patients received CAR-T cell therapy at the beginning of the study, and their M protein levels were monitored over an eighteen-month period. We first organize the M protein data into two groups, remission and relapse, and calibrate the control case of both models to these two datasets using an evolutionary algorithm. For each model, we then collect the parameter sets that yield good fitting results for both data groups and apply the Akaike Information Criterion (AIC) to identify the more plausible model for the remission and relapse groups. Next, we analyze the distributions of the collected parameter sets to identify potential biomarkers to predict patients' disease progression: remission and relapse. We also perform global sensitivity analysis to examine the correlations between M protein levels and the collected parameter sets, aiming to identify effective treatment targets and optimal treatment timing for patients with remission or relapse outcomes following CAR-T cell therapy. Next, we study how the combination therapy between CAR-T cell treatment and one of anti-PD-1, elotuzumab or daratumumab treatment can be used to improve the relapse issue, by using both models. The CAR-T cell treatment is assumed to be given once at the beginning, while the additional treatment (anti-PD-1, elotuzumab or daratumumab) is given under different treatment schedule and effect. Based on the numerical predictions for each treatment setting, we then propose recommended treatment protocols

for patients experiencing relapse. Finally, we perform identifiability analysis using the maximum likelihood function on the selected parameters for both models. Our analysis identifies structurally identifiable and practically non-identifiable parameters. We then further examine the dynamics of the model solutions associated with these practically non-identifiable parameters to propose additional experimental data that could improve their identifiability to a practical level.

The thesis is organized as follows. In Chapter 2, we introduce and explain the model created in (18; 19) and our own model. For simplicity, we call them as the general and simplified models from now on. In Chapter 3, we explain the methods used in this work. In Chapter 4, we study and compare the distributions of SS and TTSS for our models under different initial condition ranges for M protein, under one of the monotherapies anti-PD-1, elotuzumab, and daratumumab. In Chapter 5, we analyse the basic dynamics of our simplified model, apply global sensitivity analysis to investigate how the parameter values affect the equilibrium value, and provide two examples for bifurcation analysis. In Chapter 6, we calibrate both the general model and simplified model to CAR-T cell treatment data provided in (37), compare both models by using Akaike Information Criterion, perform global sensitivity analysis on both models to investigate how the parameter values affect the M protein amount at different time points. Furthermore, we study both models under the combination therapy of CAR-T cells and one of anti-PD-1, elotuzumab, or daratumumab, for patients with a relapse issue, to compare their predictions, and perform identifiability analysis on a subset of parameters. A discussion comparing the results of the two models will be given in Chapter 7.

2

Mathematical Models

2.1 General Model

We modified the model developed in (18; 19) to include the anti-PD-1, elotuzumab and daratumumab treatments and refer this model as the general model. The system network of the general model is provided in Fig. 2.1, the parameter values are listed in Table 2.1, and variables for the model are as follows:

$M(t)$: Density of M protein at time t, with unit g/dL,

$T_C(t)$: Density of CTLs at time t, with unit g/dL,

$N(t)$: Density of NK cells at time t, with unit g/dL,

$T_R(t)$: Density of regulatory T cells (T_{reg}s) at time t, with unit g/dL.

The following show the explanations of the equations for the general model, modified from (18; 19).

M protein ($M(t)$)

The dynamics of M protein is described by the following:

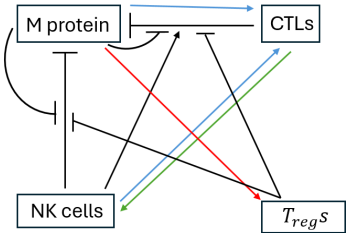

Figure 2.1: **System network for the general model.** NK cells and CTLs collaborate to deplete the production of M protein, and this depletion is inhibited by M protein and regulatory T cells. The M protein also promotes the homeostasis of CTLs and regulatory T cells. CTLs and NK cells promote each other. The anti-PD-1 treatment (F_q) enhances the homeostasis of CTLs indicated by the blue arrows, the elotuzumab treatment (F_e) promotes the homeostasis of NK cells indicated by the green arrows, and the daratumumab (F_d) inhibits the homeostasis of regulatory T cells indicated by the red arrows.

$$\frac{dM}{dt} = \underbrace{s_M}_{\text{Source}} + \underbrace{r_M\left(1-\frac{M}{K_M}\right)M}_{\text{homeostasis}} - \underbrace{\delta_M M}_{\text{Decay}} - \delta_M\left[\left(\underbrace{\frac{a_{NM}N}{b_{NM}+N}}_{\text{Depletion by NK cells}} + \underbrace{\frac{a_{CM}T_C}{b_{CM}+T_C}}_{\text{Depletion by CTLs cells}} + \underbrace{a_{CNM}\frac{N}{b_{NM}+N}\frac{T_C}{b_{CM}+T_C}}_{\text{Depletion by cooperation of NK cells and CTLs}}\right)\times\left(\underbrace{1-\frac{a_{MM}M}{b_{MM}+M}-\frac{a_{RM}T_R}{b_{RM}+T_R}}_{\text{Inhibition by M protein and T}_{\text{reg}}\text{s}}\right)\right]M. \quad (2.1.1)$$

The first term represents the constant source term for M protein (11). We assume that M protein grows logistically, which is expressed by the second term (19). The third term represents the decay of M protein. The fourth, fifth and sixth terms represent the depletion of M protein by NK cells (4; 5; 10; 27), CTLs (10; 27; 55) and the cooperation of NK cells and CTLs (31; 50), respectively, which are expressed by Michaelis-Menten type reactions. The three terms are inhibited by M protein (3; 16; 20) and T_{reg}s (6; 22; 38; 51).

CTLs ($T_C(t)$)

Table 2.1: **Parameters of the model** (2.1.6)**.** The first, second, and third columns list the parameters, description, and the range, respectively. The ranges come from (19).

Parameter	Description	Range
s_M	Constant source for M protein	0.001 g/(dL day)
r_M	Homeostasis rate for M protein	$[0.004, 0.5]$ day^{-1}
K_M	Carrying capacity for M protein	$[7, 15]$ g/dL
δ_M	Death rate for M protein	$[0.001, 0.1]$ day^{-1}
a_{NM}	Maximum loss rate of M protein by NK cells	$[0, 20]$
b_{NM}	Threshold for increase in loss rate of M protein by NK cells	$[0, 6.5 \times 10^{-2}]$ g/dL
a_{CM}	Maximum loss rate of M protein by CTLs	$[0, 20]$
b_{CM}	Threshold for increase in loss rate of M protein by CTLs	$[0, 0.15]$ g/dL
a_{CNM}	Maximum rate for NK cells efficacy from CTLs	$[0, 20]$
a_{MM}	Maximum value M protein decreases NK cells and CTLs efficacy	$[0, 1]$ $(a_{MM} + a_{RM} \leqslant 1)$
b_{MM}	Threshold for M protein decreasing NK cells and CTLs efficacy	$[0, 15]$ g/dL
a_{RM}	Maximum value T_{reg}s decreases NK cells and CTLs efficacy	$[0, 1]$ $(a_{MM} + a_{RM} \leqslant 1)$
b_{RM}	Threshold for T_{reg}s decreasing NK cells and CTLs efficacy	$[0, 1.2 \times 10^{-2}]$ g/dL
r_C	Homeostasis rate for CTLs	$[0.01, 0.5]$ day^{-1}
K_C	Carrying capacity for CTLs	$[6, 15] \times 10^{-2}$ g/dL
δ_C	Death rate for CTLs	$[0.01, 0.5]$ day^{-1}
a_{MC}	Maximum activation rate of CTLs by M protein	$[0, 10]$
b_{MC}	Threshold for activation rate of CTLs by M protein	$[0, 15]$ g/dL
a_{NC}	Maximum activation rate of CTLs by NK cells	$[0, 10]$
b_{NC}	Threshold for activation rate of CTLs by NK cells	$[0, 6.5 \times 10^{-2}]$ g/dL
f_q	Effect from anti-PD-1 treatment	$[1, \infty]$
s_N	Constant source for NK cells	$[10^{-3}, 5] \times 10^{-4}$ g/(dL day)
r_N	Homeostasis rate for NK cells	$[0.01, 0.5]$ day^{-1}
K_N	Carrying capacity for NK cells	$[3, 6.5] \times 10^{-2}$ g/dL
δ_N	Death rate for NK cells	$[0.01, 0.5]$ day^{-1}
a_{CN}	Maximum activation rate of NK cells by CTLs	$[0, 10]$
b_{CN}	Threshold for activation rate of NK cells by CTLs	$[0, 1.5 \times 10^{-1}]$ g/dL
f_e	Effect from elotuzumab treatment	$[1, \infty]$
r_R	Homeostasis rate for T_{reg}s	$[0.01, 0.5]$ day^{-1}
K_R	Carrying capacity for T_{reg}s	$[6, 12] \times 10^{-3}$ g/dL
δ_R	Death rate for T_{reg}s	$[0.01, 0.5]$ day^{-1}
a_{MR}	Maximum activation rate of T_{reg}s by M protein	$[0, 10]$
b_{MR}	Threshold for activation rate of T_{reg}s by M protein	$[0, 15]$ g/dL
f_d	Effect from daratumumab treatment	$[0, 1]$

The equation of CTLs is described by the following:

$$\frac{dT_C}{dt} = \underbrace{r_C T_C \left(1 - \frac{T_C}{K_C}\right)}_{\text{homeostasis}} \left(1 + \underbrace{\frac{a_{MC} M}{b_{MC} + M}}_{\text{Promotion by M protein}} + \underbrace{\frac{a_{NC} N}{b_{NC} + N}}_{\text{Promotion by NK cells}}\right) \times \underbrace{F_q}_{\text{Anti-PD-1 Treatment}} - \underbrace{\delta_C T_C}_{\text{Death}}. \tag{2.1.2}$$

We assume that the CTLs grows logistically (19) which is shown in the first term.

The second and third terms express the promotion of CTLs by M protein (9; 46; 55) and NK cells (1; 43; 49), respectively, which are shown by Michaelis-Menten type reactions. The last term represents the death of CTLs. The parameter F_q represents the effect from anti-PD-1 treatment. We consider $F_q \geqslant 1$ with the control case occurring when $F_q = 1$.

NK cells $(N(t))$

The equation for NK cells is as follows:

$$\frac{dN}{dt} = \underbrace{s_N}_{\text{Source}} + \underbrace{r_N N \left(1 - \frac{N}{K_N}\right)}_{\text{homeostasis}} \left(1 + \frac{a_{CN} T_C}{\underbrace{b_{CN} + T_C}_{\text{Promotion by CTLs}}}\right) \times \underbrace{F_e}_{\text{Elotuzumab Treatment}} - \underbrace{\delta_N N}_{\text{Death}}. \tag{2.1.3}$$

NK cells are differentiated from naive T cells (24), so we assume there is a constant source for NK cells, as shown in the first term. We assume that NK cells grows logistically, which is expressed by the second term (19). The third term shows the promotion of NK cells by CTLs (1; 31; 49; 50), described by a Michaelis-Menten type reaction. The last term expresses the death of NK cells. The parameter F_e represents the effect from elotuzumab treatment. We take $F_e \geqslant 1$ with the control case occurring when $F_e = 1$.

$\mathbf{T_{reg}}$s $(T_R(t))$

The equation of T_{reg}s is given as below:

$$\frac{dT_R}{dt} = \underbrace{r_R T_R \left(1 - \frac{T_R}{K_R}\right)}_{\text{homeostasis}} \left(1 + \frac{a_{MR} M}{\underbrace{b_{MR} + M}_{\text{Promotion by M protein}}}\right) \times \underbrace{F_d}_{\text{Daratumumab Treatment}} - \underbrace{\delta_R T_R}_{\text{Death}}. \tag{2.1.4}$$

We assume the growth of T_{reg}s is logistic, which is expressed by the first term (19). The second term describes the promotion of T_{reg}s by M protein (8; 14; 15; 16), expressed by a Michealis-Menten type reaction. The last term expresses the death

of T_{reg}s. The parameter F_d represents the effect of daratumumab treatment, used to deplete the number of T_{reg}s. We consider $F_d \in [0, 1]$ with the control case occurring when $F_d = 1$.

We use the following formulas to non-dimensionalize the variables and parameters

$$\hat{M} = M/M_0, \hat{T}_C = T_C/T_0, \hat{N} = N/T_0, \hat{T}_R = T_R/T_0, \hat{t} = t/\tau,$$
$$\{\hat{s}_M, \hat{r}_M, \hat{\delta}_M, \hat{r}_C, \hat{\delta}_C, \hat{s}_N, \hat{r}_N, \hat{\delta}_N, \hat{r}_R, \hat{\delta}_R\} = \tau\{s_M/M_0, r_M, \delta_M, r_C, \delta_C, s_N/T_0, r_N, \delta_N, r_R, \delta_R\},$$
$$\{\hat{b}_{CM}, \hat{b}_{NM}, \hat{b}_{RM}, \hat{K}_C, \hat{b}_{NC}, \hat{K}_N, \hat{b}_{CN}, \hat{K}_R\} = \frac{1}{T_0}\{b_{CM}, b_{NM}, b_{RM}, K_C, b_{NC}, K_N, b_{CN}, K_R\},$$
$$\{\hat{K}_M, \hat{b}_{MM}, \hat{b}_{MC}, \hat{b}_{MR}\} = \frac{1}{M_0}\{K_M, b_{MM}, b_{MC}, b_{MR}\},$$
$$\{\hat{a}_{NM}, \hat{a}_{CM}, \hat{a}_{CNM}, \hat{a}_{MC}, \hat{a}_{NC}, \hat{a}_{CN}, \hat{a}_{MR}\} = \{a_{NM}, a_{CM}, a_{CNM}, a_{NC}, a_{CN}, a_{MR}, a_{MR}\},$$

with

$$M_0 = 3 \text{ g/dL}, T_0 = 0.1 \text{ g/dL}, \text{ and } \tau = 30 \text{ days}. \tag{2.1.5}$$

Dropping the symbol '^', the non-dimensionalized model is the following:

$$
\begin{cases}
\dfrac{dM}{dt} = \underbrace{s_M}_{\text{Source}} + \underbrace{r_M\left(1-\dfrac{M}{K_M}\right)M}_{\text{homeostasis}} - \underbrace{\delta_M M}_{\text{decay}} - \delta_M\left[\left(\underbrace{\dfrac{a_{NM}N}{b_{NM}+N}}_{\text{Depletion by NK cells}} + \underbrace{\dfrac{a_{CM}T_C}{b_{CM}+T_C}}_{\text{Depletion by CTLs cells}} + \underbrace{a_{CNM}\dfrac{N}{b_{NM}+N}\dfrac{T_C}{b_{CM}+T_C}}_{\text{Depletion by cooperation of NK cells and CTLs}}\right)\times\left(\underbrace{1-\dfrac{a_{MM}M}{b_{MM}+M}-\dfrac{a_{RM}T_R}{b_{RM}+T_R}}_{\text{Inhibition by M protein and T}_{\text{regs}}}\right)\right]M \\
\dfrac{dT_C}{dt} = \underbrace{r_C T_C\left(1-\dfrac{T_C}{K_C}\right)}_{\text{homeostasis}}\left(1+\underbrace{\dfrac{a_{MC}M}{b_{MC}+M}}_{\text{Promotion by M protein}}+\underbrace{\dfrac{a_{NC}N}{b_{NC}+N}}_{\text{Promotion by NK cells}}\right)\times\underbrace{F_q}_{\text{Anti-PD-1 Treatment}} - \underbrace{\delta_C T_C}_{\text{Death}} \\
\dfrac{dN}{dt} = \underbrace{s_N}_{\text{Source}} + \underbrace{r_N N\left(1-\dfrac{N}{K_N}\right)}_{\text{homeostasis}}\left(1+\underbrace{\dfrac{a_{CN}T_C}{b_{CN}+T_C}}_{\text{Promotion by CTLs}}\right)\times\underbrace{F_e}_{\text{Elotuzumab Treatment}} - \underbrace{\delta_N N}_{\text{Death}} \\
\dfrac{dT_R}{dt} = \underbrace{r_R T_R\left(1-\dfrac{T_R}{K_R}\right)}_{\text{homeostasis}}\left(1+\underbrace{\dfrac{a_{MR}M}{b_{MR}+M}}_{\text{Promotion by M protein}}\right)\times\underbrace{F_d}_{\text{Daratumumab Treatment}} - \underbrace{\delta_R T_R}_{\text{Death}}.
\end{cases}
\tag{2.1.6}
$$

Remark 2.1.1. The dimensional and non-dimensional forms for the general model take the form of model (2.1.6), so when model (2.1.6) is referenced, it could mean either the dimensional or non-dimensional general model.

2.2 Simplified Model

Due to the complexity of model (2.1.6), we construct a simplified ODE model based on the model (2.1.6). The system network of the simplified ODE is provided in Fig. 2.2, the parameter values are listed in Table 2.2, and the model variables are the same as they were defined for model (2.1.6).

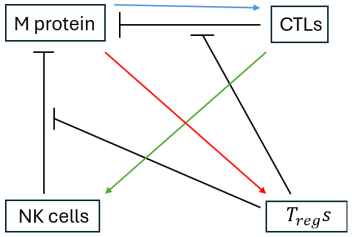

Figure 2.2: **System Network of the simplified model.** Both NK cells and CTLs deplete the production of M protein, and this depletion is inhibited by regulatory T cells. The M protein promotes the homeostasis of CTLs and regulatory T cells. CTLs promote the homeostasis of NK cells. The anti-PD-1 treatment (F_q) enhances the homeostasis of CTLs indicated by the blue arrows, the elotuzumab treatment (F_e) promotes the homeostasis of NK cells indicated by the green arrows, and the daratumumab (F_d) inhibits the homeostasis of regulatory T cells indicated by the red arrows.

The following explanations provide an interpretation for each equation for the simplified model.

M protein ($M(t)$)

The equation for M protein is shown below:

$$\frac{dM}{dt} = \underbrace{s_M}_{\text{Source}} + \underbrace{r_M \left(1 - \frac{M}{K_M}\right) M}_{\text{homeostasis}} - \underbrace{\delta_M M}_{\text{Decay}} - \left[\underbrace{(a_{NM} N}_{\text{Killing by NK cells}} + \underbrace{a_{CM} T_C}_{\text{Killing by CTLs}}) \underbrace{\frac{1}{1+T_R}}_{\text{Inhibition by T}_{\text{reg}}\text{s}} \right] M. \tag{2.2.1}$$

Comparing to Eq. (2.1.1), for simplicity, we removed the term representing the killing by the cooperation of CTLs and NK cells and replaced the Michaelis-Menten terms by linear terms. Furthermore, since the M protein promotes T_{reg}s, we combined the inhibitions from M protein and T_{reg}s by adding an indirect inhibition by T_{reg}s.

CTLs ($T_C(t)$)

The dynamics of CTLs are described as follows:

$$\frac{dT_C}{dt} = \underbrace{r_C T_C \left(1 - \frac{T_C}{K_C}\right)}_{\text{homeostasis}} \left(1 + \underbrace{a_{MC} M}_{\text{Promotion by M protein}}\right) \times \underbrace{F_q}_{\text{Anti-PD-1 Treatment}} - \underbrace{\delta_C T_C}_{\text{Death}}. \tag{2.2.2}$$

Table 2.2: **The parameter ranges for model** (2.2.5)**.** The first, second, and third columns list the parameters, description, and the range, respectively. With the exception of a_{NM}, a_{CM}, a_{MC}, a_{CN} and a_{MR}, we take 0.5 to 2 fold of the parameter ranges from Table 2.1 to obtain the ranges for the simplified model (2.2.5) For a_i, $i \in \{NM, CM, MC, CN, MR\}$, we took the upper bound of the range for a_i, from Table 2.1, and divided it by the value of b_i in Table 2.3 to obtain a new upper bound for a_i, $\tilde{a}_i$, and we took 0 to be the lower bound of a_i. For a_{NM}, and a_{CM}, we further modified their upper bounds by multiplying $\tilde{a}_{NM}$ and $\tilde{a}_{CM}$ with the upper bound of δ_M provided in Table 2.1. Finally, to obtain the upper bounds of a_i as shown, we took 2 fold of the new upper bounds, $\tilde{a}_i$.

Parameter	Description	Range
s_M	Constant source for M protein	$[0.0005, 0.002]$ g/(dL day)
r_M	Homeostasis rate for M protein	$[0.002, 1]$ day^{-1}
K_M	Carrying capacity for M protein	$[3.5, 30]$ g/dL
δ_M	Death rate for M protein	$[0.0005, 0.2]$ day^{-1}
a_{NM}	Loss rate of M protein by NK cells	$[0, 266.6]$ dL/(g day)
a_{CM}	Loss rate of M protein by CTLs	$[0, 106.66]$ dL/(g day)
r_C	Homeostasis rate for CTLs	$[0.005, 1]$ day^{-1}
K_C	Carrying capacity for CTLs	$[0.03, 0.3]$ g/dL
a_{MC}	Activation rate of CTLs by M protein	$[0, 6.666]$ dL/g
δ_C	Death rate for CTLs	$[0.005, 1]$ day^{-1}
f_q	Effect from anti-PD-1 treatment	$[1, \infty]$
s_N	Constant source for NK cells	$[5 \times 10^{-8}, 1 \times 10^{-3}]$ g/(dL day)
r_N	Homeostasis rate for NK cells	$[0.005, 1]$ day^{-1}
K_N	Carrying capacity for NK cells	$[0.015, 0.13]$ g/dL
a_{CN}	Activation rate of NK cells by CTLs	$[0, 533.334]$ g/dL
δ_N	Death rate for NK cells	$[0.005, 1]$ day^{-1}
f_e	Effect from elotuzumab treatment	$[1, \infty]$
r_R	Homeostasis rate for T_{reg}s	$[0.005, 1]$ day^{-1}
K_R	Carrying capacity for T_{reg}s	$[3 \times 10^{-3}, 0.024]$ g/dL
a_{MR}	Activation rate of T_{reg}s by M protein	$[0, 6.666]$ dL/g
δ_R	Death rate for T_{reg}s	$[0.005, 1]$ day^{-1}
f_d	Effect from daratumumab treatment	$[0, 1]$

Table 2.3: **Base values of b_{NM}, b_{CM}, b_{MC}, b_{CN}, and b_{MR} from Table 2 in (19).** The first row lists the parameter. The second row displays the base value as given in Table 2 in (19).

Parameter	b_{NM}	b_{CM}	b_{MC}	b_{CN}	b_{MR}
Value	1.5×10^{-2} g/dL	3.75×10^{-2} g/dL	3 g/dL	3.75×10^{-2} g/dL	3 g/dL

In the general model (2.1.6), CTLs and NK cells have a positive forward loop to promote each other, and then both CTLs and NK cells deplete the M protein.

Because M protein is the major component to determine the MM status, we keep the depletion terms by CTLs and NK cells in Eq. (2.2.1) and remove the promotion by NK cells in Eq. (2.2.2) to simplify the model. Thus, comparing to Eq. (2.1.2), we only keep the promotion by M protein and replace the Michaelis-Menten term by a linear term.

NK cells $(N(t))$

The equation for NK cells is given as follows:

$$\frac{dN}{dt} = \underbrace{s_N}_{\text{Source}} + \underbrace{r_N N \left(1 - \frac{N}{K_N}\right)}_{\text{homeostasis}} \left(1 + \underbrace{a_{CN} T_C}_{\text{Promotion by CTLs}}\right) \times \underbrace{F_e}_{\text{Elotuzumab Treatment}} - \underbrace{\delta_N N}_{\text{Death}}. \tag{2.2.3}$$

Comparing to Eq. (2.1.3), for simplicity, we replace the Michaelis-Menten reaction, expressing the promotion of NK cells by CTLs, with a linear term.

$\mathbf{T_{reg}}$s $(T_R(t))$

The dynamics of T_{reg}s are described as follows:

$$\frac{dT_R}{dt} = \underbrace{r_R T_R \left(1 - \frac{T_R}{K_R}\right)}_{\text{homeostasis}} \left(1 + \underbrace{a_{MR} M}_{\text{Promotion by M protein}}\right) \times \underbrace{F_d}_{\text{Daratumumab Treatment}} - \underbrace{\delta_R T_R}_{\text{Death}}. \tag{2.2.4}$$

Comparing to Eq. (2.1.4), for simplicity, we replace the Michaelis-Menten reaction, expressing the promotion of T_{reg}s by M protein, with a linear term.

The following is the dimensional simplified model:

$$
\begin{cases}
\dfrac{dM}{dt} &= \underbrace{s_M}_{\text{Source}} + \underbrace{r_M\left(1-\dfrac{M}{K_M}\right)M}_{\text{homeostasis}} - \underbrace{\delta_M M}_{\text{Decay}} - \\
&\quad \left[\underbrace{(a_{NM}N}_{\text{Killing by NK cells}} + \underbrace{a_{CM}T_C}_{\text{Killing by CTLs}}\ )\ \underbrace{\dfrac{1}{1+T_R}}_{\text{Inhibition by T}_{\text{reg}}\text{s}}\right]M \\
\dfrac{dT_C}{dt} &= \underbrace{r_C T_C\left(1-\dfrac{T_C}{K_C}\right)}_{\text{homeostasis}}\left(1+\underbrace{a_{MC}M}_{\text{Promotion by M protein}}\right)\times \underbrace{F_q}_{\text{Anti-PD-1 Treatment}} - \underbrace{\delta_C T_C}_{\text{Death}} \\
\dfrac{dN}{dt} &= \underbrace{s_N}_{\text{Source}} + \underbrace{r_N N\left(1-\dfrac{N}{K_N}\right)}_{\text{homeostasis}}\left(1+\underbrace{a_{CN}T_C}_{\text{Promotion by CTLs}}\right)\times \underbrace{F_e}_{\text{Elotuzumab Treatment}} - \underbrace{\delta_N N}_{\text{Death}} \\
\dfrac{dT_R}{dt} &= \underbrace{r_R T_R\left(1-\dfrac{T_R}{K_R}\right)}_{\text{homeostasis}}\left(1+\underbrace{a_{MR}M}_{\text{Promotion by M protein}}\right)\times \underbrace{F_d}_{\text{Daratumumab Treatment}} - \underbrace{\delta_R T_R}_{\text{Death}}.
\end{cases}
\tag{2.2.5}
$$

We use the following formulas to obtain the non-dimensionalized variables and parameters

$$
\begin{aligned}
&\hat{M} = M/M_0, \hat{T}_C = T_C/T_0, \hat{N} = N/T_0, \hat{T}_R = T_R/T_0, \hat{t} = t/\tau, \\
&\{\hat{r}_M, \hat{\delta}_M, \hat{r}_C, \hat{\delta}_C, \hat{r}_N, \hat{\delta}_N, \hat{r}_R, \hat{\delta}_R\} = \tau\{r_M, \delta_M, r_C, \delta_C, r_N, \delta_N, r_R, \delta_R\}, \\
&\{\hat{s}_M, \hat{K}_M\} = \frac{1}{M_0}\{\tau s_M, K_M\}, \{\hat{a}_{MC}, \hat{a}_{MR}\} = M_0\{a_{MC}, a_{MR}\}, \\
&\{\hat{K}_C, \hat{s}_N, \hat{K}_N, \hat{K}_R\} = \frac{1}{T_0}\{K_C, \tau s_N, K_N, K_R\}, \{\hat{a}_{NM}, \hat{a}_{CM}, \hat{a}_{CN}\} = T_0\{\tau a_{NM}, \tau a_{CM}, a_{CN}\},
\end{aligned}
$$

with M_0, T_0 and τ are defined as in Eq. (2.1.5).

Dropping the $'\hat{}'$ for convenience, the non-dimensional simplified model is shown

below

$$
\begin{cases}
\dfrac{dM}{dt} &= \underbrace{s_M}_{\text{Source}} + \underbrace{r_M\left(1-\dfrac{M}{K_M}\right)M}_{\text{homeostasis}} - \underbrace{\delta_M M}_{\text{Decay}} - \\
&\quad \left[\underbrace{(a_{NM}N}_{\text{Killing by NK cells}} + \underbrace{a_{CM}T_C}_{\text{Killing by CTLs}}\ )\ \underbrace{\dfrac{10}{10+T_R}}_{\text{Inhibition by T}_{\text{reg}}\text{s}}\right]M \\
\dfrac{dT_C}{dt} &= \underbrace{r_C T_C\left(1-\dfrac{T_C}{K_C}\right)}_{\text{homeostasis}}\left(1+\underbrace{a_{MC}M}_{\text{Promotion by M protein}}\right)\times \underbrace{F_q}_{\text{Anti-PD-1 Treatment}} - \underbrace{\delta_C T_C}_{\text{Death}} \\
\dfrac{dN}{dt} &= \underbrace{s_N}_{\text{Source}} + \underbrace{r_N N\left(1-\dfrac{N}{K_N}\right)}_{\text{homeostasis}}\left(1+\underbrace{a_{CN}T_C}_{\text{Promotion by CTLs}}\right)\times \underbrace{F_e}_{\text{Elotuzumab Treatment}} - \underbrace{\delta_N N}_{\text{Death}} \\
\dfrac{dT_R}{dt} &= \underbrace{r_R T_R\left(1-\dfrac{T_R}{K_R}\right)}_{\text{homeostasis}}\left(1+\underbrace{a_{MR}M}_{\text{Promotion by M protein}}\right)\times \underbrace{F_d}_{\text{Daratumumab Treatment}} - \underbrace{\delta_R T_R}_{\text{Death}}.
\end{cases}
\tag{2.2.6}
$$

Remark 2.2.1. Model (2.2.5) refers to the dimensional simplified model and model (2.2.6) refers to the non-dimensional simplified model.

3

Methodology

3.1 Least Squares

In this section, we will explain the method of least squares (LS), which can be used to find the optimal parameter values for a model that minimizes the error between model output and a considered data set.

Given a data set $\{(t_i, y_i)\}_{i=1}^{n}$ and a differentiable model $f(t, P)$ which depends on time t and the vector of parameters $P = [p_1, p_2, \ldots, p_k]^T$, the residual sum of squares (RSS) function, i.e. the error between the data and model output, is defined as

$$RSS(P) = \sum_{i=1}^{n} (y_i - f(t_i, P))^2. \tag{3.1.1}$$

The optimal parameter set P_{best} is defined as

$$RSS(P_{best}) = min_P\{RSS(P)\}. \tag{3.1.2}$$

The solution of Eq. (3.1.2), P_{best}, can be found by differentiating Eq. (3.1.1) with respect to each parameter p_i, $1 \leqslant i \leqslant k$, and setting the equations to zero, i.e. solving the system

$$-2\sum_{j=1}^{n}(y_j - f(t_j, P))\frac{\partial f}{\partial p_i} = 0, 1 \leqslant i \leqslant k,$$

with condition

$$x^T H(P_{best})x > 0, x \in \mathbb{R}^k - \vec{0},$$

where $H(P)$ is the Hessian matrix of $RSS(P)$ with (i,j)-entry $\dfrac{\partial^2 RSS(P)}{\partial p_i \partial p_j}, 1 \leqslant i, j \leqslant k$.

Consider an initial value problem (IVP)

$$\frac{dy}{dt} = g(y, t, P), y(t_0) = y_0(P),$$

where t is the independent variable, $y(t)$ is the state variable vector in $\mathbb{R}^m$, y_0 is the initial condition in $\mathbb{R}^m$, and P is the vector of model parameters. Given a data set $\{(t_i, y_e^o(t_i))\}_{1\leqslant i\leqslant n_i^{e,o}, 1\leqslant o\leqslant n_e^o, 1\leqslant e\leqslant n_e}$, the RSS for the IVP is

$$RSS(P) = \sum_{e=1}^{n_e}\sum_{o=1}^{n_o^e}\sum_{i=1}^{n_i^{e,o}} \omega_i^{e,o}(y_e^o(t_i) - \tilde{y}_o^e(t_i, P))^2, \tag{3.1.3}$$

where n_e is the number of experiments, n_o^e is the number of observables per experiment, $n_i^{e,o}$ is the number of data points for experiment e. Furthermore, for experiment e and observation o, $y_e^o(t_i)$ is the measured data at time t_i, $\omega_i^{e,o}$ is the weight for t_i, and $\tilde{y}_o^e(t_i, P)$ is the model output under the parameter set P. When all $\omega_i^{e,o} = 1$, we call Eq. (3.1.3) ordinary LS. Otherwise, we call Eq. (3.1.3) weighted LS.

An optimization method, evolutionary algorithm, will be discussed in the next section, to find the parameter set P_{best} that minimizes Eq. (3.1.3), namely, Eq. (3.1.2) with $RSS(P)$ as defined in Eq. (3.1.3).

3.2 Evolutionary Algorithm

In this section, we will explain the evolutionary algorithm, based on the algorithm shown in (17). This method can be used to search for the parameter set that results in the minimum of $RSS(P)$ defined as in Eqs. (3.1.1) or (3.1.3). Here are the steps:

1. The algorithm contains M generations. Each generation starts from p parameter sets, called parents. Each parent generates c parameter sets, called children, where p and c are positive integers. In the first generation, the p parents $\{P_i\}_{i=1}^{p}$ are randomly generated from considered parameter ranges.

2. In each generation, a percentage, μ, is chosen such that μp parents are randomly selected to undergo a macro-mutation, namely, applying a random perturbation from an uniform distribution on the interval $[0, n]$, $n \in \mathbb{R}^+$, to the selected μp parents. Macro-mutations are done so that the algorithm can search a wider area of the parameter space and potentially find a smaller minimum of $RSS(P)$.

3. Each parent generates c children via a micro-mutation, which will apply a random perturbation in the parent's parameters. The children are generated as follows

$$C_{ij} = P_i \cdot (\vec{1} + \lambda(\vec{\delta} - 0.5 \cdot \vec{1})),\ 1 \leqslant i \leqslant p,\ 1 \leqslant j \leqslant c,$$

   with P_i the ith parent, C_{ij} the jth child of the ith parent, λ being called the maximum possible percent change of a parameter, $\vec{\delta}$ being a random vector with entries chosen from an uniform distribution on the interval [0,1], $\vec{1}$ being a vector with 1 as all its entries, and "$\cdot$" represents component-wise multiplication.

4. For the p parents and pc children, the fitting scores are denoted by $\Omega_i = RSS(P_i)$ and $\Omega_{ij} = RSS(C_{ij})$ respectively, with $1 \leqslant i \leqslant p$ and $1 \leqslant j \leqslant c$,

where the RSS is defined as in Eq. (3.1.3).

5. A percentage s, $0 \leqslant s < 1$, is chosen, which dictates how many parents of the next generation will be chosen from $\{P_i\}_{i=1}^{p}$ of the current generation. sp parents with the smallest fitting scores Ω_i are chosen out of $\{P_i\}_{i=1}^{p}$. $(1-s)p$ children out of $\{C_{ij}\}_{1\leqslant i\leqslant p, 1\leqslant j\leqslant c}$ are chosen using a select probability $\theta_{ij} = e^{-\beta\Omega_{ij}}$, where β is the effective energy. The smaller Ω_{ij} is, the more likely child C_{ij} is chosen as a parent for the next generation. After p new parents have been chosen, repeat steps 2 to 5 until generation M is reached.

3.3 Akaike Information Criterion

In this section, we will explain the Akaike Information Criterion (AIC), as shown in (45). The AIC is a method of analysing which model is more plausible for a given data set, by taking into account both the goodness of fit and number of parameters. For a collection of r models, if $\hat{P}_i$ represents the best fit parameter set for model i, $i \in \{1, 2, \ldots, r\}$, for a given data set y, the AIC for model i is defined as

$$AIC_i = -2ln(\mathcal{L}(\hat{P}_i|y)) + 2K, \tag{3.3.1}$$

with $\mathcal{L}(\hat{P}_i|y))$ as the likelihood function evaluated at the parameter set $\hat{P}_i$ for model i for a given data set y and K is the number of estimated parameters including the variance (the bias correction term due to measurement errors). The likelihood function $\mathcal{L}(P|y)$ represents the probability of observing the parameter set P given the data set y. Setting N to be the number of data points, if $K < N/40$, Eq. (3.3.1) can be used. Otherwise, the corrected AIC is defined as

$$AICc_i = -2ln(\mathcal{L}(\hat{P}_i|y)) + \frac{2KN}{N-K-1}. \tag{3.3.2}$$

The term $-ln(\mathcal{L}(\hat{P}_i|y))$ can be replaced in two different ways. If each data point was measured independently, with the measurement error normally distributed with the same variance (i.e., Eq. (3.1.3) with all weights $\omega_i^{e,o} = 1$), then

$$-ln(\mathcal{L}(\hat{P}_i|y)) = \frac{N}{2}ln(2\pi) + \frac{N}{2}ln\left(\frac{RSS(\hat{P}_i)}{N}\right) + \frac{N}{2}. \tag{3.3.3}$$

Otherwise, the following can be used to replace $-ln(\mathcal{L}(\hat{P}_i|y))$ (i.e., Eq. (3.1.3) with some weights $\omega_i^{e,o} \neq 1$):

$$-ln(\mathcal{L}(\hat{P}_i|y)) = \frac{N}{2}ln(2\pi) + ln(\prod_{e=1}^{n_e}\prod_{o=1}^{n_o^e}\prod_{i=1}^{n_i^{e,o}}\sigma_i^{e,o}) + \frac{1}{2}RSS(\hat{P}_i), \tag{3.3.4}$$

with $\sigma_i^{e,o}$ as the standard deviation of the measurement error at time t_i for experiment e and observation o . In weighted LS (i.e., Eq. (3.1.3) with some weights $\omega_i^{e,o} \neq 1$), the weight $\omega_i^{e,o}$ at time t_i can be set as $1/(\sigma_i^{e,o})^2$. Thus, if $K < N/40$, the following formulas for the AIC of model i using Eqs. (3.3.3) and (3.3.4) can be obtained:

$$AIC_i = Nln(2\pi) + Nln\left(\frac{RSS(\hat{P}_i)}{N}\right) + N + 2K, \tag{3.3.5}$$

$$AIC_i = Nln(2\pi) + 2ln(\prod_{e=1}^{n_e}\prod_{o=1}^{n_o^e}\prod_{j=1}^{n_j^{e,o}}\sigma_j^{e,o}) + RSS(\hat{P}_i) + 2K, \tag{3.3.6}$$

and if $K > N/40$, the following formulas for the AIC of model i using Eqs. (3.3.3) and (3.3.4) can be obtained:

$$AICc_i = Nln(2\pi) + Nln\left(\frac{RSS(\hat{P}_i)}{N}\right) + N + \frac{2KN}{N-K-1}, \tag{3.3.7}$$

$$AICc_i = Nln(2\pi) + 2ln(\prod_{e=1}^{n_e}\prod_{o=1}^{n_o^e}\prod_{j=1}^{n_j^{e,o}}\sigma_j^{e,o}) + RSS(\hat{P}_i) + \frac{2KN}{N-K-1}. \tag{3.3.8}$$

Then the AIC difference for model i, $i \in \{1, 2, \dots r\}$ is defined as

$$\Delta_i = AIC_i - \min_j \{AIC_j\},$$

where AIC_i could be either the AIC or the corrected AIC. Δ_i can be interpreted as the loss of information when using model i to fit the given data set y rather than the model with the minimum AIC and a less plausible model i is associated to a higher Δ_i. Next, the AIC weight w_i for model i is defined as

$$w_i = \frac{exp(-\Delta_i/2)}{\sum_{j=1}^{r} exp(-\Delta_j/2)}. \tag{3.3.9}$$

w_i can be thought of as a probability that model i is a best fitting model to fit the considered data and thus, a higher w_i indicates model i is more plausible. In particular, model i can be taken as the best model if $w_i > 0.9$.

3.4 Identifiability

In the previous sections, we introduce the least squares method and evolutionary algorithm for optimization problems. However, these optimization methods may have a lack of identifiability, namely, optimal parameter values are non-unique. Thus, in this section, we introduce identifiability and the approaches of evaluating it.

There are two types of identifiability:

i. Structural identifiability: used to determine whether the parameter value can be uniquely determined when the model is calibrated to the data without any noise.

ii. Practical identifiability: used to determine whether the parameter value can be uniquely determined when the model is calibrated to the data with noise.

First, for structural identifiability, we consider the following ODE model:

$$\begin{cases} x' &= f(x,t,u,\mathbf{P}) \\ y &= g(x,t,\mathbf{P}) \end{cases}, \tag{3.4.1}$$

with

t : time,

u : experimental input function(s) (if it exists),

$\mathbf{P}$: vector in the parameter space $\mathbb{R}^{n_p}$,

$\tilde{P}$: an arbitrary point in $\mathbb{R}^{n_p}$,

p and $\tilde{p}$: an individual parameter in $\mathbf{P}$ and $\tilde{P}$, respectively,

y : n_y-dimensional vector of output(s) without any measurement error,

f and g : rational polynomial functions of their arguments,

u, x, y : arbitrarily differentiable.

Definition 3.4.1. (13) For a given ODE model $x' = f(x,t,u,\mathbf{P})$ and output y, a parameter p is uniquely (or globally) structurally identifiable if the equation $y(x,t,\tilde{P}) = y(x,t,\mathbf{P})$ implies $p = \tilde{p}$, for almost any $\mathbf{P}$ and almost all initial conditions. A parameter p is said to be non-uniquely (or locally) structurally identifiable if the equation $y(x,t,\tilde{P}) = y(x,t,\mathbf{P})$ implies p has a finite number of solutions, for almost any $\mathbf{P}$ and almost all initial conditions. Similarly, a model $x' = f(x,t,u,\mathbf{P})$ is said to be globally structurally identifiable for a given output y if every parameter is globally structurally identifiable.

Next, let us consider the output function with noise, namely, considering the

following ODE model:

$$\begin{cases} x' &= f(x,t,u,\mathbf{P}),\ x(0)=x_0, \\ y &= g(x,t,\mathbf{P})+\epsilon(t), \end{cases} \tag{3.4.2}$$

where $\epsilon(t)$ represents the measurement noise and it is assumed to be normally distributed, and the other components have the same definitions as Eq. (3.4.1).

Similar to the setting used in Chapter 3.3, we set $\hat{P}=(\hat{P}_1,\cdots,\hat{P}_k)$ to represent the best fitting parameter set for the considered model $x'=f(x,t,u,\mathbf{P})$ for the data y with noise ϵ, and denote $F_{ls}(P):=\min_P\{RSS(P)\}$. For normally distributed noise $\epsilon\sim N(0,\sigma)$, then we have Eq. (3.3.3) which implies

$$F_{ls}(\hat{P})=\text{constant}-2\ln(\mathcal{L}(\hat{P}|y))), \tag{3.4.3}$$

and $\hat{P}$ is the maximum-likelihood estimator for $\mathcal{L}(P|y)$. We now discuss the notion of a confidence interval for a parameter $\hat{P}_i$, which determines the region where the true value P_i^* lies with a confidence level (i.e., probability) α.

Definition 3.4.2. (2; 47) **Finite sample confidence intervals**: Let $\mathcal{L}^*(P_i)$ denote the maximum likelihood when the i-th parameter is fixed to value $\hat{P}_i$, and call it the profile likelihood of P_i. Then, the likelihood-based confidence interval for P_i at level of significance α is the set of values of P_i for which the relative negative log-likelihood at P_i is less than a threshold determined by α, namely,

$$\begin{aligned} &\{P_i:\ln(\mathcal{L}(\hat{P}))-\ln(\mathcal{L}^*(P_i))<\Delta_\alpha\},\ \text{where } 2\Delta_\alpha=\chi^2(\alpha,df), \\ \text{namely}\quad &\{P_i:F_{ls}(P_i)-F_{ls}(\hat{P})<\chi^2(\alpha,df)\}, \end{aligned} \tag{3.4.4}$$

where $\chi^2(\alpha,df)$ is the chi-squared distribution with α quantile and a number of degrees of freedom (df) equal to the number of parameters (for simultaneous confidence

intervals) or equal to 1 (for pointwise confidence intervals).

Therefore, the profile likelihoods are computed by fixing the value of one parameter at different values within an interval and finding the optimal negative log-likelihood with respect to the remaining parameters. Denote $\mathcal{A}$ as the set of parameters for model (3.4.2), in which a subset $\mathcal{B} \subseteq \mathcal{A}$ is chosen to determine their likelihood-based confidence intervals, given the data y, and here are the steps:

i. Determine $\mathcal{L}(\hat{P})$ (or $F_{ls}(\hat{P})$), where $\hat{P}$ is the best-fitting parameter set for the data y.

ii. For each $P_i \in \mathcal{B}$, an interval $[\min\ P_i, \max\ P_i]$ is selected, about the best-fit value $\hat{P}_i$, in which values are chosen for testing.
For each value of $P_i \in [\min\ P_i,\ \max\ P_i]$,

   1. Determine $\mathcal{L}$ (or F_{ls}) by estimating the best-fit estimates of $P_j \in \mathcal{A}\backslash\{P_i\}$ and record the best-fitting parameter set.

   2. Find the likelihood-based confidence interval by using $\{P_i : \ln(\mathcal{L}(\hat{P})) - \ln(\mathcal{L}^*(P_i)) < \Delta_\alpha\}$ or $\{P_i : F_{ls}(P_i) - F_{ls}(\hat{P}) < \chi^2(\alpha, df)\}$.

Based on this procedure, we summarize the criteria and properties of structural and practical identifiability:

1. A parameter P_i is **structurally non-identifiable** if the profile likelihood $\mathcal{L}^*(P_i)$ has multiple global minima in logarithmic parameter space. Then the value of parameter P_i can not be uniquely determined when the model is calibrated to noise-free data. Examples of profile likelihoods indicating a structurally non-identifiable parameter P_i are shown in Fig. 3.1(A)-(C).

2. A parameter P_i is **structurally identifiable** if the profile likelihood $\mathcal{L}^*(P_i)$ has a unique global minimum for this parameter. Then the value of parameter P_i can be uniquely determined when the model is calibrated to noise-free data.

Examples of profile likelihoods indicating a structurally identifiable parameter P_i are shown in Fig. 3.1(D)-(G).

3. A parameter P_i is **practically non-identifiable**, if the likelihood-based confidence interval has an infinite upper bound or a negative infinite lower bound. Then the value of parameter P_i cannot be uniquely determined when the model is calibrated to the data with noise. Examples of profile likelihoods indicating a practically non-identifiable parameter P_i are shown in Fig. 3.1(D)-(F).

4. A parameter P_i is **practically identifiable** if the likelihood-based confidence interval for P_i has finite upper and lower bounds. Then the value of parameter P_i can be uniquely determined when the model is calibrated to the data with noise. An example of profile likelihood indicating a practically identifiable parameter P_i are shown in Fig. 3.1(G).

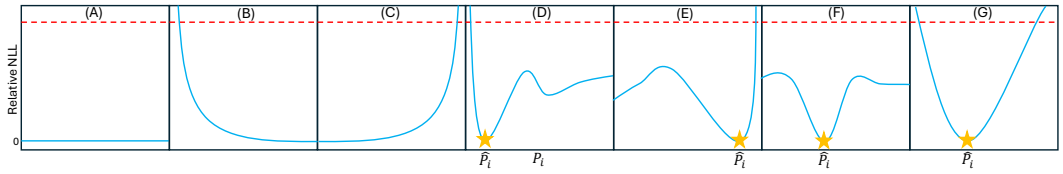

Figure 3.1: **Explanation of Profile likelihood curves.** (A)-(G) display the profile likelihood curve $\mathcal{L}^*(P_i)$, shown as the blue curve, for the parameter P_i, under various settings. The horizontal and vertical axes represent the values of P_i and the relative negative log likelihood (NLL), respectively. The red dashed line represents the threshold, as defined in Eq. (3.4.4). The yellow star in (D)-(G) indicates the best fit parameter $\hat{P}_i$. (A)-(C): Structurally non-identifiable. (D)-(F): Structurally identifiable but practically non-identifiable. (G): Structurally and practically identifiable.

4

Simulation Results

In (19), the authors studied the dynamics of model (2.1.6), under the control case (that is, $F_q = F_e = F_d = 1$), randomly generating approximately 10,000 parameter sets (each parameter set includes 30 parameters and initial conditions of 4 variables) from Table 2 in (19). Figure 2 in (19) shows the steady state distribution for each variable, when the model is simulated for 6000 days (≈ 17 *years*). The M protein distribution was skewed to the right, while the CTLs, NK cells, and T_{reg}s distributions had two peaks, one near zero and the other at a higher steady state value. The authors found that the mean for the M protein, CTLs, NK cells, and T_{reg}s distribution was 2.31 g/dL, 616 $cells/\mu L$, 260 $cells/\mu L$, and 32.2 $cells/\mu L$, respectively, consistent with the experimental data in (23; 44). Figure 3 in (19) displays the distribution of the time to steady state for the same parameter sets, using a log scale. The authors found that about 25% reached steady state in 3 months, about 50% reached their steady state in 6 months, and about 75% reached their steady state in 1 year, out of their 10000 parameter sets. The authors also found their distribution, under a log scale, was unimodal with a mean of 194 days and a median of 161 days. Figure 4A in (19) shows the boxplots of the steady state distributions from Figure 2 when parameter sets were separated by the threshold of M protein at 3 g/dL. The authors

found that T_C had wider variance in the high M protein case, and a high M protein can be linked to a lower N and higher T_R. Figure 4B in (19) shows the distribution of the loss-related term in Eq. (2.1.1) at the steady state values. The authors found that a low M protein level is more associated with higher killing by both NK cells, CTLs, consistent with experimental observations in (44). Additionally, the authors found that there were lower M protein and T_{reg}s inhibitions for the low M protein group, indicating that a decrease in T_{reg}s was more associated with a low M protein level, in the absence of treatment.

In this chapter, we will study the different dynamics between the general model and the simplified model, namely, the dimensional general model (2.1.6) and simplified model (2.2.5) for the parameter ranges in Tables 2.1 and 2.2, respectively. We do this in two ways: (i) the general model (2.1.6) under random initial conditions of M protein, and (ii) the general model (2.1.6) and the simplified model (2.2.5) under initial conditions of M protein from the experimental data shown in Figure 1 in (30).

Table 4.1: **Initial conditions for the general model** (2.1.6) **and the simplified model** (2.2.5)**.** The initial conditions for $T_C(t)$, $N(t)$, and $T_R(t)$ for the general model (2.1.6) and the simplified model (2.2.5), where the range in the third column comes from Table 2 in (19).

Initial Condition	Description	Range
T_C^0	Initial condition range of CTLs	$[4.8, 88] \times 10^{-3}$ g/dL
N^0	Initial condition range of NK cells	$[8.6, 36.8] \times 10^{-3}$ g/dL
T_R^0	Initial condition range of T_{reg}s	$[1.6, 6.8] \times 10^{-3}$ g/dL

For both (i) and (ii), we use the initial condition ranges for $T_C(t)$, $N(t)$, and $T_R(t)$ as shown in Table 4.1, as they were the ranges used in (19). For (i), we use the initial condition range $M(0) \in [0.5, 10]$ g/dL, listed in Table 2 in (19). For (ii), we take the initial condition of M protein from Figure 1 in (30), which shows the distribution of the initial levels of M protein of MGUS patients, ranging between 0 and 3 g/dL. Since 3 g/dL is the threshold for M protein that separates patients with MGUS and MM and we are considering $M(0) \in [0.5, 10]$ g/dL for (i) and $M(0) \in [0, 3]$ g/dL for

(ii), it is important that we consider (i) and (ii) separately to compare any differences in their conclusions.

4.1 Model (2.1.6) Under Random Initial Conditions

In this section, we study model (2.1.6) under random initial conditions from the ranges shown in Table 4.1 for $T_C(t)$, $N(t)$, and $T_R(t)$ and $M(0) \in [0.5, 10]$ g/dL, as given in (19). We will analyze how the distribution of steady states changes as we consider the monotherapies of anti-PD-1, elotuzumab, and daratumumab.

We generate 25000 parameter samples using latin hypercube sampling (LHS) of the parameters listed in Table 2.1 and initial conditions of 4 variables, which followed the condition $a_{MM} + a_{RM} \leqslant 1$ (used in (18; 19)) and treat each parameter set as a virtual patient.

We simulate model (2.1.6), using the virtual patients, under different monotherapies. In particular, we consider the treatment parameters $F_q \in [0, 1]$ and $F_d \in [0, 1]$ equally divided into 11 subintervals and $F_e \in [1, 10]$ equally divided into 10 subintervals. Note that $F_q = 1$, $F_e = 1$, $F_d = 1$ represents the control case. Notice that, in Chapter 2, we define the anti-PD-1 effect $F_q \geqslant 1$ to represent the promotion of CTLs homeostasis by anti-PD-1. In this Chapter, for simplicity, we set $F_q \in [0, 1]$ to consider how the variation on CTLs by F_q affects the distribution. For the considered treatment combination, we generate the solution of model (2.1.6) for each parameter set for the period $[0, 6000]$ *days* to collect both the steady state and convergence time, if possible. We compute the convergence time as the time t such that

$$\frac{||Y(t) - Y(t-1)||}{||Y(t-1)||} < 10^{-8}, \tag{4.1.1}$$

where $Y(t)$ represents the considered model solution at time t. We discard the

parameter sets which their model solutions do not satisfy condition (4.1.1) at any time t shorter than 6000 days for some treatment combination. We will refer to these collections of parameter sets for each monotherapy as the whole group. When we later divide the whole group into two groups, based on of the M component of the steady state, we will refer to the parameter sets with $M^* < 3$ (resp. $M^* > 3$) as the low (resp. high) M protein group.

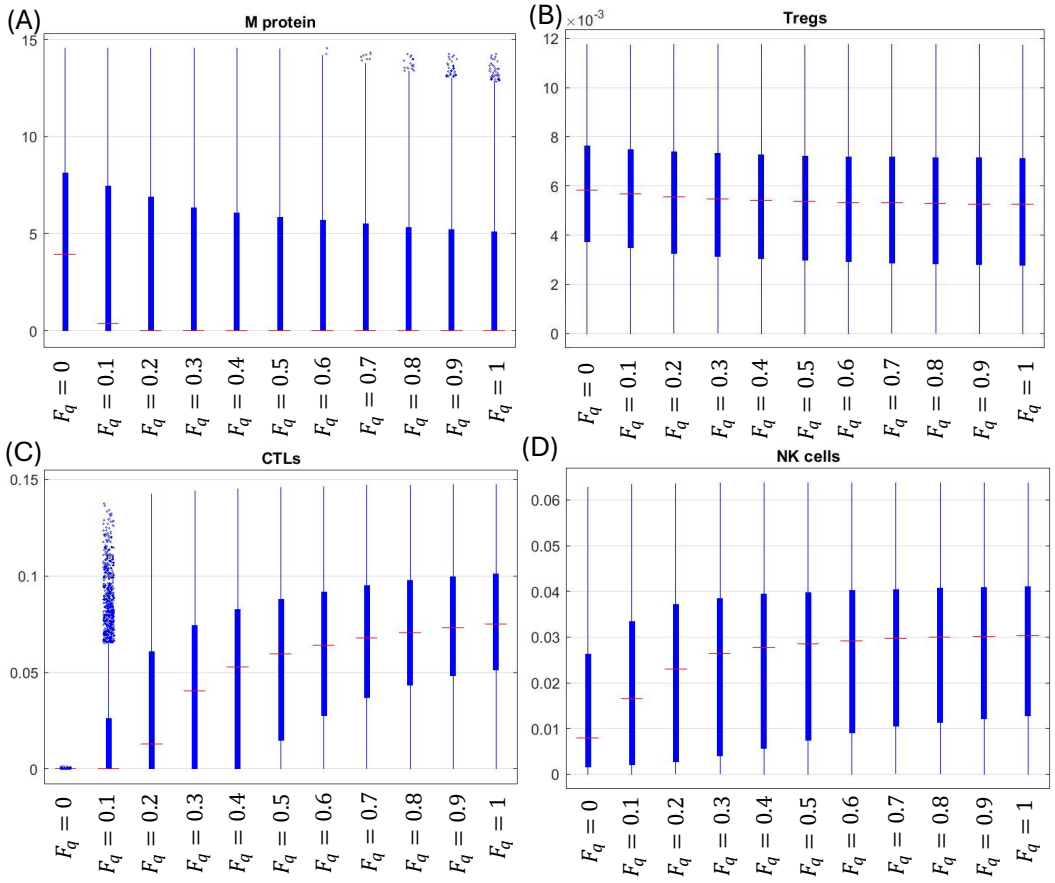

Figure 4.1: **Boxplots of SS for model** (2.1.6) **for the M protein initial condition range in (19), under anti-PD-1 monotherapy.** (A)-(D) displays the steady state boxplots for M protein, T_{reg}s, CTLs and NK cells, respectively, as the value of F_q changes, from 0 to 1 incremented by 0.1, from left bar to right bar. The vertical axis represents the value of the steady state, with the red line representing the median. The thick and thin blue lines represent the interquartile range (IQR) and the data range within 1.5×IQR. The blue dots represent the outliers.

Figs. 4.1-4.3 show the steady state boxplots for model (2.1.6) under the single effect from F_q (i.e., $F_q \in [0, 1]$ and $F_e = F_d = 1$), elotuzumab monotherapy (i.e.,

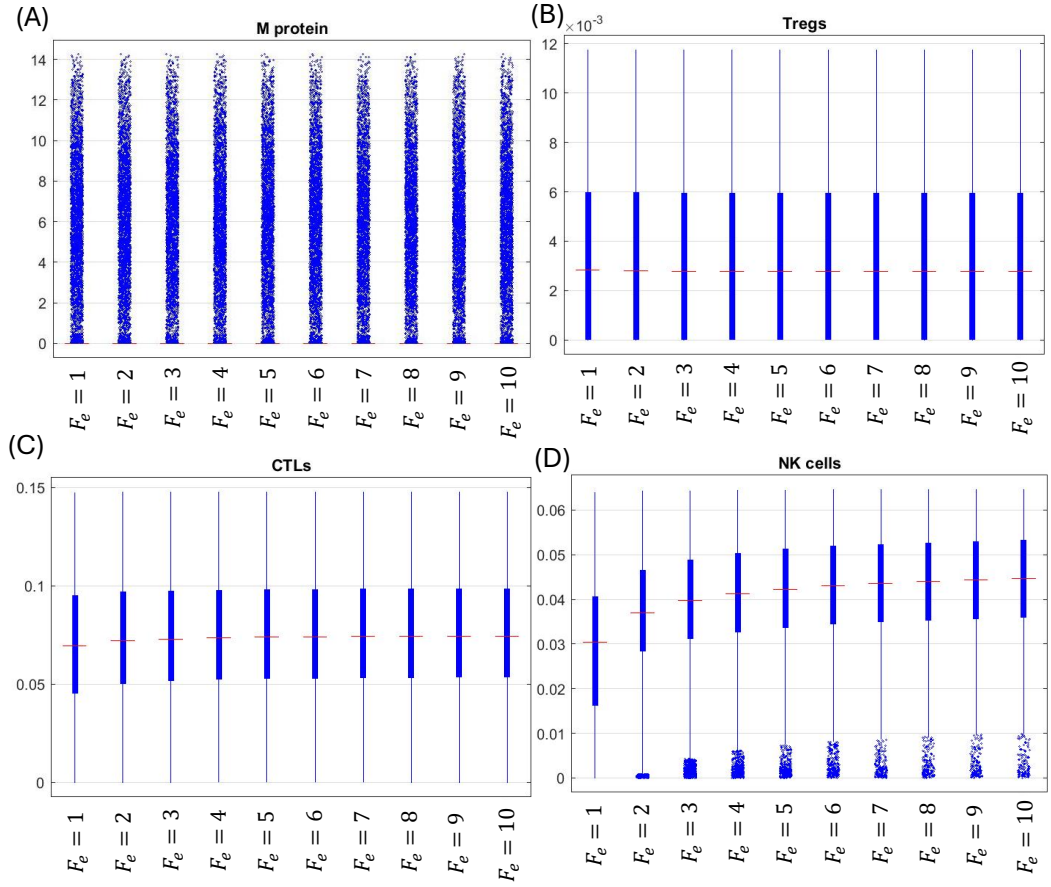

Figure 4.2: **Boxplots of SS for model** (2.1.6) **for the M protein initial condition range in (19), under elotuzumab monotherapy.** (A)-(D) displays the steady state boxplots for M protein, T_{reg}s, CTLs and NK cells, respectively, as the value of F_e changes, from 1 to 10 incremented by 1, from left bar to right bar. All symbols and definitions (vertical axis, lines, IQR, and outliers) are the same as in Fig. 4.1.

$F_e \in [1, 10]$ and $F_q = F_d = 1$) and daratumumab monotherapy (i.e., $F_d \in [0, 1]$ and $F_e = F_q = 1$), respectively. Fig. 4.1 displays that the median of the M protein and T_{reg}s boxplots slightly decrease and the median for CTLs and NK cells boxplots significantly increase when F_q is small and then slightly increase when F_q is large, as F_q increases from 0 to 1, namely, the inhibition from PD-1-PD-L1 on CTLs decreases. This indicates that increasing the effect of anti-PD-1 may help boost CTL and NK cell responses and reduce M protein and T_{reg} responses. Fig. 4.2 shows that the median of the NK cells boxplot are slightly increased as F_e increases from 1 to 10,

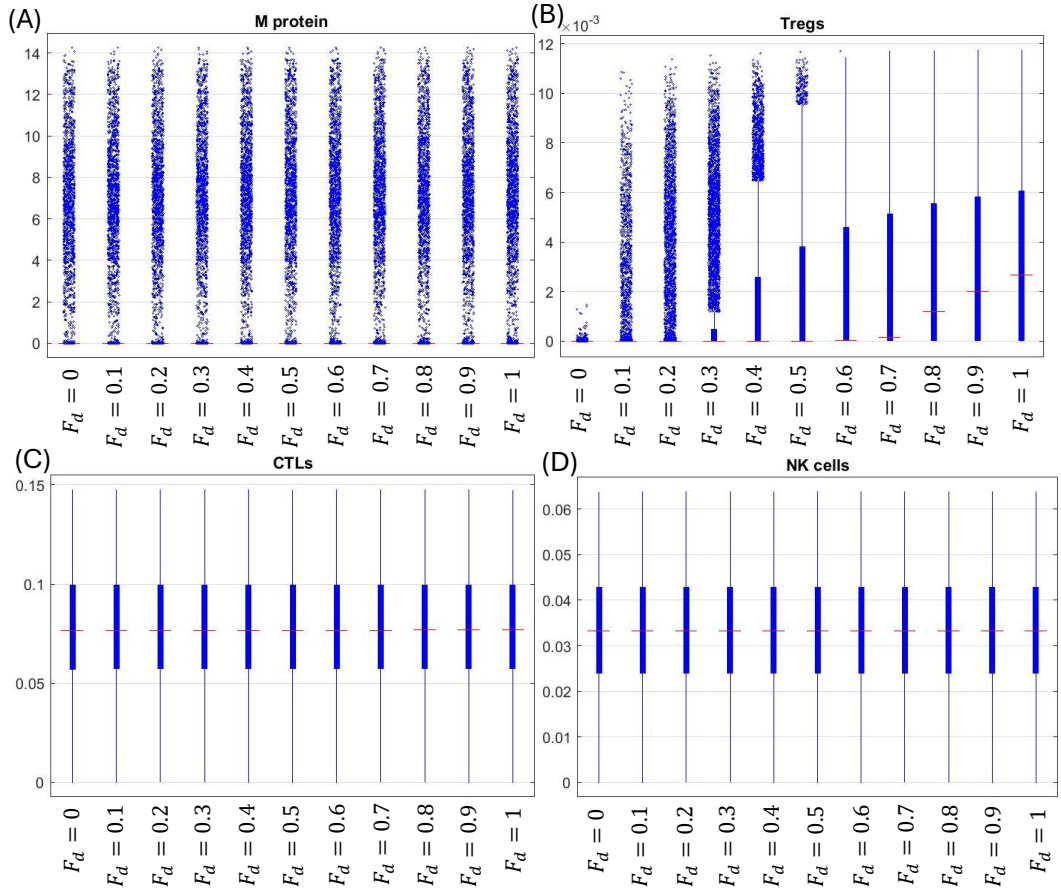

Figure 4.3: **Boxplots of SS for model** (2.1.6) **for the M protein initial condition range in (19), under daratumumab monotherapy.** (A)-(D) displays the steady state boxplots for M protein, T_{reg}s, CTLs and NK cells, respectively, as the value of F_d changes, from 0 to 1 incremented by 0.1, from left bar to right bar. All symbols and definitions (vertical axis, lines, IQR, and outliers) are the same as in Fig. 4.1.

namely, the effect of elotuzumab increases. The median of the M protein, CTLs and T_{reg}s boxplots do not significantly change. This indicates that despite the effect on NK cells as the effect of elotuzumab increased, the effect on M protein is not significant. Fig. 4.3 displays that the M protein, CTLs, and NK cells boxplots do not change significantly and the T_{reg}s boxplot has its median decrease as F_d decreases from 1 to 0.7. This indicates that the daratumumab treatment has a strong effect on T_{reg}s for high values of F_d.

Fig. 4.4 displays the boxplots for the time to steady state (TTSS) of the three

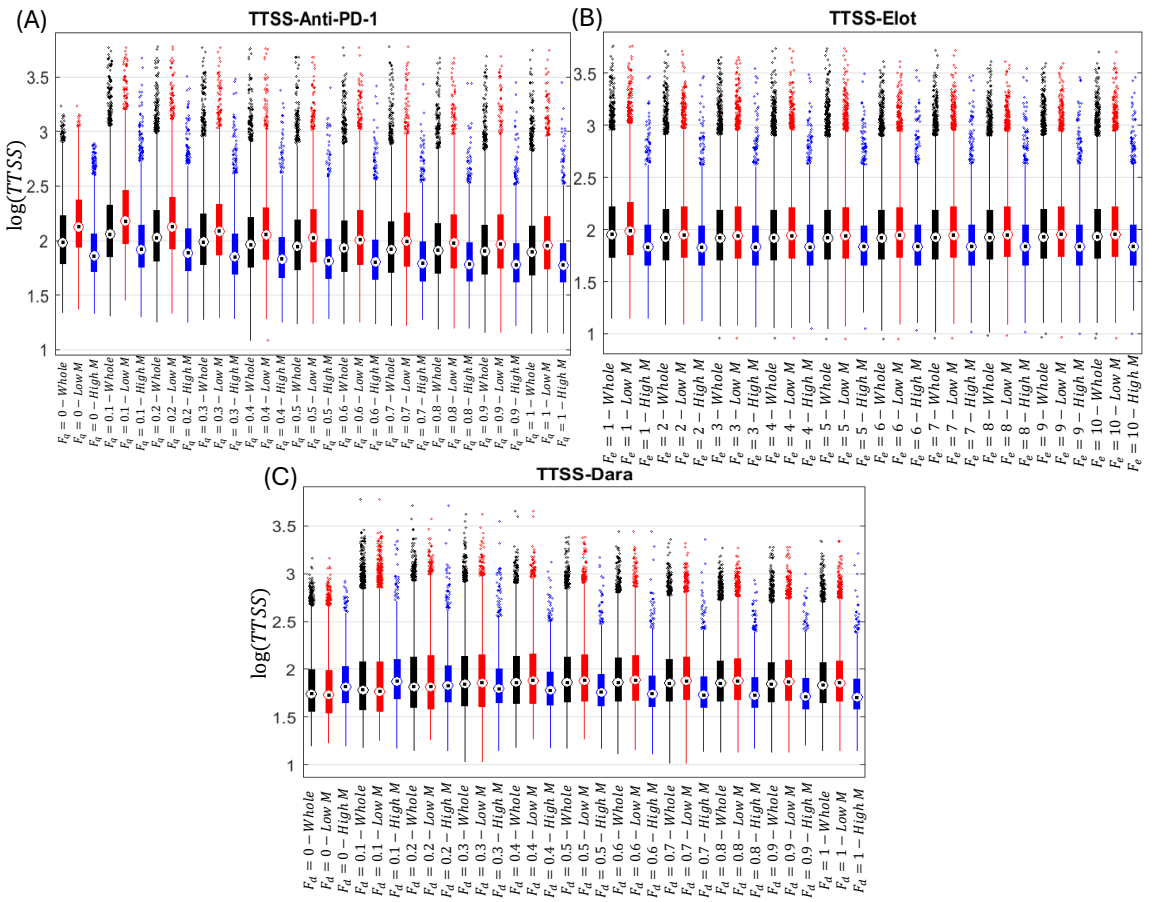

Figure 4.4: **Boxplots of TTSS for model** (2.1.6)**, using the M protein initial condition range from (19).** (A)-(C) display the boxplots for anti-PD-1, elotuzumab, and daratumumab monotherapy, respectively, as the respective treatment parameter F_q, F_e or F_d increases. The black boxplots display the TTSS distribution for all parameter sets. The red and blue boxplots show the TTSS distribution for the parameter sets separated by $M^* < 3$ and $M^* > 3$, respectively. The vertical axis represents the value of TTSS, on a log scale. The black dot inside the white circle represents the median and the thick and thin blue lines represent the interquartile range (IQR) and the data range within 1.5×IQR. The blue/red/black dots represent the outliers.

considered monotherapies, for the M protein initial condition range from (19). For each monotherapy, we first show the boxplot of TTSS for the whole group as one of the treatment parameters F_q, F_e or F_d changes, which is shown in the black boxplots in Fig. 4.4. Next, we display the boxplots of TTSS for the low and high M protein groups and their boxplots are the red and blue bars in Fig. 4.4, respectively. For the whole group boxplot (i.e., the black bars in Fig. 4.4), the median for the anti-PD-1

monotherapy decreases from 95.6 days to 77.8 days (i.e., on a log scale, 1.9805 to 1.8909) as F_q increases and the median for the daratumumab monotherapy increases from 55.5 days to 68.2 days (i.e., on a log scale, 1.7442 to 1.834) as F_d increases. For the elotuzumab treatment, the median is roughly the same for all values of F_e, at roughly 100 days (i.e., on a log scale, 2). Among these three treatments, only anti-PD-1 significantly prolongs the disease progression duration. Moreover, under the monotherapy of anti-PD-1 or elotuzumab, the patients with low M protein have a longer disease progression duration than the patients with high M protein, at any effect of treatment. However, under the daratumumab monotherapy, as F_d decreases (namely, the effect of daratumumab increases), the disease progression duration of patients with high M protein changes from shorter than the ones for the total population to longer than the ones for the total population.

Note that our result qualitatively agrees with the ones shown in (19), as the boxplots corresponding to no treatment (i.e., $F_q = F_e = F_d = 1$) have similar features. The main difference comes from time to steady state distribution, where the authors recorded a median of 161 days, compared to our median of roughly 100 days. This difference could be explained by the differences in sample size, as the authors in (19) used 10000 parameter sets and we used at most 25000 parameter sets.

4.2 Model (2.1.6) Under Specific Initial Conditions

In this section, we study model (2.1.6) under random initial conditions from the ranges in Table 4.1 for $T_C(t)$, $N(t)$, and $T_R(t)$ and the data from (30) for $M(t)$. We generate 25000 parameter sets, using the same settings as Chapter 4.1. The main difference from Chapter 4.1 is the different initial condition range found from (30). The data in (30) shows the distribution of patients' initial M protein level. According

to (30), 24% of the patients were initially between 0 and 0.5 g/dL, 19% of patients were initially between 0.51 and 1 g/dL, 33% of the patients were initially between 1.01 and 1.5 g/dL, 18% of the patients were initially between 1.51 and 2 g/dL, 5% of the patients were initially between 2.01 and 2.5 g/dL, and 1% of the patients were initially between 2.51 and 3 g/dL. Thus, we use these proportions for each subinterval to generate $M(0)$. Table 4.2 shows the number of $M(0)$ located in each range. We apply the same simulation work for these parameter sets used in Chapter 4.1 to understand how the monotherapies affect the steady state and TTSS boxplots and compare them to the conclusions of Chapter 4.1 to see how the different options of initial conditions affect the results.

Table 4.2: **M protein initial condition ranges from (30).** The first column displays the range of initial condition of M protein. The second column shows the proportion for each interval. The third column shows the number of $M(0)$ generated for each range.

Range	Percentage (%)	Number of $M(0)$
$[0, 0.5]$ g/dL	24	6000
$[0.51, 1]$ g/dL	19	4750
$[1.01, 1.5]$ g/dL	33	8250
$[1.51, 2]$ g/dL	18	4500
$[2.01, 2.5]$ g/dL	5	1250
$[2.51, 3]$ g/dL	1	250

Figs. 4.5-4.7 display the steady state boxplots for model (2.1.6) under the anti-PD-1, elotuzumab and daratumumab monotherapies, respectively, for the new initial conditions. We have the same conclusions as observed from Figs. 4.1-4.3 with the median values changing slightly. This finding suggests that the range of initial condition does not significantly affect the steady state boxplots.

Fig. 4.8 displays a similar boxplot for the TTSS as shown in Fig. 4.4, for the initial condition of M protein range from (30). The main difference is that for daratumumab, the patients with low M protein have a longer disease progression duration than the patients with high M protein, at any effect of treatment. Moreover,

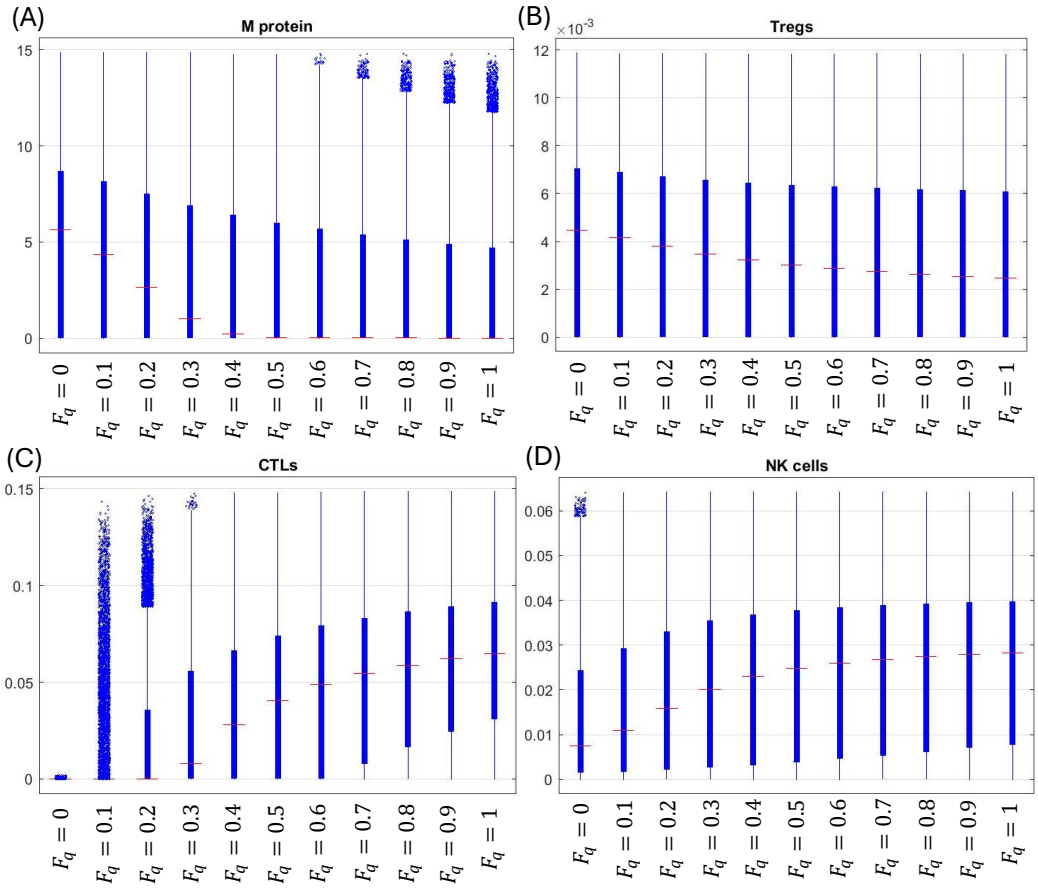

Figure 4.5: **Boxplots of SS for model** (2.1.6) **for the M protein initial condition range in (30), under anti-PD-1 monotherapy.** (A)-(D) displays the steady state boxplots for M protein, T_{reg}s, CTLs and NK cells, respectively, as the value of F_q changes, from 0 to 1 incremented by 0.1, from left bar to right bar. All symbols and definitions (vertical axis, lines, IQR, and outliers) are the same as in Fig. 4.1.

as the effect of daratumumab decreases (i.e., as F_d increases from 0 to 1), the disease progression duration of patients with high M protein changes from similar to that of the total population to shorter than that of the total population. Otherwise, we have similar conclusions when comparing to Fig. 4.4. Comparing these results with the ones in Chapter 4.1, the range of the initial condition of M protein does not significantly affect the distribution of steady state and TTSS, hence we only consider the M protein initial condition range from (30) in the steady state boxplots for model (2.2.5).

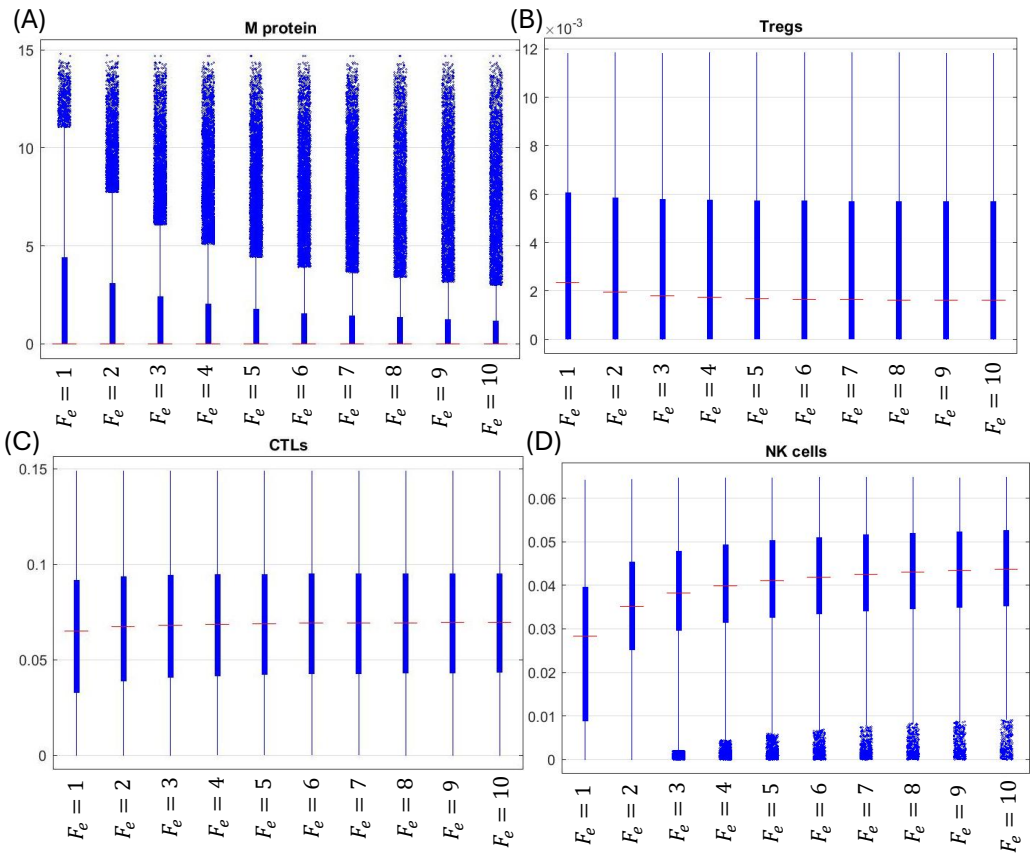

Figure 4.6: **Boxplots of SS for model** (2.1.6) **for the M protein initial condition range in (30), under elotuzumab monotherapy.** (A)-(D) displays the steady state boxplots for M protein, T_{reg}s, CTLs and NK cells, respectively, as the value of F_e changes, from 1 to 10 incremented by 1, from left bar to right bar. All symbols and definitions (vertical axis, lines, IQR, and outliers) are the same as in Fig. 4.1.

4.3 Model (2.2.5) Under Specific Initial Conditions

In this section, we apply the same process done in Chapter 4.2 on model (2.2.5), with initial condition generated from Table 4.2 for $M(t)$ and from Table 4.1 for $T_C(t)$, $N(t)$, and $T_R(t)$. We generated 25000 parameter sets containing the parameters from Table 2.2 and the initial conditions for 4 variables, using the LHS method. We will then compare and contrast the conclusions of this section to the conclusions of Chapters 4.1 and 4.2.

Figs. 4.9-4.11 display the steady state boxplots for model (2.2.5) under the anti-

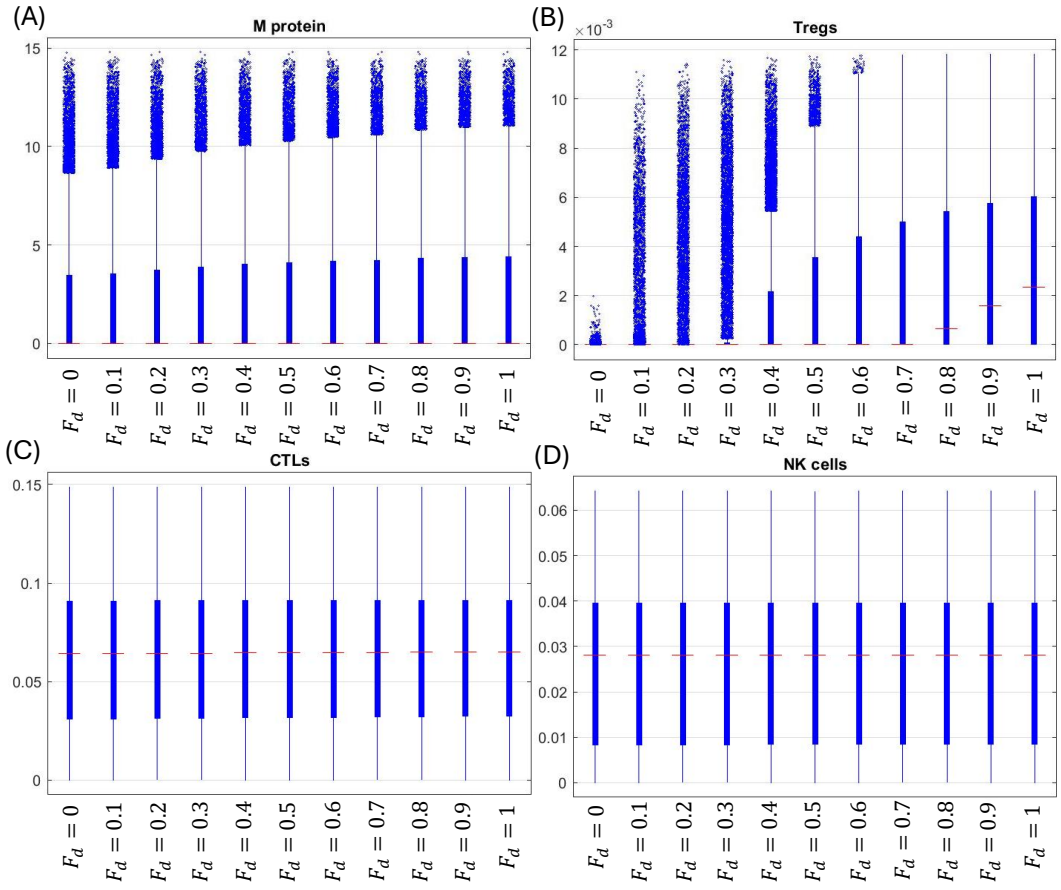

Figure 4.7: **Boxplots of SS for model** (2.1.6) **for the M protein initial condition range in (30), under daratumumab monotherapy.** (A)-(D) displays the steady state boxplots for M protein, T_{reg}s, CTLs and NK cells, respectively, as the value of F_d changes, from 0 to 1 incremented by 0.1, from left bar to right bar. All symbols and definitions (vertical axis, lines, IQR, and outliers) are the same as in Fig. 4.1.

PD-1, elotuzumab, and daratumumab monotherapies, respectively. We have similar patterns and conclusions as for Figs. 4.1-4.3 and Figs. 4.5-4.7 with slightly different median values.

Fig. 4.12 shows the TTSS boxplots for model (2.2.5) under different monotherapies. Comparing to Figs. 4.4 and 4.8, we find that none of the monotherapies can make significant changes on the medians of TTSS for the whole group or separated groups, suggesting that none of the monotherapies can improve the disease progression duration and there is no significant difference between patients with low or high

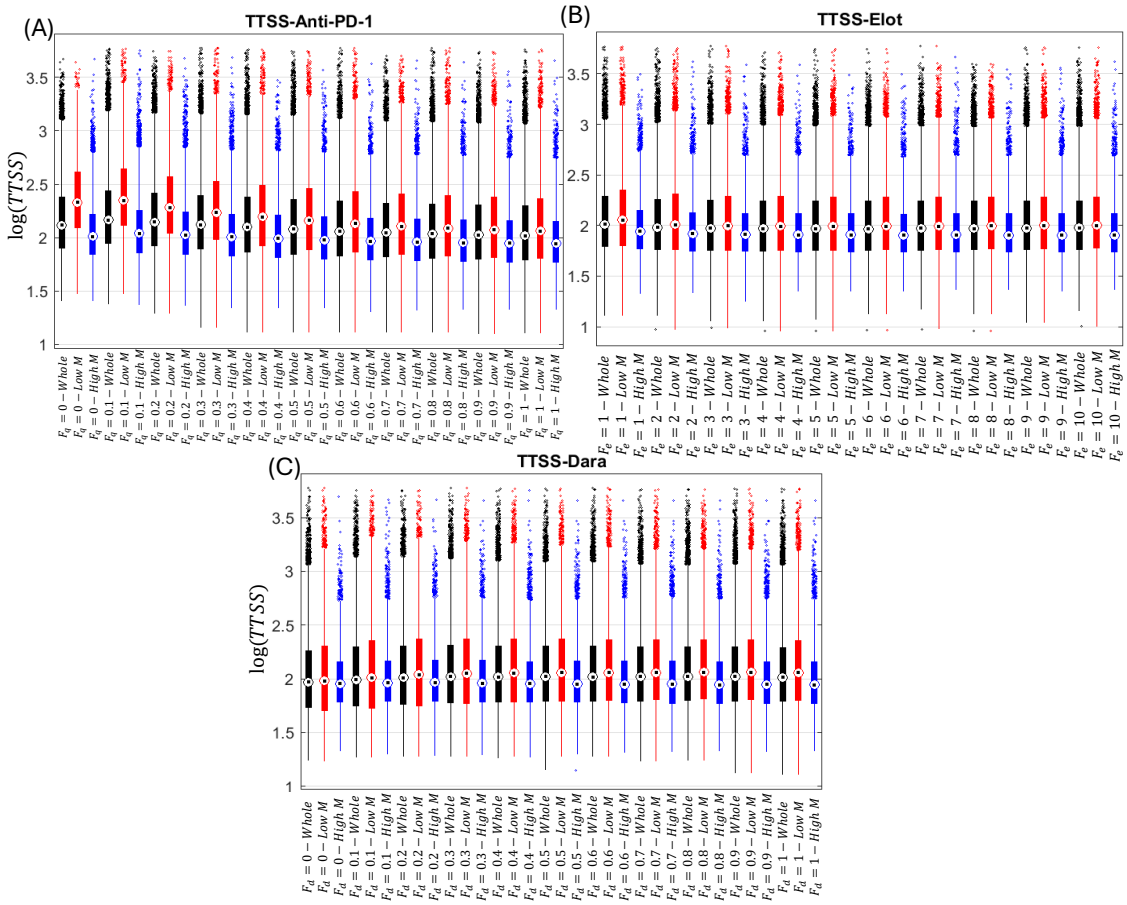

Figure 4.8: **Boxplots for TTSS for model** (2.1.6)**, using the M protein initial condition range from (30).** (A)-(C) display the boxplots for anti-PD-1, elotuzumab, and daratumumab monotherapy, respectively, as the respective treatment parameter F_q, F_e or F_d increases. All symbols and definitions (boxplot, vertical axis, median, IQR, and outliers) are the same as in Fig. 4.4.

M protein.

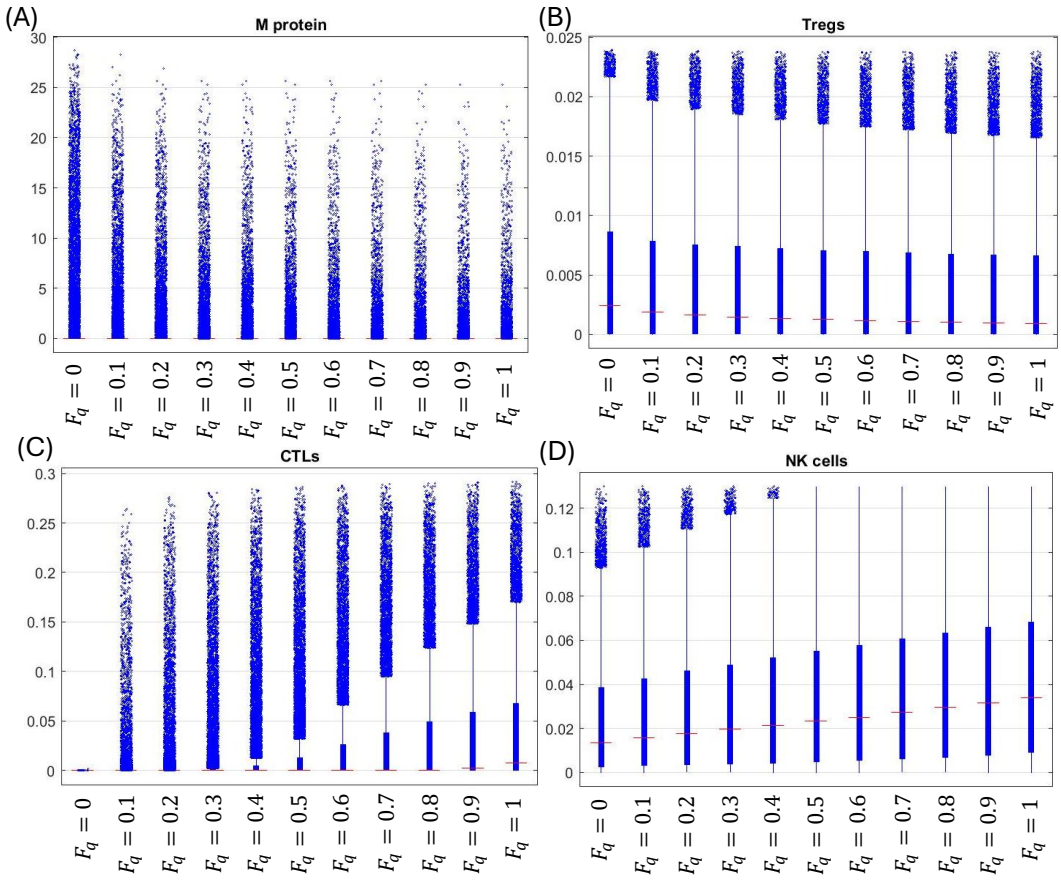

Figure 4.9: **Boxplots of SS for model** (2.2.5) **for the M protein initial condition range in (30), under anti-PD-1 monotherapy.** (A)-(D) displays the steady state boxplots for M protein, T_{reg}s, CTLs and NK cells, respectively, as the value of F_q changes, from 0 to 1 incremented by 0.1, from left bar to right bar. All symbols and definitions (vertical axis, lines, IQR, and outliers) are the same as in Fig. 4.1.

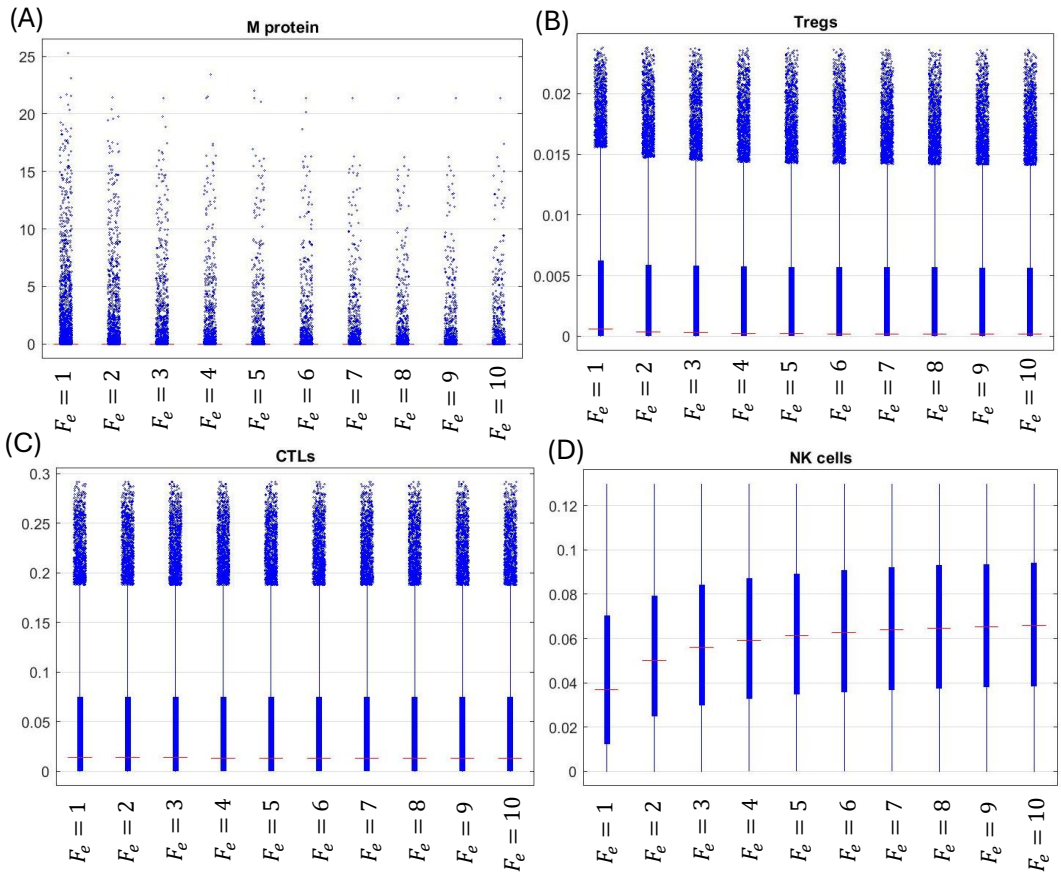

Figure 4.10: **Boxplots of SS for model** (2.2.5) **for the M protein initial condition range in (30), under elotuzumab monotherapy.** (A)-(D) displays the steady state boxplots for M protein, T_{reg}s, CTLs and NK cells, respectively, as the value of F_e changes, from 1 to 10 incremented by 1, from left bar to right bar. All symbols and definitions (vertical axis, lines, IQR, and outliers) are the same as in Fig. 4.1.

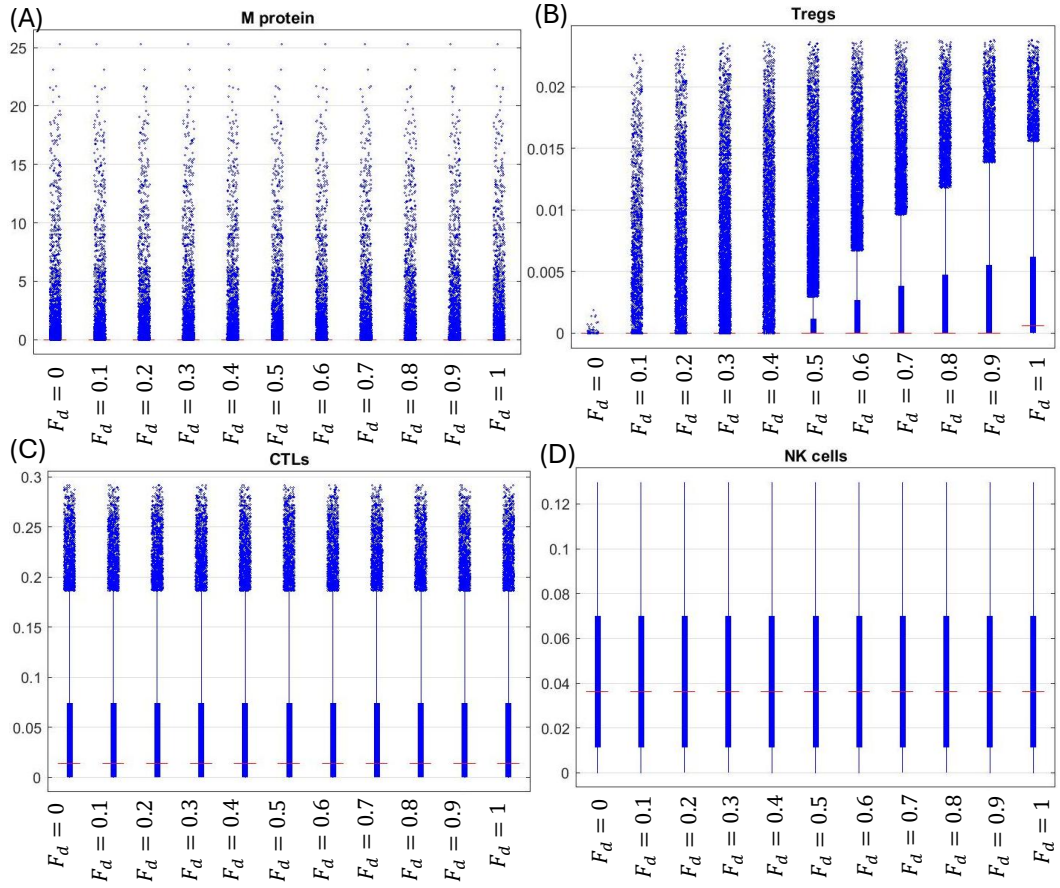

Figure 4.11: **Boxplots of SS for model** (2.2.5) **for the M protein initial condition range in (30), under daratumumab monotherapy.** (A)-(D) displays the steady state boxplots for M protein, T_{reg}s, CTLs and NK cells, respectively, as the value of F_d changes, from 0 to 1 incremented by 0.1, from left bar to right bar. All symbols and definitions (vertical axis, lines, IQR, and outliers) are the same as in Fig. 4.1.

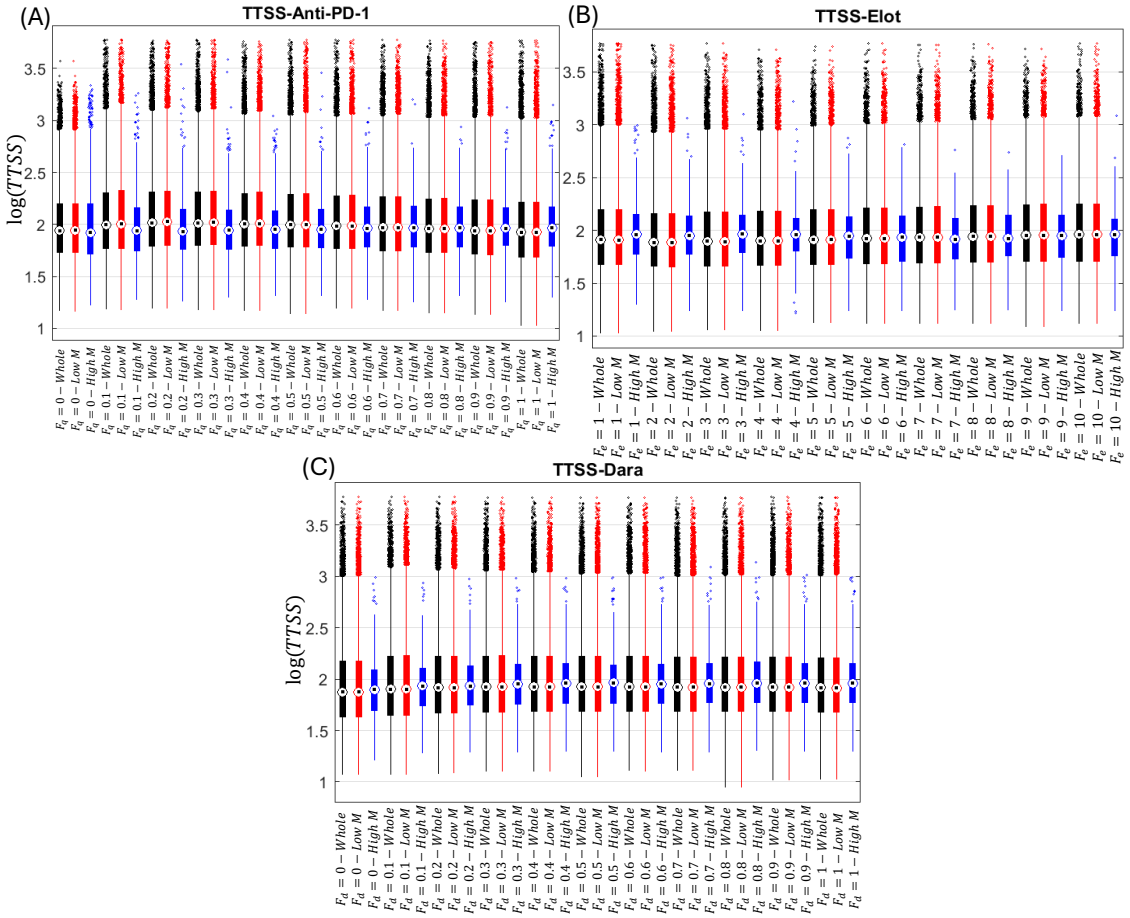

Figure 4.12: **Boxplots for TTSS for model** (2.2.5)**, using the M protein initial condition range from (30).** (A)-(C) display the boxplots for anti-PD-1, elotuzumab, and daratumumab monotherapy, respectively, as the respective treatment parameter F_q, F_e or F_d increases. All symbols and definitions (boxplot, vertical axis, median, IQR, and outliers) are the same as in Fig. 4.4.

5

Mathematical Analysis

In (18), the authors analyzed model (2.1.6), under the control case (i.e., $F_q = F_e = F_d = 1$). They reduced model (2.1.6) from four to two variables, $M(t)$ and $T_C(t)$, using the assumption that $N(t)$ and $T_R(t)$ were constants due to the experimental data in (44). They showed that the reduced model had two types of equilibria, $E_1^* := (M^*, 0)$ and $E_2^* := (M^*, T_C^*)$. For the equilibrium E_1^*, there was a critical M, M_c, such that E_1^* is unstable if $M^* > M_c$, whereas E_1^* is locally stable if $M^* < M_c$. For the equilibrium E_2^*, the authors demonstrated that $T_C^* > 0$ in the region $\{M > M_c\}$ and proved a sufficient condition for the local stability of E_2^*.

However, in (44), there is not enough evidence to support that $N(t)$ and $T_R(t)$ are constants. The experimental data in (44) is cell population across different disease states (e.g., healthy, MGUS, symptomatic MM) at one time point. In particular, NK cells and $\mathrm{T_{reg}}$s had similar distributions across the different disease states. Therefore, we keep all four variables in our analysis for model (2.2.5) to better study the possible dynamics of multiple myeloma.

In this chapter, we analyze the dynamics of model (2.2.5). We will show the positive invariant set and boundness of solutions, existence and local stability of different types of equilibria. We then provide some numerical testing for bifurcation

analysis based on these dynamics.

5.1 Existence of Solutions

In this section, we demonstrate the existence of solutions by the following two propositions.

Proposition 5.1.1. $R_4^{nonneg} = \{(x_1, x_2, x_3, x_4) | x_i \geqslant 0, i = \{1, 2, 3, 4\}\}$ *is a positive invariant set of model* (2.2.5)*, if* $(M(0), T_C(0), N(0), T_R(0)) \in R_4^{nonneg}$.

Proof. First, we consider the case that $(M(0), T_C(0), N(0), T_R(0)) \in R_4^+$, where $R_4^+ = \{(x_1, x_2, x_3, x_4) | x_i > 0, i = \{1, 2, 3, 4\}\}$. Assume that there is a time $\tau_1 > 0$ in which any component reaches zero. If that component is M, namely,

$$\frac{dM}{dt}(\tau_1) = s_M \geqslant 0.$$

Then, $M(t)$ stays nonnegative for all $t \geqslant 0$. If that component is T_C, then $\frac{dT_C}{dt}(\tau_1) = 0$. By existence and uniqueness of solutions, $T_C \equiv 0$. However, this is a contradiction to the assumption that $T_C(0) > 0$. Thus, $T_C(t) > 0$ for all $t \geqslant 0$. Similar arguments can be made to show that N and T_R are nonnegative if $(M(0), T_C(0), N(0), T_R(0)) \in R_4^+$. A similar argument shows that if the initial condition of any component is zero, the solution is nonnegative for all $t \geqslant 0$. □

We next show the solutions of model (2.2.5) are bounded.

Proposition 5.1.2. *The solutions to model* (2.2.5) *are bounded, if the initial condition is in* R_4^{nonneg}.

Proof. First observe that for Eq. (2.2.1)

$$\frac{dM}{dt} = s_M + r_M \left(1 - \frac{M}{K_M}\right) M - \delta_M M - \left[(a_{NM} N + a_{CM} T_C) \frac{1}{1 + T_R}\right] M \leqslant s_M + r_M \left(1 - \frac{M}{K_M}\right) M = F_1(M),$$

due to the positivity of solutions. We analyze the behaviour of the solutions of $\frac{dM}{dt} = F_1(M)$ by looking at the stability of the fixed points,

$$M^* = M_\pm = \frac{r_M \pm \sqrt{r_M^2 + 4r_M s_M/K_M}}{2r_M/K_M}.$$

Since $F_1(M) > 0$ if $0 \leqslant M < M_+$, and $F_1(M) < 0$ if $M > M_+$, the only positive fixed point M_+ is asymptotically stable. Hence $M(t) \leqslant M_+ + \epsilon_1 =: B_M$, for all $\epsilon_1 > 0$, when t is large enough. Therefore, $M(t)$ is bounded.

For Eq. (2.2.2), due to a similar reason, we have

$$\frac{dT_C}{dt} = r_C T_C \left(1 - \frac{T_C}{K_C}\right)(1 + a_{MC}M) - \delta_C T_C \leqslant r_C T_C \left(1 - \frac{T_C}{K_C}\right) A_M = F_2(T_C),$$

where $A_M = 1 + a_{MC}B_M$ and $M \leqslant B_M$, when time is large enough. $F_2(T_C)$ is the logistic equation, so all solutions are bounded by $K_C + \epsilon_2$, for all $\epsilon_2 > 0$, when time t is large enough. Thus, $T_C(t)$ is bounded. A similar argument leads to the boundness of $N(t)$ and $T_R(t)$. □

5.2 Existence and Local Stability of Equilbria

In this section, we consider model (2.2.5) under the control case, i.e., $F_q = F_e = F_d = 1$. According to Eqs. (2.2.1) and (2.2.3), the equilibrium values M^* and N^* are nonzero; Thus, we find different types of nonnegative equilibria: $(M^*, 0, N^*, 0)$, $(M^*, 0, N^*, T_R^*)$, $(M^*, T_C^*, N^*, 0)$, and (M^*, T_C^*, N^*, T_R^*) with the condition for their existence and local stability. For simplicity, these four equilibria are named type 1, type 2, type 3, and type 4, respectively.

Proposition 5.2.1. *If $T_C^* = T_R^* = 0$, model (2.2.5) has the equilibrium $X_1^* :=$*

$(M^*, 0, N^*, 0)$, *with*

$$N^* = \frac{r_N - \delta_N + \sqrt{(r_N - \delta_N)^2 + 4r_N s_N/K_N}}{2r_N/K_N},$$

and

$$M^* = \frac{r_M - \delta_M - a_{NM}N^* + \sqrt{(r_M - \delta_M - a_{NM}N^*)^2 + 4r_M s_M/K_M}}{2r_M/K_M}.$$

Proof. When $T_C^* = T_R^* = 0$, the equilibrium $(M^*, 0, N^*, 0)$ satisfies the following equations

$$M' = s_M + r_M\left(1 - \frac{M^*}{K_M}\right)M^* - \delta_M M^* - a_{NM}N^*M^* = 0, \tag{5.2.1}$$

$$N' = s_N + r_N N^*\left(1 + \frac{N^*}{K_N}\right) - d_N N^* = 0. \tag{5.2.2}$$

Eq. (5.2.2) leads to

$$N^* = N_\pm = \frac{r_N - \delta_N \pm \sqrt{(r_N - \delta_N)^2 + 4r_N s_N/K_N}}{2r_N/K_N},$$

and we set $N^* = N_+ > 0$. Solving Eq. (5.2.1) for M^*, we obtain

$$M^* = M_\pm = \frac{r_M - \delta_M - a_{NM}N^* \pm \sqrt{(r_M - \delta_M - a_{NM}N^*)^2 + 4r_M s_M/K_M}}{2r_M/K_M},$$

and we set $M^* = M_+ > 0$. □

Proposition 5.2.2. *If*

$$T_C^* = 0, M^* > \frac{\delta_R - r_R}{r_R a_{MR}}, K_M(-\delta_R K_R + r_R + K_R r_R + a_{MR}M^* r_R + a_{MR}K_R r_R M^*) \neq 0,$$
$$K_M(\delta_R K_R - (1 + K_R)r_R)s_M < 0, \tag{5.2.3}$$

there exists at least one nonnegative equilibrium $X_2^* := (M^*, 0, N^*, T_R^*)$*, where*

$$N^* = \frac{r_N - \delta_N + \sqrt{(r_N - \delta_N)^2 + 4r_N s_N/K_N}}{2r_N/K_N}, T_R^* = -\frac{K_R}{r_R}\frac{\delta_R - r_R - a_{MR}r_R M^*}{1 + a_{MR}M^*},$$

and M^* *is a positive root of the following polynomial*

$$F(M) := \alpha_3 M^3 + \alpha_2 M^2 + \alpha_1 M + \alpha_0,$$

with

$$\begin{aligned}
\alpha_3 &= r_M(1 + K_R)r_R a_{MR},\\
\alpha_2 &= -\delta_R K_R r_M + (r_M + K_R r_M + a_{MR}K_M(\delta_M + \delta_M K_R + a_{NM}N^* - (1 + K_R)r_M))r_R,\\
\alpha_1 &= K_M(\delta_R K_R r_M + a_{NM}r_R N^* + \delta_M(-\delta_R K_R + r_R + K_R r_R) - (1 + K_R)r_R(r_M + a_{MR}s_M)),\\
\alpha_0 &= K_M s_M(\delta_R K_R - (1 + K_R)r_R).
\end{aligned}$$

Proof. When $T_C^* = 0$, the equilibrium $(M^*, 0, N^*, T_R^*)$ satisfies the following equations:

$$M' = s_M + r_M\left(1 - \frac{M^*}{K_M}\right)M^* - \delta_M M^* - \frac{a_{NM}N^*}{1 + T_R^*}M^* = 0, \tag{5.2.4}$$

$$N' = s_N + r_N N^*\left(1 + \frac{N^*}{K_N}\right) - d_N N^* = 0, \tag{5.2.5}$$

$$T_R' = r_R T_R^*\left(1 - \frac{T_R^*}{K_R}\right)(1 + a_{MR}M^*) - \delta_R T_R^* = 0. \tag{5.2.6}$$

N^* is derived from Eq. (5.2.5), as stated in Proposition 5.2.1.

Eq. (5.2.6) provides

$$T_R^* = \frac{K_R}{r_R}\frac{r_R - \delta_R + a_{MR}r_R M^*}{1 + a_{MR}M^*} > 0, \text{ due to } M^* > \frac{\delta_R - r_R}{a_{MR}r_R}. \tag{5.2.7}$$

Substituting Eq. (5.2.7) into Eq. (5.2.4), we get

$$-\delta_M M^* + r_M M^* - \frac{r_M}{K_M}(M^*)^2 - \frac{a_{NM} M^* N^*}{1 + \frac{K_R(\delta_R - r_R - a_{MR} M^*)}{r_R(1 + a_{MR} M^*)}} + s_M = 0,$$

namely,

$$\frac{F(M^*)}{K_M(-\delta_R K_R + r_R + K_R r_R + a_{MR} M^* r_R + a_{MR} K_R r_R M^*)} = 0,$$

where

$$F(M) = \alpha_3 M^3 + \alpha_2 M^2 + \alpha_1 M + \alpha_0,$$

with

$$\begin{aligned}
\alpha_3 &= r_M(1 + K_R) r_R a_{MR}, \\
\alpha_2 &= -\delta_R K_R r_M + (r_M + K_R r_M + a_{MR} K_M(\delta_M + \delta_M K_R + a_{NM} N^* - (1 + K_R) r_M)) r_R, \\
\alpha_1 &= K_M(\delta_R K_R r_M + a_{NM} r_R N^* + \delta_M(-\delta_R K_R + r_R + K_R r_R) - (1 + K_R) r_R(r_M + a_{MR} s_M)), \\
\alpha_0 &= K_M s_M(\delta_R K_R - (1 + K_R) r_R).
\end{aligned}$$

By condition (5.2.3), we only consider $F(M^*) = \alpha_3(M^*)^3 + \alpha_2(M^*)^2 + \alpha_1 M^* + \alpha_0 = 0$. Since $\alpha_3 > 0$ and $\alpha_0 < 0$, we have $F(0) < 0$ and $\lim_{M \to \infty} F(M) = \infty$, due to condition (5.2.3). Thus, by the Intermediate Value Theorem, there is at least one positive root of $F(M)$, called M^*, such that there is a nonnegative equilibrium $(M^*, 0, N^*, T_R^*)$. □

Proposition 5.2.3. *If $T_R^* = 0$ and $M^* > \frac{\delta_C - r_C}{a_{MC} r_C}$, then there exists at least one nonnegative equilibrium $X_3^* := (M^*, T_C^*, N^*, 0)$, where*

$$T_C^* = T_C^*(M^*) = \frac{K_C(r_C - d_C + a_{MC} r_C M^*)}{r_C(1 + a_{MC} M^*)},$$

$N^* = N^*(M^*)$ is a positive root of the polynomial

$$s_N + r_N N(1 - N/K_N)T(M^*) - \delta_N N,$$

with $T(M^*) = 1 + a_{CN}T_C^*(M^*)$, and M^* is a positive root of the function

$$G(M) := s_M + r_M M(1 - M/K_M) - \delta_M M - (a_{NM}N^*(M) + a_{CM}T_C^*(M))M.$$

Proof. When $T_R^* = 0$, the equilibrium $(M^*, T_C^*, N^*, 0)$ satisfies the following:

$$\begin{aligned} M' &= s_M + r_M \left(1 - \frac{M^*}{K_M}\right) M^* - \delta_M M^* \\ &-(a_{NM}N^* + a_{CM}T_C^*)M^* = 0, \qquad (5.2.8) \\ T_C' &= r_C T_C^* \left(1 - \frac{T_C^*}{K_C}\right)(1 + a_{MC}M^*) - \delta_C T_C^* = 0, \qquad (5.2.9) \\ N' &= s_N + r_N N^* \left(1 + \frac{N^*}{K_N}\right)(1 + a_{CN}T_C^*) - d_N N^* = 0. \qquad (5.2.10) \end{aligned}$$

Eq. (5.2.9) leads to

$$T_C^*(M^*) = \frac{K_C(r_C - \delta_C + a_{MC}r_C M^*)}{r_C(1 + a_{MC}M^*)} > 0, \text{ due to } M^* > \frac{\delta_C - r_C}{a_{MC}r_C}. \qquad (5.2.11)$$

Set $T(M^*) = 1 + a_{CN}T_C^*(M^*)$. Substituting $T(M^*)$ in Eq. (5.2.10) and expanding out in powers of N^*, we have

$$\frac{r_N}{K_N}T(M^*)N^{*2} - (r_N T(M^*) - \delta_N)N^* - s_N = 0. \qquad (5.2.12)$$

Since $\frac{r_N}{K_N}T(M^*) > 0$ and $s_N > 0$, Eq. (5.2.12) has at least one positive root $N^*(M^*)$, by the Intermediate Value Theorem. Next, we analyze the behaviours of $T_C^*(M)$,

$T(M)$ and $N^*(M)$ as $M \to \infty$. We obtain that

$$\begin{aligned} \lim_{M\to\infty} T_C^*(M) &= K_C > 0, \\ \lim_{M\to\infty} T(M) &= 1 + a_{CN}K_C > 0. \end{aligned} \tag{5.2.13}$$

Eq. (5.2.13) implies that $\lim_{M\to\infty} N^*(M)$ is a positive, finite constant as $\frac{r_N}{K_N}(1 + a_{CN}K_C) > 0$ and $s_N > 0$. Set $\lim_{M\to\infty} N^*(M) = N_1$, $0 < N_1 < \infty$.

Finally, from Eq. (5.2.8), we obtain the following equation:

$$P(M^*) = 0, \tag{5.2.14}$$

where

$$P(M) = s_M + r_M M(1 + M/K_M) - \delta_M M - (a_{NM}N^*(M) + a_{CM}T_C^*(M))M.$$

When $M = 0$, $P(0) = s_M > 0$. By Eq. (5.2.13)

$$\lim_{M\to\infty} P(M) = \lim_{M\to\infty} M^2 \left(\frac{s_M}{M^2} + \frac{r_M - \delta_M - a_{NM}N_1 - a_{CM}K_C}{M} - \frac{r_M}{K_M} \right) = -\infty. \tag{5.2.15}$$

Thus, by the Intermediate Value Theorem, we have at least one positive root M^* of $P(M)$. Thus, $(M^*, T_C^*, N^*, 0)$ exists. □

Proposition 5.2.4. *If $M^* > max\{\frac{\delta_C - r_C}{a_{MC}r_C}, \frac{\delta_R - r_R}{a_{MR}r_R}\}$ and $K_R(r_R - \delta_R) > -r_R$, then there exists at least one positive equilibrium $X_4^* := (M^*, T_C^*, N^*, T_R^*)$, where*

$$T_C^* = T_C^*(M^*) = \frac{K_C(r_C - d_C + a_{MC}r_C M^*)}{r_C(1 + a_{MC}M^*)},\ T_R^* = T_R^*(M^*) = \frac{K_R(r_R - \delta_R + a_{MR}M^* r_R)}{r_R(1 + a_{MR}M^*)},$$

and $N^* = N^*(M^*)$ is a positive root of the polynomial

$$s_N + r_N N(1 - N/K_N)T(M^*) - \delta_N N,$$

with $T(M^*) = 1 + a_{CN}T_C^*(M^*)$. *Additionally,* M^* *is a positive root of the function*

$$P_1(M) := s_M + r_M M(1 - M/K_M) - \delta_M M - \frac{(a_{NM}N^*(M) + a_{CM}T_C^*(M))M}{1 + T_R^*(M)}.$$

Proof. The equilibrium (M^*, T_C^*, N^*, T_R^*) satisfies the following equations:

$$\begin{aligned}
M' &= s_M + r_M \left(1 - \frac{M^*}{K_M}\right) M^* - \delta_M M^* - \\
&\left[(a_{NM}N^* + a_{CM}T_C^*)\frac{1}{1 + T_R^*}\right] M^* = 0, && (5.2.16)\\
T_C' &= r_C T_C^* \left(1 - \frac{T_C^*}{K_C}\right)(1 + a_{MC}M^*) - \delta_C T_C^* = 0, && (5.2.17)\\
N' &= s_N + r_N N^* \left(1 + \frac{N^*}{K_N}\right)(1 + a_{CN}T_C^*) - d_N N^* = 0, && (5.2.18)\\
T_R' &= r_R T_R^* \left(1 - \frac{T_R^*}{K_R}\right)(1 + a_{MR}M^*) - \delta_R T_R^* = 0. && (5.2.19)
\end{aligned}$$

Eqs. (5.2.17) and (5.2.18) lead to Eqs. (5.2.11) and (5.2.12), given $M^* > (\delta_C - r_C)/a_{MC}r_C$. Thus, Eq. (5.2.13) holds.

Solving Eq. (5.2.19) as a function of M^*, we obtain

$$T_R^*(M^*) = \frac{K_R(r_R - \delta_R + a_{MR}r_R M^*)}{r_R(1 + a_{MR}M^*)} > 0, \text{ due to } M^* > (\delta_R - r_R)/a_{MR}r_R,$$

and we have

$$\frac{dT_R^*}{dM^*} = \frac{K_R a_{MR}\delta_R}{r_R(1 + a_{MR}M^*)^2}.$$

Hence, $T_R^*(M^*)$ is increasing as M^* increases.

For Eq. (5.2.16), we have, replacing M^* with M,

$$P_1(M) = s_M + r_M M(1 + M/K_M) - \delta_M M - \left(\frac{a_{NM}N^*(M) + a_{CM}T_C^*(M)}{1 + T_R^*(M)}\right) M = 0.$$

When $M = 0$,

$$P_1(0) = s_M - \left(\frac{a_{NM} N^*(0) + a_{CM} T_C^*(0)}{1 + T_R^*(0)} \right) \times 0.$$

Since $K_R(r_R - \delta_R) > -r_R$, we have $T_R^*(0) = K_R(r_R - \delta_R)/r_R > -1$. Since $T_R^*(M)$ is increasing, $T_R^*(M) > -1$ for all $M \geqslant 0$. Thus, $1/(1 + T_R^*(M))$ is defined for all $M \geqslant 0$. Thus, $P_1(M) = s_M > 0$. Additionally, $\lim_{M\to\infty} T_R^*(M) = K_R > 0$ and thus,

$$\lim_{M\to\infty} P_1(M) = \lim_{M\to\infty} M^2 \left(\frac{s_M}{M^2} + \frac{r_M - \delta_M - a_{NM} N_1 - a_{CM} K_C}{(1 + K_R)M} - \frac{r_M}{K_M} \right) = -\infty.$$

Thus, by the Intermediate Value Theorem, there exists at one positive root M^* of $P_1(M)$ and (M^*, T_C^*, N^*, T_R^*) exists. □

Table 5.1: **Conditions for existence of X_1^*, X_2^*, X_3^*, and X_4^*.** The first column lists the equilibrium. The second column displays the conditions for existence, as shown in Propositions 5.2.1, 5.2.2, 5.2.3, and 5.2.4.

Equilibria	Conditions
X_1^*	N/A
X_2^*	$T_C^* = 0,\ M^* > \dfrac{\delta_R - r_R}{r_R a_{MR}}$ $K_M(-\delta_R K_R + r_R + K_R r_R + a_{MR} r_R M^* + a_{MR} K_R r_R M^*) \neq 0$ $K_M(\delta_R K_R - (1 + K_R) r_R) s_M < 0$
X_3^*	$T_R^* = 0,\ M^* > \dfrac{\delta_C - r_C}{a_{MC} r_C}$
X_4^*	$M^* > max\left\{ \dfrac{\delta_C - r_C}{a_{MC} r_C}, \dfrac{\delta_R - r_R}{a_{MR} r_R} \right\}$ $K_R(r_R - \delta_R) > -r_R$

Table 5.1 summarizes the conditions for the existence of X_1^*, X_2^*, X_3^*, and X_4^*. Consider the biological meaning of the equilibria. In all four types, M^* and N^* are always positive, showing that M protein and NK cells are always present. CTLs inhibit M protein by killing myeloma cells (10; 27; 55) and T_{reg}s promote M protein by inhibiting the killing of myeloma cells by CTLs and NK cells (6; 22; 38; 51). Therefore, the equilibrium $X_2^* = (M^*, 0, N^*, T_R^*)$ is the worst case for a patient and the equilibrium $X_3^* = (M^*, T_C^*, N^*, 0)$ is the best case for a patient. The equilibrium

$X_1^* = (M^*, 0, N^*, 0)$ is the second best case for a patient, as there are no T_{reg}s but there is only NK cells present, as compared to CTLs and NK cells present for X_3^*. The equilibrium $X_4^* = (M^*, T_C^*, N^*, T_R^*)$ could be good or bad for a patient, depending on the balance of T_C^* and T_R^* and the level of M^*. Thus, we need to consider the local stability of each type of equilibria so that we can find potential strategies or reactions that could change a patient's disease outcome.

For the local stability, we compute the Jacobian matrix of model (2.2.5) at the considered equilibrium (M^*, T_C^*, N^*, T_R^*):

$$J := \begin{bmatrix} J_{11} & J_{12} & J_{13} & J_{14} \\ J_{21} & J_{22} & 0 & 0 \\ 0 & J_{32} & J_{33} & 0 \\ J_{41} & 0 & 0 & J_{44} \end{bmatrix},$$

with

$$\begin{aligned}
&J_{11} = r_M - 2\frac{r_M}{K_M}M^* - \delta_M - \frac{(a_{NM}N^* + a_{CM}T_C^*)}{1+T_R^*},\ J_{12} = -a_{CM}\frac{M^*}{1+T_R^*},\\
&J_{13} = -a_{NM}\frac{M^*}{1+T_R^*},\ J_{14} = \frac{(a_{NM}N^* + a_{CM}T_C^*)M^*}{(1+T_R^*)^2},\ J_{21} = a_{MC}r_C T_C^*\left(1 - \frac{T_C^*}{K_C}\right),\\
&J_{22} = (1 + a_{MC}M^*)\left(r_C - 2\frac{r_C}{K_C}T_C^*\right) - \delta_C,\ J_{32} = a_{CN}r_N N^*\left(1 - \frac{N^*}{K_N}\right),\\
&J_{33} = (1 + a_{CN}T_C^*)\left(r_N - 2\frac{r_N}{K_N}N^*\right) - \delta_N,\ J_{41} = a_{MR}r_R T_R^*\left(1 - \frac{T_R^*}{K_R}\right),\\
&J_{44} = (1 + a_{MR}M^*)\left(r_R - 2\frac{r_R}{K_R}T_R^*\right) - \delta_R.
\end{aligned}$$

The characteristic polynomial for J is

$$P(\lambda) = \lambda^4 + S_1\lambda^3 + S_2\lambda^2 + S_3\lambda + S_4,$$

with

$$\begin{aligned}
S_1 &= -J_{11} - J_{22} - J_{33} - J_{44}, \\
S_2 &= J_{33}J_{44} + J_{11}J_{22} + J_{11}J_{44} + J_{11}J_{33} + J_{22}J_{33} + J_{22}J_{44} - J_{41}J_{14} - J_{21}J_{12}, \\
S_3 &= J_{14}J_{33}J_{41} + J_{14}J_{22}J_{41} + J_{12}J_{21}J_{44} + J_{12}J_{21}J_{33} - J_{22}J_{33}J_{44} - J_{11}J_{33}J_{44} \\
&\quad -J_{11}J_{22}J_{44} - J_{11}J_{22}J_{33} - J_{13}J_{21}J_{32}, \\
S_4 &= J_{11}J_{22}J_{33}J_{44} + J_{13}J_{21}J_{32}J_{44} - J_{14}J_{22}J_{33}J_{41} - J_{21}J_{12}J_{33}J_{44}.
\end{aligned}$$

By using Routh-Hurwitz criterion, we have the following theorem for the local stability.

Theorem 5.2.5. *For model* (2.2.5)*, the considered equilibrium* (M^*, T_C^*, N^*, T_R^*) *is locally asymptotically stable if and only if*

$$D_1 = S_1 > 0, D_2 = S_1S_2 - S_3 > 0, D_3 = S_1S_2S_3 - S_3^2 - S_1^2S_4 > 0, \text{ and } D_4 = S_4D_3 > 0.$$

Now, let us consider a special case of Theorem 5.2.5, when we have $T_C^* = T_R^* = 0$. By substituting the equilibrium values shown in Proposition 5.2.1, we have the following result:

Corollary 5.2.6. *For the equilibrium* X_1^* *in Proposition 5.2.1, let* $r_C = c\delta_C$ *and* $r_R = r\delta_R$*, then* $X_1^* = (M^*, 0, N^*, 0)$ *is locally asymptotically stable if and only if*

$$r < \frac{1}{1 + a_{MR}M^*} \text{ and } c < \frac{1}{1 + a_{MC}M^*}. \tag{5.2.20}$$

Proof. The Jacobian for X_1^* is

$$J_1 := \begin{bmatrix}
r_M - 2\frac{r_M}{K_M}M^* - \delta_M - a_{NM}N^* & -a_{CM}M^* & -a_{NM}M^* & a_{NM}N^*M^* \\
0 & (1 + a_{MC}M^*)r_C - \delta_C & 0 & 0 \\
0 & a_{CN}r_NN^*(1 - \frac{N^*}{K_N}) & r_N(1 - \frac{2N^*}{K_N}) - \delta_N & 0 \\
0 & 0 & 0 & (1 + a_{MR}M^*)r_R - \delta_R
\end{bmatrix},$$

where the eigenvalues are the diagonal entries. Substituting the exact values for M^* and N^* of X_1^* from Proposition 5.2.1 into $r_M - 2\frac{r_M}{K_M}M^* - \delta_M - a_{NM}N^*$ gets

$$-\sqrt{(r_M - \delta_M - a_{NM}N^*)^2 + 4r_M s_M/K_M} < 0.$$

Similarly for $r_N(1 - \frac{2N^*}{K_N}) - \delta_N$, we get

$$-\sqrt{(r_N - \delta_N)^2 + 4r_N s_N/K_N} < 0.$$

For the other two eigenvalues, we have

$$(1 + a_{MC}M^*)r_C - \delta_C = \delta_C(c(1 + a_{MC}M^*) - 1) < 0,$$

and

$$(1 + a_{MR}M^*)r_R - \delta_R = \delta_R(r(1 + a_{MR}M^*) - 1) < 0,$$

due to the condition (5.2.20). Since all eigenvalues are negative, $X_1^* = (M^*, 0, N^*, 0)$ is locally asymptotically stable under the condition (5.2.20).

Next, if $(M^*, 0, N^*, 0)$ is locally asymptotically stable, the eigenvalues of J_1 are negative. From the above equations, we derive $r < \frac{1}{1+a_{MR}M^*}$ and $c < \frac{1}{1+a_{MC}M^*}$. □

Remark 5.2.7. In the treatment case, the treatment parameters F_q, F_e, and F_d result in a change in parameter values for r_C, r_N, and r_R, respectively. Therefore, the above analysis holds for the treatment case.

5.3 Numerical Testing

In (18), the authors showed that changing the parameter a_{CNM} for model (2.1.6), under the control case (i.e., $F_q = F_e = F_d = 1$), can affect the model dynamics. Using a particular parameter set, the authors showed that for a sufficiently low value

of a_{CNM}, there is only one stable equilibrium with a high M protein level and for a sufficiently high value of a_{CNM}, there is only one stable equilibrium with a lower M protein level. Furthermore, for a moderate value of a_{CNM}, there were two stable equilibria, one with a lower M protein level and one with a higher M protein level and the basin of attraction increased for the lower M protein equilibrium as a_{CNM} increased. Finally, for a particular parameter set, it was found that a sufficiently high M protein initial value led to a significantly higher M protein level compared to a lower M protein initial value. In (19), the authors found a parameter set for which different initial values of M protein lead to two different long-term behaviour. It was shown that a sufficiently high M protein initial value led to a significantly higher M protein level, as compared to a sufficiently low M protein initial value which led to a low M protein level. Additionally, small changes to the homeostasis rate or degradation rate of M protein can lead to different steady state values of M protein.

In this section, we only consider the parameter sets of model (2.2.5) used in Chapter 4.3. We focus on model (2.2.5) and investigate the relation between the long-term behaviour of solutions and the parameters. We first study the distribution of parameters that induce different types of equilibria and their local stability. We then perform global sensitivity analysis to study the correlation between parameters and stable equilibria. Finally, we use bifurcation analysis to study how the parameter values change the local stability of equilibria.

5.3.1 Parameter Distributions

In this section, we use the parameter sets generated in Chapter 4.3 to generate the parameter distribution of each type of equilibrium. For each parameter set, we use the symbolic toolbox package in MATLAB to algebraically generate all its non-negative equilibria and then calculate all the eigenvalues to determine the local stability of each equilibrium. Notice that the parameter set may induce multiple non-

negative equilibria, because X_1^* always exists. Based on this result, we categorize these parameter sets into four groups that these four groups represent the parameter set induces the equilibrium X_1^*, X_2^*, X_3^*, and X_4^*, respectively. Moreover, in each group, we further categorize the parameter sets into the following four subsets:

(i) L+S: the equilibrium is locally asymptotically stable (due to the negative real parts of all eigenvalues) with $M^* < 3$,

(ii) L+US: the equilibrium is unstable (due to at least one eigenvalue having a positive real part) with $M^* < 3$,

(iii) H+S: the equilibrium is locally asymptotically stable (due to the negative real parts of all eigenvalues) with $M^* > 3$, and

(iv) H+US: the equilibrium is unstable (due to at least one eigenvalue having a positive real part) with $M^* > 3$.

Figs. 5.1-5.4 display the distribution of these four groups for each type of equilibrium. First, Fig. 5.1 shows the distribution for type 1 equilibrium $X_1^* = (M^*, 0, N^*, 0)$ and have the following observations:

(i) The values of r_C and r_R are relatively lower when X_1^* is stable than the ones when X_1^* is unstable. This suggests that a lower homeostasis rate of CTLs and $\mathrm{T_{regs}}$s may lead to elimination of CTLs and $\mathrm{T_{reg}}$s.

(ii) The values of a_{MC} is relatively lower only for the H+S group, indicating that a low promotion rate of CTLs by M protein may lead to severe MM and elimination of CTLs and $\mathrm{T_{reg}}$s, namely, X_1^* with $M^* > 3$.

(iii) The values of δ_N and r_M are relatively lower when $M^* < 3$, suggesting for X_1^* that a lower death rate of NK cells or a lower homeostasis rate of M protein may lead to low M protein in the long term.

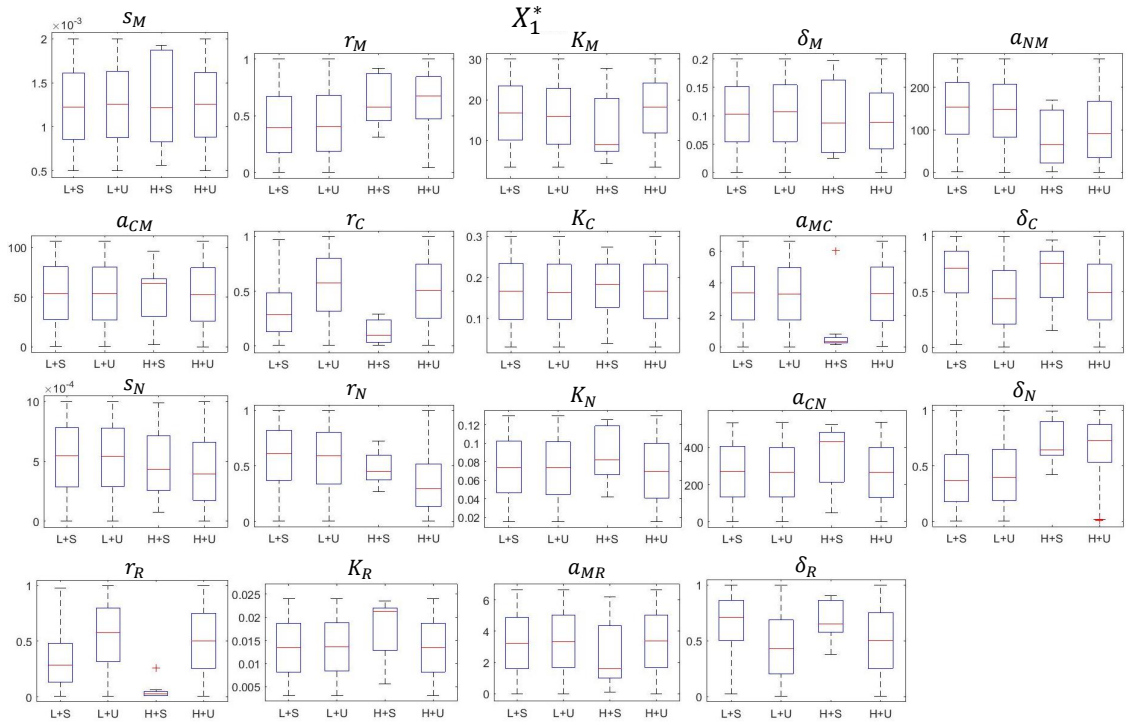

Figure 5.1: **Parameter boxplots for X_1^*.** Each subfigure displays the boxplot of parameter values inducing equilibrium X_1^* in L+S, L+U, H+S, and H+U, from left to right boxes.

(iv) The values of δ_C and δ_R are relatively higher when X_1^* is stable, so a fast death rate of CTLs or $\mathrm{T_{reg}}$s may lead to the long term behaviour of X_1^*.

(v) The value of a_{NM} is relatively lower when $M^* > 3$, indicating that a slower killing rate by NK cells may lead to severe MM.

Fig. 5.2 displays the result for the type 2 equilibrium $X_2^* = (M^*, 0, N^*, T_R^*)$ and we have the following observations:

(i) The value r_C is relatively lower and the value of δ_C is relatively higher when X_2^* is stable. Thus, a slower homeostasis rate or fast death rate of CTLs may lead to elimination of CTLs.

(ii) Similar to the (ii) of X_1^* that low promotion rate of CTLs by M protein may lead to severe MM and elimination of CTLs.

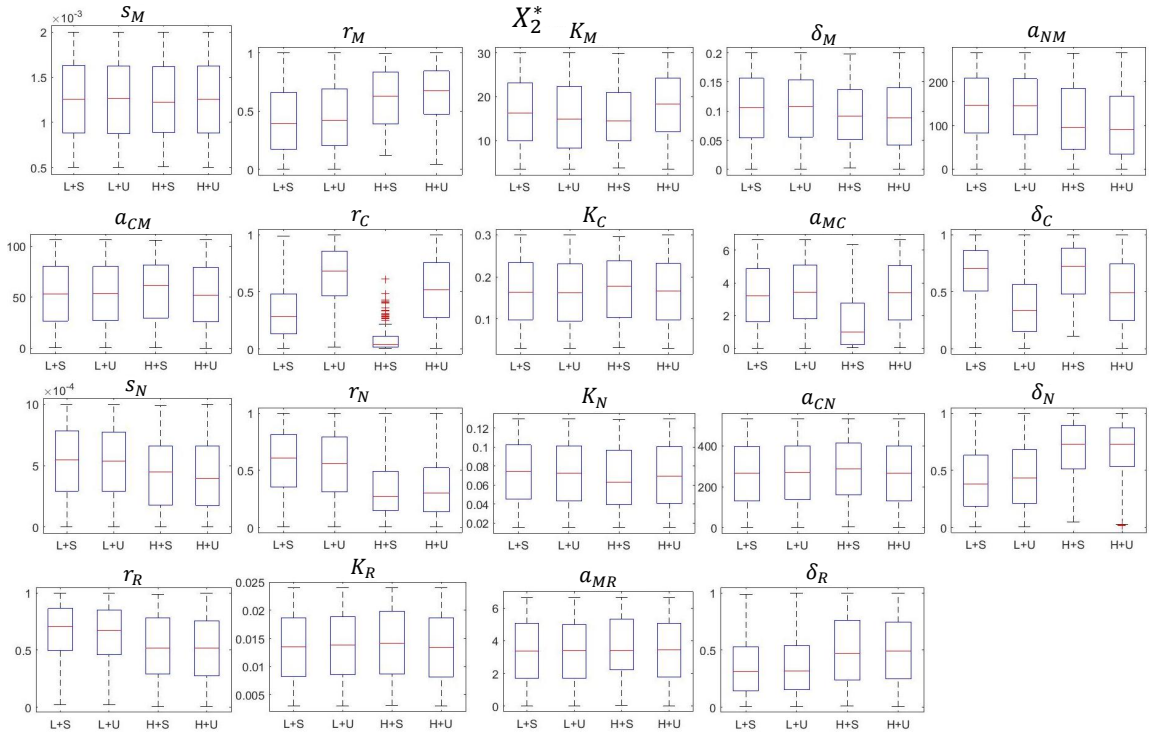

Figure 5.2: **Parameter boxplots for X_2^*.** Each subfigure displays the boxplot of parameter values inducing equilibrium X_2^* in L+S, L+U, H+S, and H+U, from left to right boxes.

(iii) The value of r_N is relatively higher and the value of δ_N is relatively lower when $M^* < 3$, indicating that growing NK cells may control the disease progression.

(iv) The values of r_M and δ_R are relatively higher when $M^* > 3$, suggesting that a faster homeostasis rate of M protein or faster death rate of T_{reg}s may lead to severe MM.

Fig. 5.3 displays the result for the type 3 equilibrium $X_3^* = (M^*, T_C^*, N^*, 0)$ and we have the following observations:

(i) The value of r_C is relatively higher when $M^* < 3$, suggesting that a higher homeostasis rate of CTLs may lead to a low M protein in the long term.

(ii) The value of r_R is relatively low and the value of δ_R is relatively high when X_3^* is stable, indicating a slower homeostasis rate or a fast death rate of T_{reg}s may

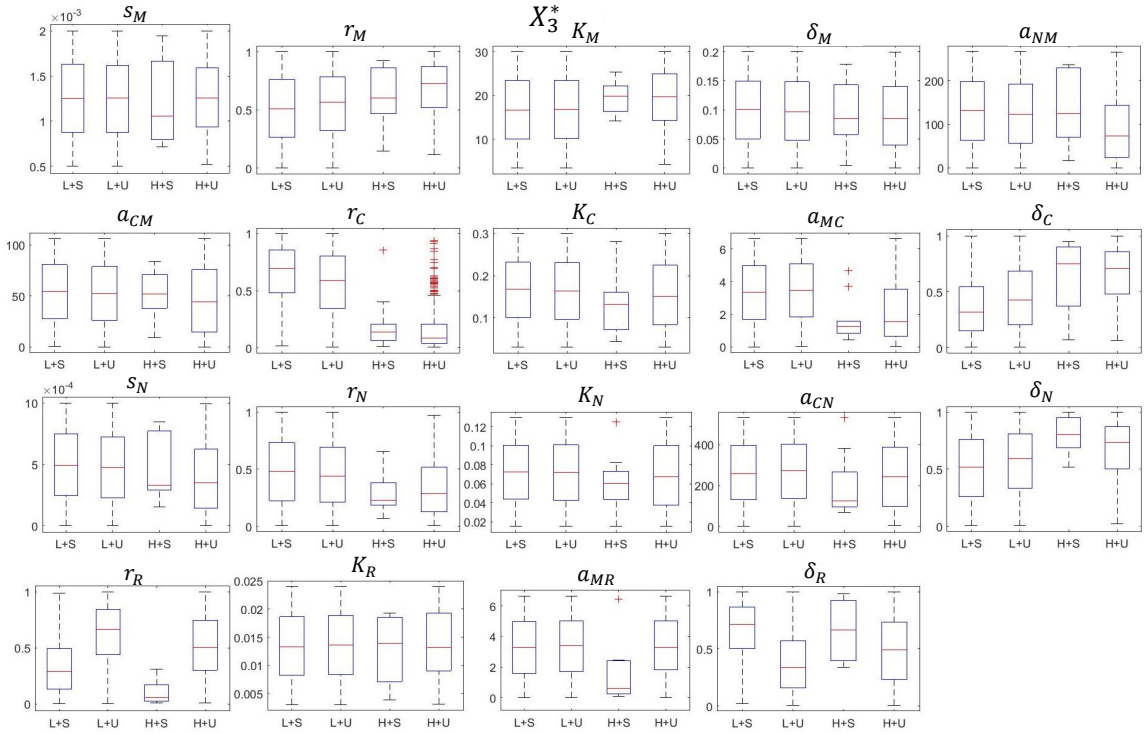

Figure 5.3: **Parameter boxplots for X_3^*.** Each subfigure displays the boxplot of parameter values inducing equilibrium X_3^* in L+S, L+U, H+S, and H+U, from left to right boxes.

lead to elimination of T_{reg}s.

(iii) The values of a_{MR} and a_{MC} are relatively lower only for the H+S group. This suggests that a low promotion rate of T_{reg}s or CTLs may lead to severe MM and elimination of T_{reg}s, namely, X_3^* with $M^* > 3$.

Fig. 5.4 displays the result for the type 4 equilibrium $X_4^* = (M^*, T_C^*, N^*, T_R^*)$. We have the observation that the value of r_C is relatively higher and the value of δ_C is relatively lower for the L+S group, indicating that a high homeostasis rate and a lower death rate of CTLs may lead to a long term behaviour of X_4^* with $M^* < 3$.

Next, we redisplay Figs. 5.1-5.4 by comparing four types of equilibria, and only consider the stable cases in Figs. 5.5 and 5.6, as the unstable cases would not be observed numerically. Since by Proposition 5.2.1 that $X_1^* = (M^*, 0, N^*, 0)$ always

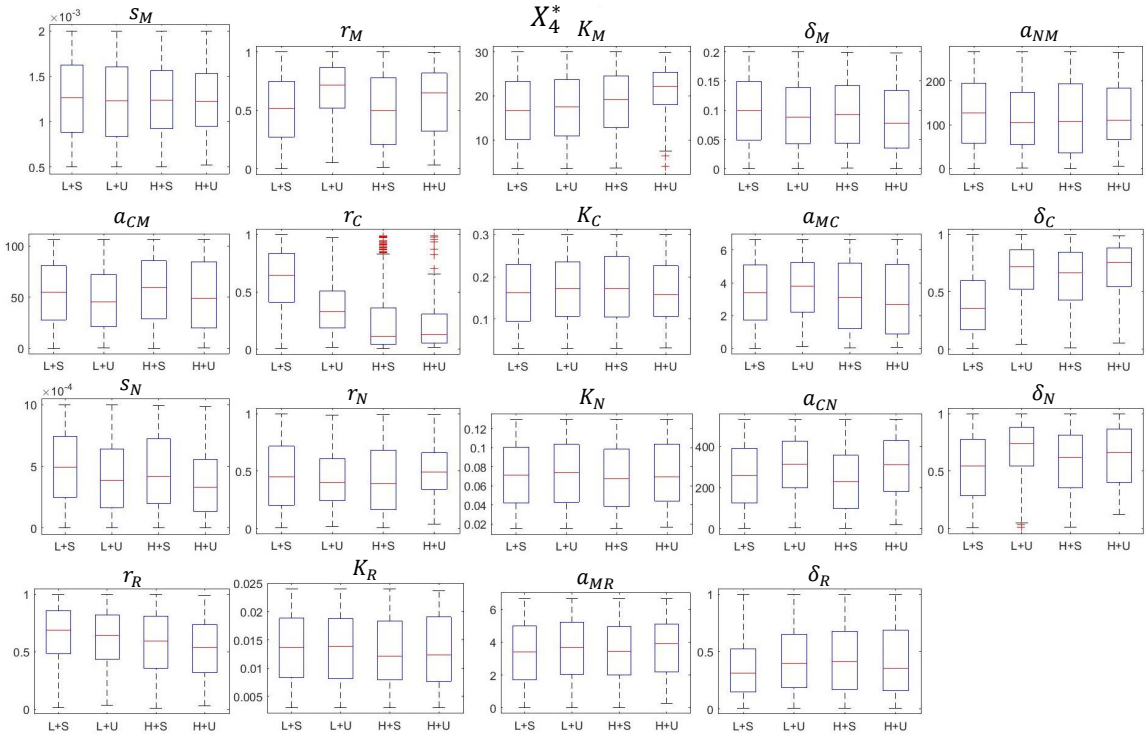

Figure 5.4: **Parameter boxplots for X_4^*.** Each subfigure displays the boxplot of parameter values inducing equilibrium X_4^* in L+S, L+U, H+S, and H+U, from left to right boxes.

exists for model (2.2.5), we only consider the equilibria $X_2^* = (M^*, 0, N^*, T_R^*)$, $X_3^* = (M^*, T_C^*, N^*, 0)$ and $X_4^* = (M^*, T_C^*, N^*, T_R^*)$. Recall that X_2^* and X_3^* represent the worst and best case for patients and X_4^* is the uncertain case.

Fig. 5.5 shows the parameter boxplots for the L+S group and we find that:

(i) The values of r_M, r_C, δ_N, and δ_R are lower for X_2^* and higher for X_3^*, hence higher production of M protein or CTLs, or death rate of NK cells or $\mathrm{T_{reg}}$s could control the disease progression at a low level of M protein, and vice versa.

(ii) The value of δ_C and r_N are higher for X_2^* and lower for X_3^*, hence lower death rate of CTLs or homeostasis rate of NK cells could control the disease progression at a low level of M protein, and vice versa.

(iii) The higher value of r_R or lower value of δ_R could lead to X_4^*. Hence, the disease progression highly depends on a patient's condition (namely, the parameter

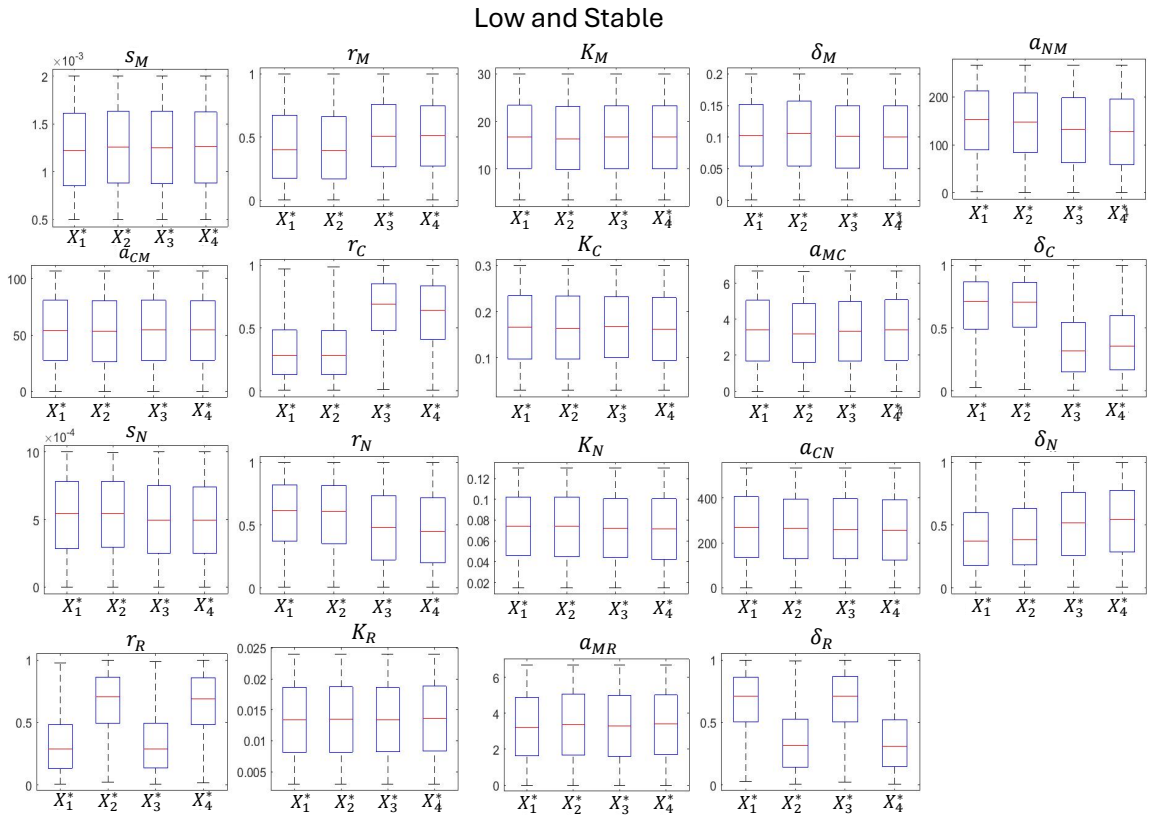

Figure 5.5: **Parameter boxplots for low and stable equilibrium.** Each subfigure displays the boxplot of parameter values inducing $M^* < 3$ for the stable equilibrium X_1^*, X_2^*, X_3^*, and X_4^*, from left to right boxes.

values) when the homeostasis rate of T_{reg}s is high or the death rate of T_{reg}s is low.

Fig. 5.6 shows the results when the equilibrium is in the H+S group and find that:

(i) The values of a_{NM}, and δ_R are lower for X_2^* and higher for X_3^*. Hence, higher killing rate of M protein by NK cells, or death rate of T_{reg}s could control the disease progression at a high level of M protein, and vice versa.

(ii) The values of K_C, a_{MC}, a_{CN}, r_R and a_{MR} are higher for X_2^* and lower for X_3^*, hence lower carrying capacity of CTLs or promotion rate of CTLs by M protein, promotion rate of NK cells by CTLs, and the promotion rate of T_{reg}s

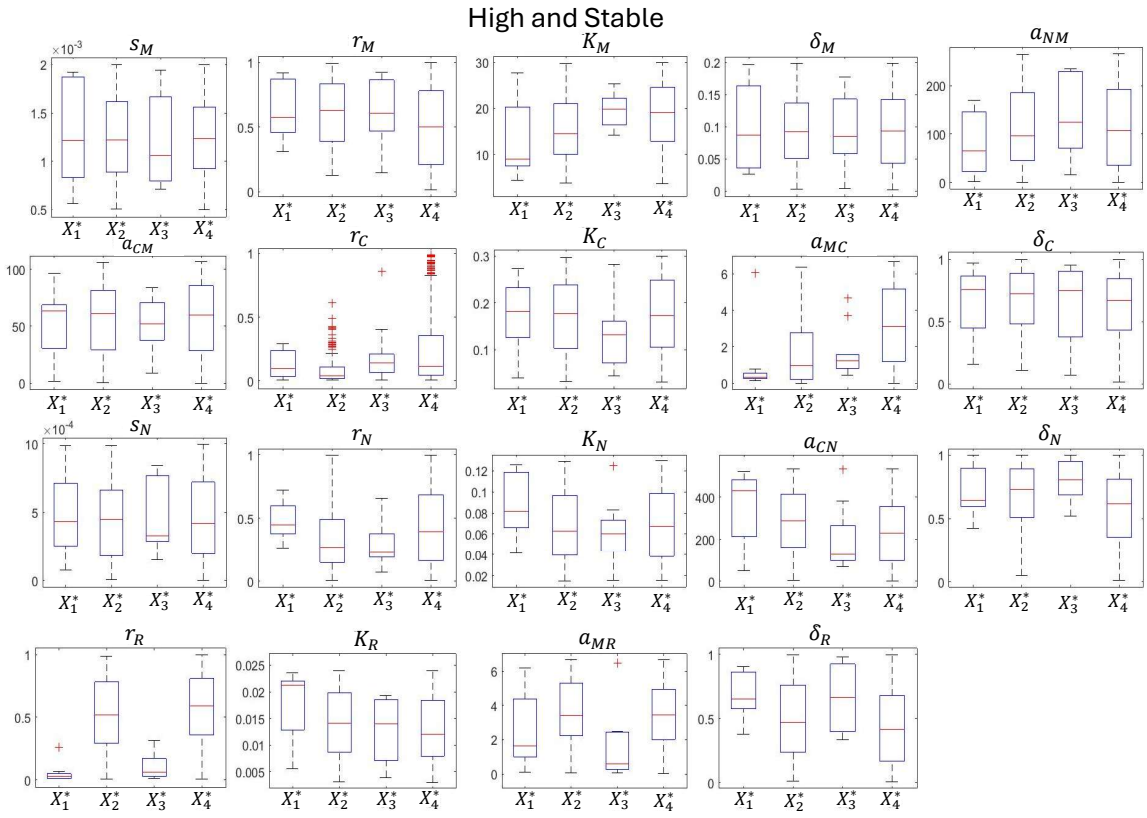

Figure 5.6: **Parameter boxplots for high and stable equilibrium.** Each subfigure displays the boxplot of parameter values inducing $M^* > 3$ for the stable equilibrium X_1^*, X_2^*, X_3^*, and X_4^*, from left to right boxes.

by M protein could control the disease progression at a high level of M protein, and vice versa.

(iii) The higher value of a_{MC} and r_R could lead to X_4^*, hence the disease progression highly depends on a patient's condition (namely, the parameter values) when the promotion rate of CTLs by M protein or homeostasis rate of T_{reg}s is high.

5.3.2 Sensitivity Analysis

Next, based on the four groups of parameter sets for the four types of equilibria that we found in Chapter 5.3.1, we perform the global sensitivity analysis outlined

in (35) to study how all parameters listed in Table 2.2 affect the equilibria X_1^*, X_2^*, X_3^*, and X_4^*. Because the size of parameter sets for the four types of equilibria generated in Chapter 5.3.1 is not large enough to analyze the correlation, we perform latin hypercube sampling (LHS) to generate 200000 parameter sets using the ranges listed in Table 2.2 and then perform the same analytical process used in Chapter 5.3.1 to categorize parameter sets into four groups that these four groups represent the parameter set induces the locally stable equilibrium X_1^*, X_2^*, X_3^*, and X_4^*, respectively. Next, we compute the Partial Rank Correlation Coefficients (PRCCs) and p-values of the parameters with respect to the components of the stable equilibrium. In doing this, we had 29198 samples for stable X_1^*, 32363 samples for stable X_2^*, 40000 samples for stable X_3^*, and 58556 samples for stable X_4^*. A parameter with a positive PRCC indicates increasing the parameter value increases the considered model output, while a parameter with a negative PRCC indicates that the opposite relation. Tables 5.2-5.5 show the PRCCs for the parameters to the components M^*, T_C^*, N^*, and T_R^* under different types of equilibrium, respectively.

Let us first consider the M^* component for each equilibria in Table 5.2. The parameters δ_N, s_M and r_M are positively correlated to all types of equilibrium, where δ_N is much stronger than s_M and s_M is much stronger than r_M. Thus, the reduction of M protein is most sensitive to the decreasing of the death rate of NK cells, is minor sensitive to the decreasing of the constant source of M protein, and less sensitive to the decreasing of the homeostasis rate of M protein. The parameters a_{NM}, r_N, K_N, s_N, δ_M, r_R and r_C are negatively correlated to all types of equilibrium, where a_{NM}, r_N and K_N are much stronger than s_N and s_N are much stronger than δ_M and r_R. Hence, the reduction of M protein is most sensitive to the increasing of killing rate of M protein by NK cells, or homeostasis rate of NK cells or carrying capacity of NK cells, is minor sensitive to the increasing of the constant source for NK cells and less sensitive to the increasing of the degradation rate of M

Table 5.2: **PRCCs of the parameters in model** (2.2.5) **with respect to** M^***.** The first column lists the parameters. The second, third, fourth and fifth columns display their PRCCs to the M^* of the equilibria X_1^*, X_2^*, X_3^*, and X_4^*, respectively. All PRCCs have p-value less than 0.05, except those marked with a superscript $*$.

Parameter	X_1^*	X_2^*	X_3^*	X_4^*
s_M	0.3985	0.3513	0.5268	0.4318
r_M	0.1197	0.1995	0.07202	0.1097
K_M	-0.006166^*	-0.01343	-0.000693^*	-0.00361^*
δ_M	-0.04348	-0.04881	-0.01879	-0.02228
a_{NM}	-0.6337	-0.6188	-0.6214	-0.5586
a_{CM}	0.002228^*	-0.001441^*	-0.3641	-0.3069
r_C	-0.01545	-0.0964	-0.4139	-0.5504
K_C	0.007307^*	-0.005784^*	-0.4068	-0.3347
a_{MC}	-0.006443^*	-0.06424	0.01631	-0.04416
δ_C	0.01123^*	0.05082	0.6246	0.6705
s_N	-0.09526	-0.1252	-0.02202	-0.05379
r_N	-0.6626	-0.674	-0.321	-0.3484
K_N	-0.4786	-0.4321	-0.4842	-0.4012
a_{CN}	$8.88 \times 10^{-5*}$	0.00893^*	-0.1875	-0.1825
δ_N	0.8018	0.8044	0.238	0.2531
r_R	-0.01613	-0.0638	-0.02356	-0.06008
K_R	-0.006169^*	-0.0034^*	-0.003388^*	-0.004896^*
a_{MR}	-0.01059^*	0.008391^*	-0.01959	0.004143^*
δ_R	0.01315	0.06109	0.006056^*	0.06366

protein or homeostasis rate of T_{reg}s. Moveover, r_C has a weak effect on X_1^* and X_2^* and a strong effect on X_3^* and X_4^*, so increasing the homeostasis rate of CTLs may weakly improve the worst case X_2^* for patients and strongly improve the best case X_3^* or the uncertain case X_4^* for patients. The parameters a_{CM}, K_C and a_{CN} are negatively correlated to the equilibria X_3^* and X_4^*, where a_{CM} and K_C are stronger than a_{CN}. Hence, the reduction of M protein is most sensitive to the increase of the promotion rate of CTLs by M protein or carrying capacity of CTLs and less sensitive to the increase of promotion rate of NK cells by CTLs for the equilibria X_3^* and X_4^*. The parameter δ_C is positively correlated to M^* for the equilibria X_2^*, X_3^* and X_4^*, indicating that the reduction of M protein in X_2^*, X_3^*, and X_4^* is sensitive to a decrease in the death rate of CTLs. Moveover, δ_C has a weak effect on X_2^* and

Table 5.3: **PRCCs of the parameters in model** (2.2.5) **with respect to T_C^*.** The first column lists the parameters. The second and third columns display their PRCCs to the T_C^* of the equilibria X_3^* and X_4^*, respectively. All PRCCs have p-value less than 0.05, except those marked with a superscript $*$.

Parameter	X_3^*	X_4^*
s_M	-0.005648^*	-0.0008234
r_M	0.0187	0.07139
K_M	0.003633^*	0.0204
δ_M	-0.0007574^*	-0.01572
a_{NM}	0.02903^*	-0.01037
a_{CM}	-0.04206	-0.1027
r_C	0.6291	0.6274
K_C	0.7286	0.6113
a_{MC}	-0.01342	0.01232
δ_C	-0.8424	-0.8161
s_N	-0.01315	-0.00836
r_N	0.0195	-0.0032^*
K_N	0.008753^*	0.005381^*
a_{CN}	-0.0039^*	-0.0169
δ_N	-0.02718	-0.02423
r_R	0.007436^*	0.008281
K_R	0.001457^*	0.003179^*
a_{MR}	-0.001885^*	-0.002622^*
δ_R	-0.003912^*	-0.008088^*

a strong effect on X_3^* and X_4^*, and hence decreasing the death rate of CTLs may weakly improve the worst case X_2^* and strongly improve the best case X_3^* and the uncertain case X_4^* for patients.

Consider the T_C^* components for the X_3^* and X_4^* equilibria in Table 5.3. The parameters K_C and r_C are strongly positively correlated to X_3^* and the parameters r_M and r_N are weakly positively correlated to X_3^*. These results suggest that, when the patients are in the best situation X_3^*, an increase in CTLs is more sensitive to an increase in the homeostasis rate or carrying capacity of CTLs and less sensitive to an increase in the homeostasis rate of either M protein or NK cells. The parameter δ_C is strongly negatively correlated to X_3^* and the parameters a_{CM}, a_{MC}, s_N, and δ_N are weakly negatively correlated to X_3^*. Hence, when the patients are in the best

Table 5.4: **PRCCs of the parameters for model** (2.2.5) **with respect to** N^***.** The first column lists the parameters. The second, third, fourth and fifth columns display the PRCCs to the N^* of the equilibria X_1^*, X_2^*, X_3^*, X_4^*, respectively. All PRCCs have p-value less than 0.05, except those marked with a superscript $*$.

Parameter	X_1^*	X_2^*	X_3^*	X_4^*
s_M	-0.004534^*	-0.001565^*	-0.01228	-0.007912^*
r_M	0.1147	0.09075	0.01615	0.01578
K_M	-0.0006833^*	0.01066^*	$1.54 \times 10^{-5*}$	0.005677^*
δ_M	-0.01711	-0.02719	0.005248^*	-0.004428^*
a_{NM}	-0.07258	-0.06047	-0.002111^*	-0.02341
a_{CM}	-0.001603^*	-0.003003^*	-0.03218	-0.05119
r_C	-0.002968^*	0.04948	0.2764	0.3914
K_C	-0.001991^*	0.001359^*	0.1949	0.1541
a_{MC}	0.001869^*	0.003338	-0.02501	0.01443
δ_C	-0.007931^*	-0.03142	-0.4272	-0.4885
s_N	0.1299	0.1978	0.03821	0.09906
r_N	0.7526	0.7805	0.4938	0.5298
K_N	0.6488	0.6049	0.7862	0.6977
a_{CN}	-0.00375^*	-0.01001^*	0.3441	0.3228
δ_N	-0.8767	-0.887	-0.3746	-0.3896
r_R	0.01201	0.03502	0.02034	0.0425
K_R	0.00829^*	0.002221^*	0.009527^*	0.003293^*
a_{MR}	0.005762^*	-0.002132^*	0.01448	-0.008129
δ_R	-0.009037^*	-0.03324	-0.003539^*	-0.0475

situation X_3^*, an increase in CTLs is more sensitive to a decrease of the death rate of CTLs and less sensitive to a decrease in the killing rate of M protein by CTLs, the promotion rate of CTLs by M protein, the carrying capacity of NK cells or the death rate of NK cells.

The parameters r_C and K_C are strongly positively correlated to X_4^* and the parameters r_M, a_{MC}, r_R and K_M are weakly positively correlated to X_4^*. These results hint that, when the patients are in the uncertain situation X_4^*, an increase in CTLs is more sensitive to an increase the homeostasis rate or carrying capacity of CTLs and less sensitive to an increase in either the homeostasis rate of M protein, the promotion rate of CTLs by M protein, the homeostasis rate of T_{reg}s, or the carrying

Table 5.5: **PRCCs of the parameters in model** (2.2.5) **with respect to T_R^*.** The first column lists the parameters. The second and third columns display their PRCCs to the T_R^* of the equilibria X_2^* and X_4^*, respectively. All PRCCs have p-value less than 0.05, except those marked with a superscript $*$.

Parameter	X_2^*	X_4^*
s_M	0.00508*	-0.002635*
r_M	0.1557	0.05096
K_M	-0.03553	0.0167
δ_M	-0.02989	-0.01649
a_{NM}	-0.101	-0.06025
a_{CM}	0.006101*	-0.0171
r_C	-0.1639	-0.3234
K_C	-0.005865*	-0.02413
a_{MC}	-0.1195	-0.08611
δ_C	0.07876	0.2743
s_N	-0.06087	-0.01925
r_N	-0.1648	-0.08292
K_N	-0.03141	-0.01259
a_{CN}	0.008763*	-0.01851
δ_N	0.1936	0.06246
r_R	0.4235	0.4251
K_R	0.7183	0.7288
a_{MR}	0.04087	0.0779
δ_R	-0.7441	-0.7425

capacity of M protein. The parameter δ_C is strongly negatively correlated to X_4^* and the parameters $s_M,\ \delta_M,\ a_{NM},\ a_{CM},\ s_N,\ a_{CN}$ and δ_N are weakly negatively correlated to X_4^*. These results indicate that, when patients are in the uncertain situation X_4^*, an increase in CTLs is more sensitive to a decrease in the death rate of CTLs and less sensitive to a decrease in either the constant source of M protein, the death rate of M protein, the killing rates of M protein by CTLs and NK cells, the constant source for NK cells, the promotion rate of NK cells by M protein, or the death rate of NK cells.

Consider the N^* components for the equilibria, shown in Table 5.4. The parameters $r_M,\ s_N,\ r_N,\ K_N$ and r_R are positively correlated to all types of equilibria, where K_N and r_N are much stronger than $r_M,\ s_N$ and r_R. This suggests that an increase

in NK cells is most sensitive to an increase in the homeostasis rate of NK cells or carrying capacity of NK cells and less sensitive to an increase in the homeostasis rate of T_{reg}s, homeostasis rate of M protein or constant source of NK cells. The parameter a_{CM} is negatively correlated and the parameters K_C and a_{CN} are positively correlated to the equilibria X_3^* and X_4^*, where K_C and a_{CN} are much stronger than a_{CM} in magnitude. This suggests that an increase in NK cells is most sensitive to an increase in the carrying capacity of CTLs or the promotion rate of NK cells by CTLs and less sensitive to a decrease in the killing rate of M protein by CTLs. The parameter r_C is positively correlated and the parameter δ_C is negatively correlated to the equilibria $X_2^*,\ X_3^*$ and X_4^*. This indicates that an increase in NK cells is sensitive to an increase of the homeostasis rate of CTLs or a decrease of the death rate of CTLs. Moreover, r_C and δ_C have a weak effect for X_2^* and a strong effect for X_3^* and X_4^*. This suggest that changing either the homeostasis rate or the death rate of CTLs has a weaker effect on the worst case X_2^* and has a stronger effect on the best case X_3^* and the uncertain case X_4^* for patients. The parameter δ_N is negatively correlated for all types of equilibria, suggesting that an increase in NK cells is sensitive to a decrease in the death rate of NK cells. Furthermore, δ_N has a stronger effect on X_1^* and X_2^* and a weaker effect on X_3^* and X_4^*. Hence, decreasing the death rate of NK cells has a strong effect on the worst case X_2^* and has a weaker effect on the best case X_3^* and the uncertain case X_4^*.

Consider the T_R^* components for the equilibria X_2^* and X_4^*, shown in Table 5.5. The parameters $r_M,\ \delta_C,\ \delta_N,\ r_R,\ K_R$ and a_{MR} are positively correlated both types of equilibrium, where r_R and K_R are much stronger than $r_M,\ \delta_C,\ \delta_N$ and a_{MR}. This indicates that the reduction of T_{reg}s is most sensitive to a decrease in the homeostasis rate or carrying capacity of T_{reg}s and less sensitive to a decrease in the homeostasis rate of M protein, death rate of CTLs or NK cells or the promotion rate of T_{reg}s by M protein. Moreover, r_M and δ_N have a weaker effect on X_4^* and a moderate

effect on X_2^*, indicating that decreasing the homeostasis rate of M protein and the death rate of NK cells may improve the worst case X_2^* more than for the uncertain case X_4^* for patients. Additionally, δ_C has a stronger effect for X_4^* compared to X_2^*, indicating that decreasing the death rate of CTLs may weakly improves the worst case X_2^* and strongly improve the uncertain case X_4^*. The parameters $\delta_M,\ a_{NM},\ r_C,\ a_{MC},\ s_N,\ r_N,\ K_N$ and δ_R are negatively correlated to both equilibrium, where δ_R is much stronger than r_N and a_{NM}, and r_N and a_{NM} are stronger than $\delta_M,\ a_{NM},\ a_{MC},\ r_C,\ s_N,\ r_N$ and K_N. This suggests that the reduction of $\mathrm{T_{reg}}$s is most sensitive to the increase in the death rate of $\mathrm{T_{reg}}$s and moderately sensitive to an increase in either the homeostasis rate of NK cells or the killing rate of M protein by NK cells. Moreover, r_C has a weaker effect on X_2^* and a stronger effect on X_4^*, indicating that increasing the homeostasis rate of CTLs may weakly improve the worst case X_2^* and strongly improve the uncertain case X_4^* for patients. Furthermore, r_N and s_N have a stronger effect on X_2^* and a weaker effect on X_4^*, suggesting that increasing either the homeostasis rate or constant source of NK cells may strongly improve the worst case X_2^* and weakly improve the uncertain case X_4^*.

The parameters $a_{CM},\ K_C$ and a_{CN} are negatively correlated to the equilibrium X_4^*, indicating that increasing the promotion of CTLs by M protein, the carrying capacity of CTLs, or the promotion of NK cells by CTLs may lead to a reduction in $\mathrm{T_{reg}}$s. The parameter K_M is negatively correlated to X_2^* and positively correlated to X_4^*, suggesting that the carrying capacity of M protein could be used to determine a patient's long term disease progression.

5.3.3 Bifurcation Analysis

Considering the importance of the parameters r_C and r_R found in the stability of X_1^* in Corollary 5.2.6, in the parameter distributions and in the sensitivity analysis, we provide two examples of bifurcation diagrams to display how the values of r_C and

r_R affect the number and local stability of equilibria. We generate the bifurcation diagrams in this subsection using the Matlab package matcont.

Noticing that the values of r_C and r_R affect the stability of X_1^* and the existence of X_2^*, X_3^* and X_4^*, we set $r_C = c\delta_C$, $r_R = r\delta_R$, $r^* = 1/(1 + a_{MR}M_1^*)$ and $c^* = 1/(1 + a_{MC}M_1^*)$, where M_1^* is the M component in the equilibrium X_1^*, as shown in Corollary 5.2.6. Then, we vary the values of r_C and r_R by changing c and r within the intervals $r \in [0, 3r^*]$ and $c \in [0, 3c^*]$ equally divided into 51 grids. In Chapter 4, we use the LHS method with parameter ranges from Table 2.2 to generate 25000 parameter sets. Within these parameter sets, we select two sets that one set induces a type 1 equilibrium X_1^* with its $M_1^* < 3$ and the other set induces a type 1 equilibrium X_1^* with its $M_1^* > 3$. Table 5.6 displays the values for these two parameter sets.

Table 5.6: **Parameter values for the bifurcation examples.** The first column lists the parameter. The second and third columns list the parameter values where the corresponding model (2.2.5) generates the type 1 equilibrium X_1^* with $M_1^* < 3$ and $M_1^* > 3$, respectively.

Parameter	$M_1^* < 3$	$M_1^* > 3$
s_M	0.0007 g/(dL day)	0.0017 g/(dL day)
r_M	0.356 day^{-1}	0.7635 day^{-1}
K_M	29.7443 g/dL	25.4672 g/dL
δ_M	0.151 day^{-1}	0.182 day^{-1}
a_{NM}	59.3234 dL/(g day)	63.7661 dL/(g day)
a_{CM}	69.7445 dL/(g day)	88.3295 dL/(g day)
r_C	0.1088 day^{-1}	0.4489 day^{-1}
K_C	0.1025 g/dL	0.2096 g/dL
a_{MC}	5.6735 dL/g	3.1256 dL/g
δ_C	0.6767 day^{-1}	0.586 day^{-1}
s_N	0.0006 g/(dL day)	0.0008 g/(dL day)
r_N	0.7875 day^{-1}	0.5429 day^{-1}
K_N	0.0874 g/dL	0.0396 g/dL
a_{CN}	480.5674 dL/g	262.6044 dL/g
δ_N	0.9573 day^{-1}	0.572 day^{-1}
r_R	0.7715 day^{-1}	0.9994 day^{-1}
K_R	0.0122 g/dL	0.0088 g/dL
a_{MR}	6.5069 dL/g	1.8308 dL/g
δ_R	0.1267 day^{-1}	0.0084 day^{-1}

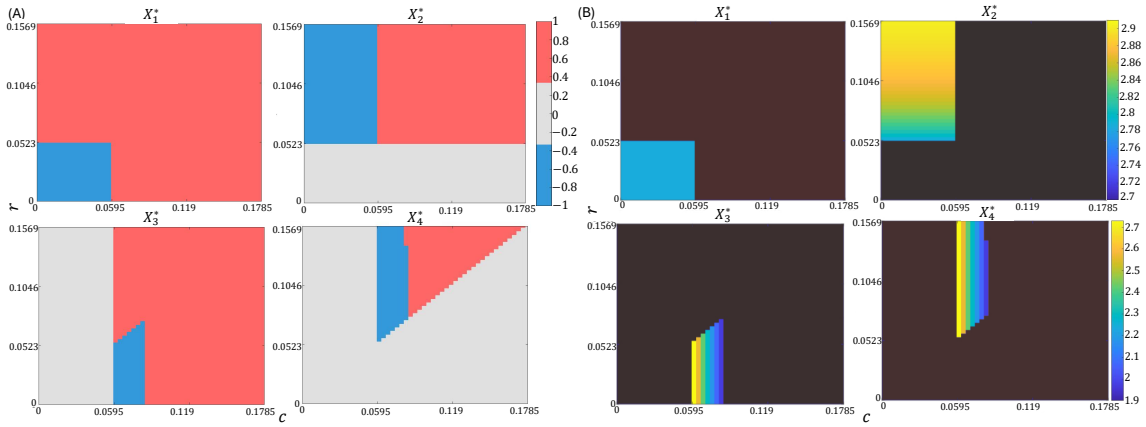

Figure 5.7: **Bifurcation example with $M_1^* < 3$.** (A) shows the bifurcation diagrams for X_1^* (top left corner), X_2^* (top right corner), X_3^* (bottom left corner), and X_4^* (bottom right corner), using the parameter set in the second column of Table 5.6. For this example, $r^* = 0.0523$ and $c^* = 0.0595$. The horizontal and vertical axes represent the values of c and r, respectively. The value represents the stability of the equilibria, with 1 (red) meaning unstable, -1 (blue) meaning locally asymptotically stable and 0 (grey) meaning no equilibria. (B) shows the value of M^* for each equilibrium type in the stable regions in (A). The horizontal and vertical axes represent the values of c and r, respectively. The colour bar only represents the value of M^* in the stable regions and the black area indicates no corresponding stable equilibrium.

Fig. 5.7 shows the bifurcation diagram for model (2.2.5) with bifurcation parameters c and r (namely, r_C and r_R) and parameter values listed in the second column of Table 5.6, except for r_C and r_R. Due to Proposition 5.2.1 and Corollary 5.2.6, $X_1^* = (M_1^*, 0, N_1^*, 0)$ always exists and it is locally asymptotically stable when $0 \leqslant r < r^*$ and $0 \leqslant c < c^*$ and unstable when $r > r^*$ or $c > c^*$. The dynamics is observed in Fig. 5.7A and we find that X_2^* only exists when $r > r^*$, and it is locally asymptotically stable when $0 \leqslant c < c^*$ and unstable when $c > c^*$. X_3^* only exists when $c > c^*$ and X_4^* only exists when $c > 1.138r$ and $c > c^*$. Moreover, X_3^* is locally asymptotically stable when $c \in [c^*, c^* + 0.0226]$ and $r < 0.879c$, and X_4^* is locally asymptotically stable when $c \in [c^*, c^* + 0.0226]$ and $r > 0.879c$. Hence, when $0 \leqslant c < c^*$, a patient's situation could change from regular status (i.e., X_1^*) to the worst case (i.e., X_2^*) as r_R increases (namely, as r increases). On the other hand, when $0 \leqslant r < r^*$, a patient's situation could change from regular status to the

best case (i.e., X_3^*) as r_C increases (namely as c increases). Additionally, when c is slightly higher than c^*, a patient's situation may get worse as r_R increases (namely, change from X_3^* to X_4^*).

Next, in Fig. 5.7B, we further analyze how the M^* value of each equilibrium type changes as r and c change, in the regions where the equilibrium is locally asymptotically stable. For type 1 equilibrium, fixing either r or c has no effect on the value of M^*. For type 2 equilibrium, fixing c leads to an increase in M^* (from 2.789 to 2.903) as r increases. This result suggests that decreasing r_R improves the patient's long term behaviour from high M protein to low M protein status. For type 3 equilibrium, fixing r leads to a decreasing value of M^* as c increases. This result indicates that increasing r_C further improves the patient's long term behaviour by reducing the amount of M protein. For type 4 equilibrium, fixing r leads to a decreasing value of M^* as c increases, whereas fixing c leads to an insignificant increase in M^* as r increases. This result suggests that, when patients are in the certain status X_4^*, increasing r_C improves the patient's long term behaviour by reducing the amount of M protein.

Next, we use the Matlab package *matcont* to generate the bifurcation diagrams, Fig. 5.8, for model (2.2.5) at different values of r_R with bifurcation parameter c (i.e., r_C) and other parameter values being listed in the second column of Table 5.6. From Fig. 5.8, we find the following bifurcations:

(i) For $r = 0.04$ and $c \in [0, 0.1]$, we have a transcritical bifurcation at $c \approx 0.0595$ from X_1^* to X_3^* and a Hopf bifurcation at $c \approx 0.08538$.

(ii) For $r = 0.06$ and $c \in [0, 0.1]$, we have a transcritical bifurcation at $c \approx 0.0595$ from X_2^* to X_4^* and a transcritical bifurcation at $c \approx 0.0643$ from X_4^* to X_3^*. Then, at $c \approx 0.0821$, we have a Hopf bifurcation.

(iii) For $r = 0.1$ and $c \in [0, 0.1]$, we have a transcritical bifurcation at $c \approx 0.0579$

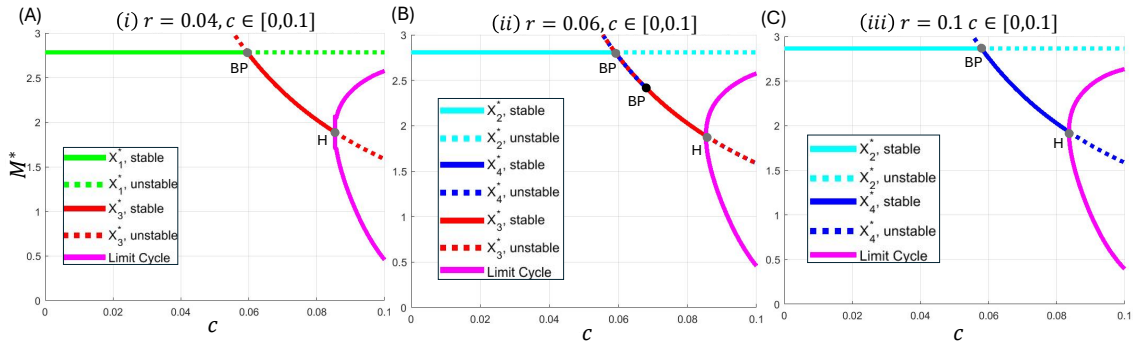

Figure 5.8: **Bifurcation diagrams for model** (2.2.5) **with** $M_1^* < 3$**.** The bifurcation diagrams of model (2.2.5) with bifurcation parameter c for cases: (A) $r = 0.04$, (B) $r = 0.06$ and (C) $r = 0.1$. We used the parameter values in the second column of Table 5.6, except for r_C and r_R. The horizontal and vertical axes represent the value of the bifurcation parameter c and the value of the M^* component of the corresponding equilibrium with unit g/dL, respectively. The green, cyan, red and blue curves represents the M^* value for the X_1^*, X_2^*, X_3^* and X_4^* equilibrium, respectively; the solid and dotted line styles represent the locally stable and unstable regions, respectively. The gray circle marked as BP represents the branch point at (A) $c \approx 0.0595$, (B) $c \approx 0.05913$, and (C) $c \approx 0.0579$. The black circle in (B), marked as BP, represents the branch point at $c \approx 0.06822$. The gray circle marked as H represents the Hopf bifurcation occurring at (A) $c \approx 0.08538$, (B) $c \approx 0.08538$, and (C) $c \approx 0.08365$. The pink curves display the generated limit cycle after the bifurcation point H, where the vertical distance between the two pink curves represents the amplitude of the limit cycle.

from X_2^* to X_4^*, and then we have a hopf bifurcation at $c \approx 0.08365$.

Combining the findings from Figs. 5.7 and 5.8, it suggests that:

(i) when fixing $r < r^* = 0.0523$, the model dynamics shift from a locally stable X_1^* to a locally stable X_3^* to an oscillation pattern, as r_C increases.

(ii) when fixing $0.0523 \leqslant r \leqslant 0.0753$, the model dynamics shift from a locally stable X_2^* to a locally stable X_4^* to a locally stable X_3^* to an oscillation pattern, as r_C increases.

(iii) when fixing $r > 0.0753$, the model dynamics shift from a locally stable X_2^* to a locally stable X_4^* to an oscillation pattern, as r_C increases.

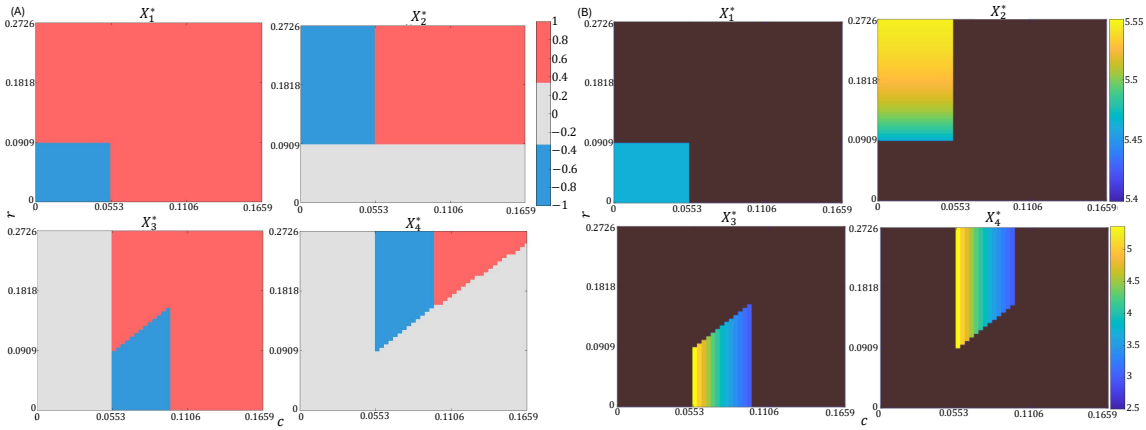

Figure 5.9: **Bifurcation example with $M_1^* > 3$.** (A) shows the bifurcation diagram for X_1^* (top left corner), X_2^* (top right corner), X_3^* (bottom left corner), and X_4^* (bottom right corner), using the parameter set in the third column of Table 5.6. For this example, we have $r^* = 0.0909$ and $c^* = 0.0553$. All symbols and definitions (axes and values for stability) are the same as in Fig. 5.7A. (B) shows the value of M^* for each equilibrium type in the stable regions in (A). The horizontal and vertical axes represent the values of c and r, respectively. All symbols and definitions (axes and colour bar) are the same as in Fig. 5.7B.

Fig. 5.9A shows the bifurcation diagram for model (2.2.5) with bifurcation parameters c and r and parameter values listed in the third column of Table 5.6, except for r_C and r_R. The equilibria X_1^* and X_2^* have a similar behaviour to those of Fig.

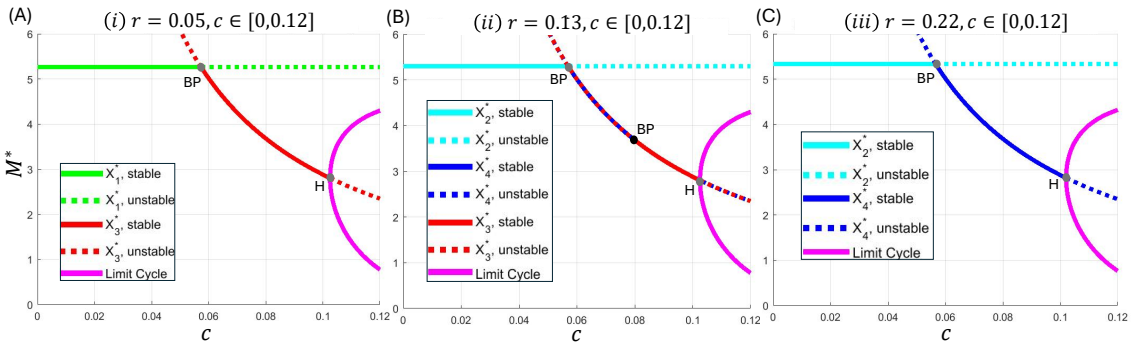

Figure 5.10: **Bifurcation diagrams for model** (2.2.5) **with** $M_1^* > 3$**.** The bifurcation diagrams of model (2.2.5) with bifurcation parameter c for cases: (A) $r = 0.05$, (B) $r = 0.13$ and (C) $r = 0.22$. We used the parameter values in the third column of Table 5.6, except for r_C and r_R. All symbols and definitions (axes, curves, and bifurcation types) are the same as in Fig. 5.8. The gray circle marked as BP represents the branch point at (A) $c \approx 0.0573$, (B) $c \approx 0.0573$, and (C) $c \approx 0.05697$. The black circle in (B), marked as BP, represents the branch point at $c \approx 0.0805$. The gray circle marked as H represents the Hopf bifurcation occurring at (A) $c \approx 0.1025$, (B) $c \approx 0.1025$, and (C) $c \approx 0.102$.

5.7, except for the different values of r^* and c^*. The equilibria X_3^* and X_4^* have similar behaviours when compared to Fig. 5.7, the differences being mainly the stability region for X_3^* is $c \in [c^*, c^* + 0.0409]$ and $r < 1.47c$ and the stability region for X_4^* is $c \in [c^*, c^* + 0.0409]$ and $r > 1.47c$. We also investigate how the M^* value for each equilibrium type changes as r and c change, in Fig. 5.9B, and we have similar conclusions compared to Fig. 5.7B.

Similar to Fig. 5.8, Fig. 5.10 shows the bifurcation diagrams for model (2.2.5) with $M^* > 3$, and we find that

(i) For $r = 0.05$ and $c \in [0, 0.12]$, we have a transcritical bifurcation at $c \approx 0.0573$ from X_1^* to X_3^* and a Hopf bifurcation at $c \approx 0.1025$.

(ii) For $r = 0.13$ and $c \in [0, 0.12]$, we have a transcritical bifurcation at $c \approx 0.05697$ from X_2^* to X_4^*, then a transcritical bifurcation at $c \approx 0.0805$ from X_4^* to X_3^*. We then have a Hopf bifurcation at $c \approx 0.1025$.

(iii) For $r = 0.22$ and $c \in [0, 0.12]$, we have a transcritical bifurcation at $c \approx 0.0566$

from X_2^* to X_4^* and a Hopf bifurcation at $c \approx 0.102$.

Hence, we have a similar transition of model dynamics as Fig. 5.8.

We can conclude for these two examples that for a low homeostasis rate of CTLs (r_C), we need a low homeostasis rate of T_{reg}s (r_R) to avoid the worst case X_2^* as the long term behaviour. For a medium homeostasis rate of CTLs, we either have the best case X_3^* for a low r_R or the uncertain case X_4^* for a high r_R. If the homeostasis rate of CTLs is high, the most likely outcome for a patient is oscillatory behaviour. Furthermore, when we consider the regions of stability for the equilibrium X_2^*, X_3^*, and X_4^*, fixing the homeostasis rate of CTLs leads to an increasing M protein as r_R increases when the patient is in the worst case, i.e., type 2 equilibrium, while fixing the homeostasis rate of T_{reg}s leads to a decreasing M protein as r_C increases when the patient is in the best or uncertain case, i.e., type 3 or type 4 equilibrium. These two examples show that depending on a patient's long term disease progression, changing the homeostasis rate of either CTLs or T_{reg}s can impact the long behaviour of patients by changing the M protein level.

6

Application to CAR-T Cell Treatment

The goal of this chapter is to apply both the general model (2.1.6) and the simplified model (2.2.6) to the treatment of CAR-T cells, using the experimental data from (37), by splitting the data into two groups: remission and relapse. We define the remission group as the patients whose M protein level at the end of experiment is less than the M protein level right after CAR-T cell treatment, and define the relapse group as the patients whose M protein level at the end of experiment is greater than the M protein level right after CAR-T cell treatment. We apply the evolutionary algorithm to both the general model (2.1.6) and the simplified model (2.2.6) to find the best fitting parameter sets for these two groups (i.e., the parameter values under the CAR-T cell treatment). We will then (i) use the Akaike Information Criterion (AIC) to select the most plausible model, (ii) construct parameter distributions to identify potential biomarkers, (iii) perform global sensitivity analysis to identify potential treatment targets for patients in remission and relapse, (iv) study how to improve the relapse issue after CAR-T cell treatment by combining with anti-PD-1, elotuzumab or daratumumab for the general model (2.1.6) and the simplified

model (2.2.6) and (v) perform identifiability analysis to determine the uniqueness of parameter values in model calibration for both models.

6.1 Experimental Data

Chimeric antigen receptor (CAR)-T cell treatment involves enhancing T cells with synthetic receptors and infusing them back into a patient to help train immune cells to recognize and kill tumour cells more effectively (52). In addition, the synthetic receptors can be used to bind to specific antigens on tumour cells so CAR-T cells can also kill tumour cells (36). For MM, there are some antigens used for CAR-T cell treatment such as B cell maturation antigen (BCMA), expressed on plasma cells and myeloma cells (41), and CD38, expressed on myeloma cells (40). BCMA-targeted CAR-T cells have shown great effect for those patients for which other treatments fail (41) and anti-CD38 CAR-T cells have a strong effect against myeloma cells with high expression of CD38 (40). Additionally, anti-CD19 CAR-T cells and anti-PD-1 have shown to be an effective treatment for relapsed B-cell acute lymphoblastic leukemia (32). Thus, we consider combination therapy with CAR-T cells for the treatment of MM.

In (37), the authors made use of bispecific BM38 (BMCA+CD38) CAR-T cells on 23 patients with refractory or relapsed MM. These patients are marked by numbers from 1 to 23. Patients were divided into different CAR-T cell doses of 0.5×10^6, 1×10^6, 2×10^6, 3×10^6 or 4×10^6 cells/kg, with patients labeled 1 and 2 receiving dose 0.5×10^6 cells/kg, patients labeled 3 and 4 receiving dose 1×10^6 cells/kg, patients 5-7 receiving dose 2×10^6 cells/kg, patients 8-10 receiving dose 3×10^6 cells/kg, and patients 11-23 receiving dose 4×10^6 cells/kg. CAR-T cells were infused only once at the start of the study. Some patients received a second dose of CAR-T cells in a follow-up appointment and due to limitations in the general model (2.1.6) and

the simplified model (2.2.6), we cannot apply this second dose within the models. Thus, we assume all patients have CAR-T cells infused only once at the start of the experiment. Patient responses were measured on day 14 ± 2 and 28 ± 2 and on follow-up sessions, which were monthly for the first 6 months and every 3 months afterwards, up to 2 years. Bone marrow was collected from patients to measure both MM burden, which includes the immunoglobulins IgG, IgA, IgM, IgE, IgD, LAM and KAP, and BCMA and CD38 expression on MM cells. The sum of all these immunoglobulins represent the M protein level for a general patient. Since immunoglobulin (i.e., M protein) can be measured for MM burden and acts as its surrogate, we use their data to study the progression of MM under CAR-T cell treatment by using the general model (2.1.6) and the simplified model (2.2.6).

The authors collected data for 19 of these patients on the concentration of the immunoglobulins IgG, IgA, IgM, KAP and LAM over several months, measured as time since CAR-T cell infusion. For simplicity, we assume that the infusion of CAR-T cells only changes the reaction rates in the general model (2.1.6) and the simplified model (2.2.6), instead of the system networks. We then calibrate the general model (2.1.6) and the simplified model (2.2.6) to the total amount of immunoglobulin (i.e., M protein) for patients in the remission and relapse groups in (37).

We extracted the data for each patient in (37) using the Matlab package *grabit*. Since M protein can be any of the types of immunoglobulin (21; 25; 34; 39) measured in (37), we add up the amount of all immunoglobulin for each patient to obtain the amount of M protein for each patient and normalize the data by dividing by the value at $t = 0$ months. We further nondimensionalize the time component of the data by using $\tau = 1\ month = 30\ days$ as defined in Eq. (2.1.5).

Our focus is on two trends in the data, either a good response or a weak response to the CAR-T cell treatment. Patients labeled 1, 2, 3, 8, 11, 12, 13, 15, 17, 18 and 20 have a good response to treatment, as most of their M protein data are

below 1 across the time scale $[0, 18]$ months and we call this group of data "Group I". Furthermore, patients labeled 4, 5, 7, 14, 16 and 21 have a weak response to treatment as their M protein data increases and stays above 1 after some time. We exclude patient 21, as their data lacked a point at $t = 0$ months, and call this group of data "Group II". Fig. 6.1 shows the final M protein data for Groups I and II that will be used for the model calibration of the general model (2.1.6) and the simplified model (2.2.6).

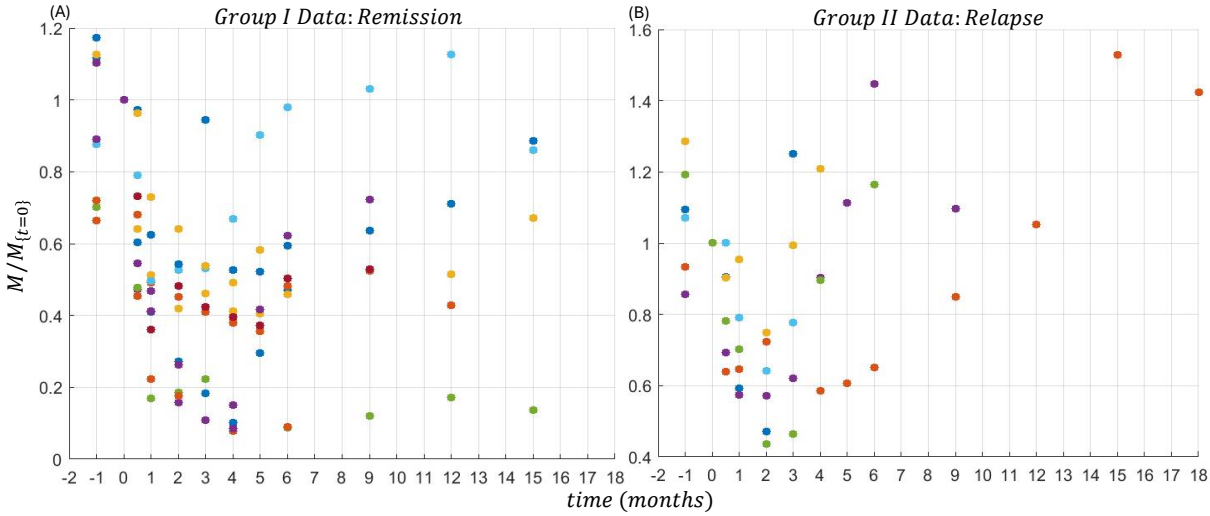

Figure 6.1: **M protein data in (37).** (A) and (B) display the time series data for M protein for Group I and Group II, respectively. The horizontal and vertical axes represent the time with unit month and M protein normalized by initial condition, respectively. The different dot colours represent the data for different patients. The data point at $t = -1$ months represent the patient's M protein concentration at enrollment of the study.

6.2 Model Calibration

In this section, we calibrate the non-dimensional general model (2.1.6) and simplified model (2.2.6) to the data in Group I and Group II by using the evolutionary algorithm. We then study the distribution of parameter sets with numerical solution close to the data to select potential biomarkers to distinguish Groups I and II.

Finally, we will apply AIC to study which model is more plausible for Groups I and II.

For the initial conditions, we used the mean of the ranges in Table 4.1 for $T_C(t)$, $N(t)$ and $T_R(t)$ (namely, $T_C(0) = 4.64 \times 10^{-2}$ g/dL, $N(0) = 2.27 \times 10^{-2}$ g/dL and $T_R(0) = 4.2 \times 10^{-3}$ g/dL). For $M(t)$, we use $M(0) = 1.5$ g/dL, which is close to the median serum M protein in Table 1 in (37).

Given there is one type of observation for each patient (namely, M protein), we simplify Eq. (3.1.3) and obtain the residual sum of squares (RSS) function as

$$RSS(P) = \sum_{p=1}^{n_e} \sum_{i=1}^{n_i^p} \omega_i^p (y_p(t_i) - \tilde{y}^p(t_i, P))^2, \tag{6.2.1}$$

where n_e is the number of patients, n_i^p is the number of observations for patient p, $1 \leqslant p \leqslant n_e$, $y_p(t_i)$ is the experimental data at time t_i for patient p, $\tilde{y}^p(t_i, P)$ is the predicted output at time t_i for the parameter set P and ω_i^p is the associated weight for patient p at time t_i. We use Eq. (6.2.1) to calibrate the general model (2.1.6) and the simplified model (2.2.6) to all M protein data shown in Fig. 6.1. For Group I, we take $\omega_i^p = 1$ for all times t and for Group II, we take $\omega_i^p = 3$ for $t = 12,\ 15$ and 18 months and $\omega_i^p = 1$ otherwise to obtain a good fitting result. For the evolutionary algorithm, we used 100 generations with 50 parents and 10 children each, with micro-mutation rate $\lambda = 0.25$ and effective energy $\beta = 2$. For Group I, we used a macro-mutation rate of $\mu = 0.5$ for model (2.1.6) and $\mu = 0.2$ for model (2.2.6) and for Group II, we used a macro-mutation rate of $\mu = 0.3$ for model (2.1.6) and $\mu = 0.5$ for model (2.2.6). Finally, for the next generation of parents, 10% (i.e., 5) came from the parents in the current generation and the remaining 90% (i.e., 45) came from the children.

We define the best fitting parameter set P_{best} as in Eq. (3.1.2). We then generate cohort virtual patients for both Groups I and II by selecting parameter sets $P \in \tilde{P} =$

$\{P|RSS(P) < 1.2RSS(P_{best})\}$. Tables 6.1 and 6.2 show the best fitting parameter set P_{best} for the general model (2.1.6) and the simplified model (2.2.6), respectively, for Groups I and II. Fig. 6.2 displays the fitting results from P_{best} and $\tilde{P}$.

For the solutions from P_{best} related to Group I (i.e., the black curves in Figs. 6.2A and 6.2C), both the general model (2.1.6) and the simplified model (2.2.6) have a decreasing trend near $t = 0$ months and an increasing trend after $t = 2$ months, but the M protein of model (2.1.6) flattens out while the M protein of model (2.2.6) slowly increases. For the solutions from $\tilde{P}$ related to Group I (i.e., the multi-coloured curves in Figs. 6.2A and 6.2C), some of the solutions for model (2.1.6) flatten out right after a decreasing trend and some initially have an increasing trend for a brief amount of time before going in a decreasing trend.

For the solutions from P_{best} related to Group II (i.e., the black curves in Figs. 6.2B and 6.2D), we have a decreasing trend near $t = 0$ months and a flattening trend near $t = 18$ months for both models. The best fits differ in how the M protein grows after $t = 2$ months, as for model (2.1.6), M protein increases fast but has a secondary increasing trend near $t = 12$ months, whereas for model (2.2.6), M protein has a slow increasing trend until $t = 8$ months where the M protein starts to have a faster increasing trend. For the solutions from $\tilde{P}$ related to Group II (i.e., the multi-coloured curves in Figs. 6.2B and 6.2D), they behave similarly to the solution using P_{best} for model (2.1.6) and the others have an increasing trend between $t = 4$ months and $t = 6$ months which then flatten out by $t = 8$ months for model (2.2.6). We find that model (2.1.6) fits the early period better as it captures the decreasing trend in the early period, whereas model (2.2.6) fits the later period better as it smoothly increases as time increases to 18 months (i.e., no sudden increasing trend). We will further demonstrate this finding by using AIC.

To analyse the distribution of $\tilde{P}$, we generate boxplots for each parameter in Figs. 6.3 and 6.4 for the general model (2.1.6) and the simplified model (2.2.6),

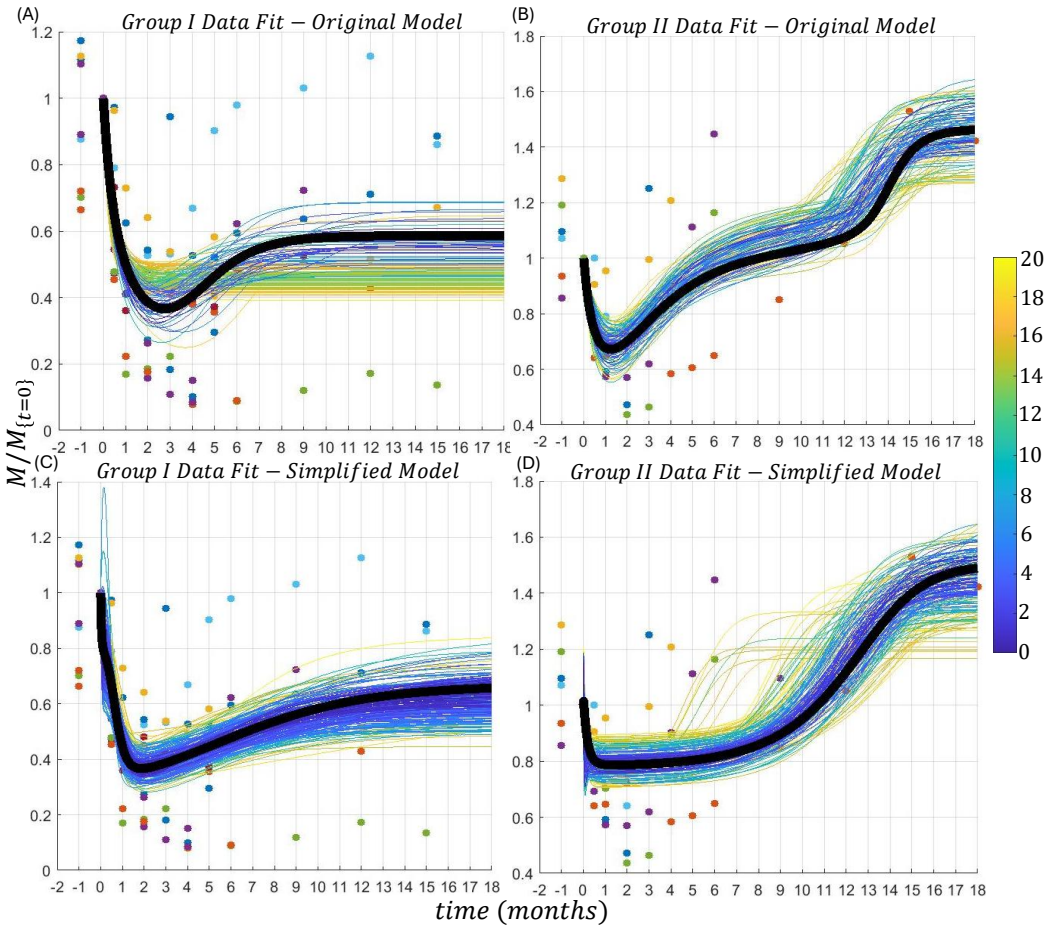

Figure 6.2: **Fitting result for the cohort virtual patients.** (A) and (B) display the fitting results for Group I and Group II for model (2.1.6), respectively. (C) and (D) displays the fitting result for Group I and Group II for model (2.2.6), respectively. The horizontal and vertical axes represent the time with unit month and M protein normalized by initial condition, respectively. The black curve displays the solution using the best fit parameter set P_{best} and the thin multi-coloured curves are solutions using the parameter sets $\tilde{P} - \{P_{best}\}$, where the colour indicates the percentage difference $100 \times (RSS(P) - RSS(P_{best}))/RSS(P_{best})$, $P \in \tilde{P} - \{P_{best}\}$ shown by the colour bar.

respectively, and compare how the ranges differ between Group I and Group II to identify potential biomarkers to identify a patient in Group I (namely, remission after CAR-T cell treatment) and II (namely, relapse after CAR-T cell treatment).

From Fig. 6.3, we find that

(i) The distribution of parameters a_{NM}, b_{NM}, r_C, K_C, δ_C, a_{MC}, b_{MC}, r_N, b_{CN}, r_R and a_{MR} are relatively higher for Group I. This indicates that a patient with

Table 6.1: P_{best} **of model** (2.1.6) **for Groups I and II.** The first column lists the parameter. The second and third columns display the non-dimensional parameter values for the best fitting result P_{best} for Group I and Group II, respectively. The last row displays the $RSS(P_{best})$ of model (2.1.6) for Groups I and II.

Parameter	Group I	Group II
s_M	0.0183	0.0361
r_M	0.9269	2.021
K_M	0.4236	1.2099
δ_M	0.2218	0.8335
a_{NM}	4.2264	0.4704
b_{NM}	0.4854	0.0373
a_{CM}	10.6939	8.5048
b_{CM}	4.2702	3.7568
a_{CNM}	9.5447	3.9026
a_{MM}	0.1071	0.028
b_{MM}	1.8963	0.3407
a_{RM}	0.2334	0.9664
b_{RM}	0.1177	0.3722
r_C	3.619	0.1856
K_C	0.5359	0.153
δ_C	6.3106	0.662
a_{MC}	4.5084	1.4795
b_{MC}	3.4661	1.9318
a_{NC}	0.8499	1.821
b_{NC}	1.6712	0.18
s_N	0.1083	0.0056
r_N	2.9626	1.9605
K_N	1.0531	1.1215
δ_N	4.1563	7.6169
a_{CN}	21.8732	33.6013
b_{CN}	0.233	0.0675
r_R	3.0302	3.3671
K_R	0.0759	0.17
δ_R	18.634	45.0742
a_{MR}	3.5658	0.3462
b_{MR}	1.1851	4.2615
RSS	4.101	1.534

a relatively higher loss rate of M protein by NK cells, or threshold for loss rate of M protein by NK cells, or homeostasis rate of CTLs, or carrying capacity of CTLs, or death rate of CTLs, or activation rate of CTLs by M protein, or threshold for activation rate of CTLs by M protein, homeostasis rate for NK

Table 6.2: P_{best} **of model** (2.2.6) **for Groups I and II.** The first column lists the parameter. The second and third columns display the non-dimensional parameter values for the best fitting result P_{best} for Group I and Group II, respectively. The last row displays the $RSS(P_{best})$ of model (2.2.6) for Groups I and II.

Parameter	Group I	Group II
s_M	10.3612	4.0118
r_M	2.2617	0.4609
K_M	79.1896	13.38
δ_M	25.6894	1.8251
a_{NM}	1.2661	6.6964
a_{CM}	5.5989	1.125
r_C	0.2352	2.4978
K_C	1.641	0.3397
a_{MC}	2.7527	4.0658
δ_C	0.7036	2.3193
s_N	2.5429	97.9868
r_N	0.9226	12.5585
K_N	42.2795	0.5248
a_{CN}	11.8440	11.6189
δ_N	1.1391	10.8385
r_R	65.5737	0.1557
K_R	1.5702	14.7969
a_{MR}	3.5912	8.0362
δ_R	2.89	0.2321
RSS	4.052	1.899

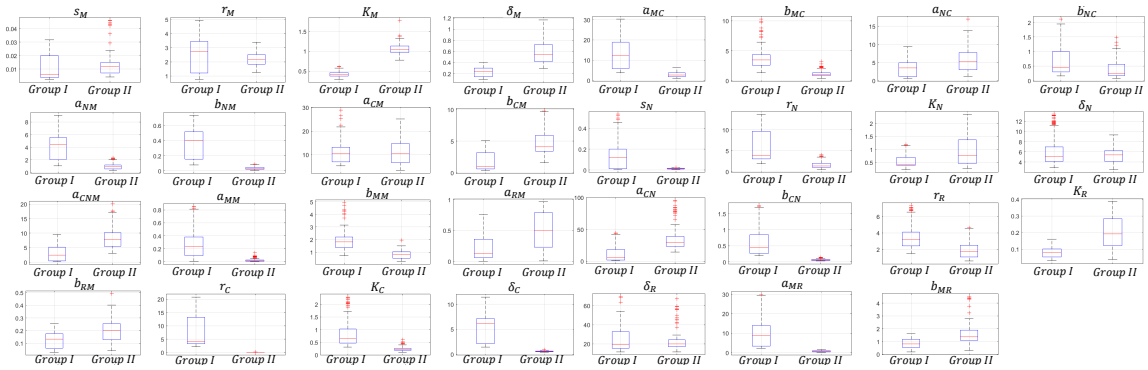

Figure 6.3: **Distributions of $\tilde{P}$ for model** (2.1.6)**.** The first and second boxplots in each subfigure display the distribution of the corresponding parameter of $\tilde{P}$ for model (2.1.6) from Group I and Group II, respectively.

cells, or threshold for activation rate of NK cells by CTLs, or homeostasis rate of T_{reg}s, or activation rate of T_{reg}s by M protein may stay in remission after

CAR-T cell treatment (namely, stays in Group I).

(ii) The distribution of parameters K_M, δ_M, b_{CM}, a_{CNM}, K_N, and a_{CN} were relatively higher in Group II. This indicates that a patient with a relatively carrying capacity of M protein, or higher death rate of M protein, or threshold for increase in loss rate of M protein by CTLs, or killing rate of M protein by cooperation of NK cells and CTLs, or carrying capacity of NK cells, or activation rate of NK cells by CTLs may relapse after CAR-T cell treatment (namely, stays in Group II).

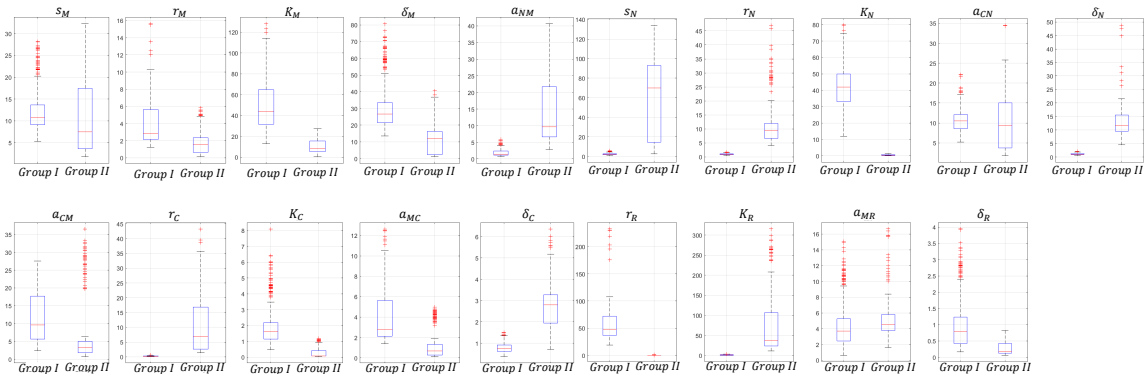

Figure 6.4: **Distributions of $\tilde{P}$ for model** (2.2.6)**.** The first and second boxplots in each subfigure display the distribution of the corresponding parameter of $\tilde{P}$ for model (2.2.6) from Group I and Group II, respectively.

From Fig. 6.4, we find that

(i) The distribution of parameters r_M, K_M, δ_M, a_{CM}, K_C, a_{MC}, K_N, and r_R are relatively higher in Group I. This suggests that a patient with a relatively higher homeostasis rate, carrying capacity, or death rate of M protein, or killing rate of M protein by CTLs, or carrying capacity of CTLs, or activation rate of CTLs by M protein, or carrying capacity of NK cells, or the homeostasis rate of T_{reg}s may stay in remission after CAR-T cell treatment (namely, stays in Group I).

(ii) The distribution of parameters a_{NM}, r_C, δ_C, s_N, r_N, δ_N, and K_R are relatively higher in Group II. This indicates that a patient with relatively higher killing rate of M protein by NK cells, or homeostasis rate of CTLs, or death rate of CTLs, or the carrying capacity of T_{reg}s, or the constant source, homeostasis rate, or death rate of NK cells may relapse after CAR-T cell treatment (namely, stays in Group II).

Comparing the distribution of similar parameters between the general model (2.1.6) and the simplified model (2.2.6) from Figs. 6.3 and 6.4, we find that

(i) The relative relation between Groups I and II of parameters K_C, a_{MC}, and r_R are similar between the general model (2.1.6) and the simplified model (2.2.6). Hence, no matter which model is more plausible, we can still use these three parameters as a biomarker to predict a patient's situation after CAR-T cell treatment.

(ii) The relative relation between Groups I and II of parameters K_M, δ_M, a_{NM}, r_C, δ_C, r_N, and K_N are opposite between the general model (2.1.6) and the simplified model (2.2.6). Thus, when experimental data for measuring any of these seven parameters becomes available, then these seven parameters can be used to identify which model is more plausible.

Next, we apply the AIC method to study which of the general model (2.1.6) or the simplified model (2.2.6) is more plausible for the data in Fig. 6.1. Table 6.3 displays the number of observations, estimated parameters and the $RSS(P_{best})$ for both Groups I and II for the general model (2.1.6) and the simplified model (2.2.6). Both Groups I and II satisfy the condition $K > N/40$, and thus we use the corrected AIC. In particular, we use Eq. (3.3.7) for Group I, since we used $\omega_i^p = 1$ for all times, and Eq. (3.3.8) for Group II, since we used $\omega_i^p = 3$ for $t = 12,\ 15$ and 18 months.

For the Group II data, since we used a weight of 3 at times $t = 12, 15$ and 18

months, the substitution $\sigma_i^p = 1/\sqrt{3}$ for 3 of the σ_i^p's and 1 for the remaining σ_i^p's is applied to Eq. (3.3.8) to obtain

$$2ln(\prod_{p=1}^{n_e}\prod_{i=1}^{n_i^p}\sigma_i^p) = 2ln\left(\frac{1}{\sqrt{27}}\right) = ln\left(\frac{1}{27}\right),$$

and obtain the following AIC for the general model (2.1.6) and the simplified model (2.2.6):

$$AIC = Nln(2\pi) + ln\left(\frac{1}{27}\right) + RSS(P_{best}) + \frac{2KN}{N-K-1}, \tag{6.2.2}$$

where $RSS(P_{best})$ is the RSS of the considered model.

Table 6.3: **Number of observations, parameters and RSS for the general model** (2.1.6) **and the simplified model** (2.2.6)**.** The first column displays the model. The second and third columns represent the number of Group I and Group II observations, respectively. The fourth column displays the number of estimated parameters, namely, the number of parameters add one. The fifth and sixth columns represent the $RSS(P_{best})$ for Group I and Group II, respectively.

Model	Group I Data (N)	Group II Data (N)	Parameters (K)	Group I RSS	Group II RSS
(2.1.6)	95	38	32	4.101	1.534
(2.2.6)	95	38	20	4.052	1.899

Using either Eq. (3.3.7) for Group I data or Eq. (6.2.2) for Group II data and Eq. (3.3.9) for the AIC weight, we generate Table 6.4 to display the final results of the AIC analysis.

Table 6.4: **AIC results for the general model** (2.1.6) **and the simplified model** (2.2.6)**.** The first column displays the model. The second and third (resp. fourth and fifth) columns represent the AIC and AIC weight for the data from Group I (resp. Group II).

Model	Group I AIC	Group I Weight	Group II AIC	Group II Weight
(2.1.6)	69.1058	4.0785×10^{-11}	554.4773	7.49×10^{-87}
(2.2.6)	21.2604	1	157.8547	1

We find that the simplified model (2.2.6) is more plausible for both Group I and Group II, due to it having fewer parameters compared to the general model (2.1.6)

and this agrees with our previous observation about fitting results of the general model (2.1.6) and the simplified model (2.2.6) with respect to Group II data.

6.3 Sensitivity Analysis

In this section, we perform the global sensitivity analysis outlined in (35) (also explained in Chapter 5.3.2) to study how all parameters listed in Table 6.5 affect the M protein concentration at $t = 3,\ 6,\ 9,\ 12,\ 15$ and 18 months for the general model (2.1.6) and the simplified model (2.2.6) only under CAR-T cell treatment. We perform LHS to generate 20000 parameter sets within the ranges in Table 6.5 and compute the PRCCs with p-values of the parameters to the M protein amount. The PRCC results for the general model (2.1.6) and the simplified model (2.2.6) under CAR-T cell monotherapy are shown in Fig. 6.5. The global sensitivity analysis will be used to study: (i) how the parameters of the general model (2.1.6) and the simplified model (2.2.6) under CAR-T cell treatment affect the M protein concentration after infusion, (ii) how the anti-PD-1, elotuzumab and daratumumab monotherapies could potentially affect the M protein value for patients, and (iii) select the parameters for the identifiability analysis.

When considering the PRCCs for model (2.1.6) between Groups I and II (shown in Fig. 6.5A), we find that the sign of the PRCCs do not change across the time scale $[3, 18]$ months and the PRCCs between Groups I and II have the same sign for all times, for the parameters significantly affecting the result (namely, with p-value smaller than 0.05), and the only thing that changes is the magnitude of PRCC across the time interval $[3, 18]$ months. Therefore, these significant parameters have the same effect (namely, positive or negative correlation) on M protein level over time and for all types of patients. However, the effect level by these parameters increases or decreases as time goes on, or is stronger or weaker on patients in Group

Table 6.5: **Parameter ranges for sensitivity analysis of the general model** (2.1.6) **and the simplified model** (2.2.6)**.** The first and fourth columns display the parameters for the general model (2.1.6) and the simplified model (2.2.6), respectively. The second and third (resp. fifth and sixth) columns show the non-dimensional parameter ranges for Groups I and II for model (2.1.6) (resp. (2.2.6)).

Parameter	(2.1.6)-Group I	(2.1.6)-Group II	Parameter	(2.2.6)-Group I	(2.2.6)-Group II
s_M	[0.0023,0.0315]	[0.004,0.0461]	s_M	[5.3511,28.2095]	[1.7762,32.2723]
r_M	[0.7643,4.9325]	[1.2566,3.3817]	r_M	[1.2576,15.6438]	[0.136,5.8372]
K_M	[0.2888,0.6111]	[0.7719,1.7778]	K_M	[12.7112,128.1547]	[0.3922,27.3147]
δ_M	[0.098,0.3969]	[0.297,1.1633]	δ_M	[13.6062,80.7435]	[1.0828,40.5861]
a_{NM}	[1.0661,9.083]	[0.3445,2.327]	a_{NM}	[0.6667,5.8917]	[2.8728,40.672]
a_{CM}	[5.3222,28.8701]	[3.5494,25.1059]	a_{CM}	[2.4681,27.5436]	[0.7445,36.5254]
r_C	[2.1701,20.4862]	[0.0317,0.1856]	r_C	[0.0687,0.62]	[1.4045,43.2527]
K_C	[0.3082,2.2915]	[0.0994,0.5983]	K_C	[0.4691,8.0949]	[0.0297,1.1722]
δ_C	[1.4266,11.446]	[0.3809,0.9008]	δ_C	[0.3671,1.5004]	[0.7116,6.355]
a_{MC}	[3.7692,30.3017]	[1.0173,6.2778]	a_{MC}	[1.3774,12.6422]	[0.122,4.9825]
s_N	[0.0052,0.5339]	[0.0048,0.0271]	s_N	[0.8426,5.6866]	[2.7138,134.3022]
r_N	[1.8399,13.7524]	[0.4873,4.0698]	r_N	[0.495,1.7996]	[4.0617,47.1008]
K_N	[0.2328,1.2083]	[0.2773,2.3503]	K_N	[11.9231,79.8028]	[0.0979,1.3813]
δ_N	[2.9033,13.4082]	[2.5476,9.3554]	δ_N	[0.5345,2.1264]	[4.4816,48.8648]
a_{CN}	[0.9697,44.2166]	[14.4578,95.4063]	a_{CN}	[5.1991,22.2219]	[1.8198,34.5621]
r_R	[1.4935,7.3296]	[0.5841,4.6838]	r_R	[18.7880,233.008]	[0.1093,1.0624]
K_R	[0.0317,0.161]	[0.0392,0.3885]	K_R	[0.3688,3.506]	[11.1514,315.7534]
δ_R	[11.7278,69.7053]	[11.4763,67.3956]	δ_R	[0.1664,3.95]	[0.0587,0.8234]
a_{MR}	[2.2317,29.9832]	[0.1446,1.6433]	a_{MR}	[0.6155,15.0984]	[1.6179,16.6669]
b_{NM}	[0.0777,0.7374]	[0.008,0.0919]			
b_{CM}	[0.3848,5.0827]	[1.5734,9.7506]			
a_{CNM}	[0.2077,9.5447]	[3.0716,20.1037]			
a_{MM}	[0.0053,0.8573]	[0.0002,0.14]			
b_{MM}	[0.722,4.9264]	[0.2846,1.9673]			
a_{RM}	[0.0018,0.7609]	[0.0035,0.9664]			
b_{RM}	[0.0287,0.2531]	[0.0416,0.4919]			
b_{MC}	[1.2864,10.2855]	[0.3947,3.2657]			
a_{NC}	[0.6601,9.3906]	[1.2595,16.9552]			
b_{NC}	[0.1659,2.1151]	[0.0786,1.4897]			
b_{CN}	[0.194,1.7527]	[0.0251,0.1459]			
b_{MR}	[0.1719,1.6069]	[0.3033,4.5247]			

II. For instance, δ_M, a_{NM}, a_{NC} and r_N have stronger negative effect on Group II than on Group I, but the effect strength of δ_M and a_{NM} decreases and the effect strength of a_{NC} and r_N increases as time goes on. Hence, increasing one of $\delta_M,\ a_{NM},\ a_{NC}$, or r_N could efficiently reduce the M protein level and hence reduce the relapse for patients in Group II, but δ_M and a_{NM} work in a short time period while a_{NC} and r_N work in a long time period. On the other hand, $r_M,\ K_M,\ \delta_C,\ s_M,\ b_{NC}$ and δ_N

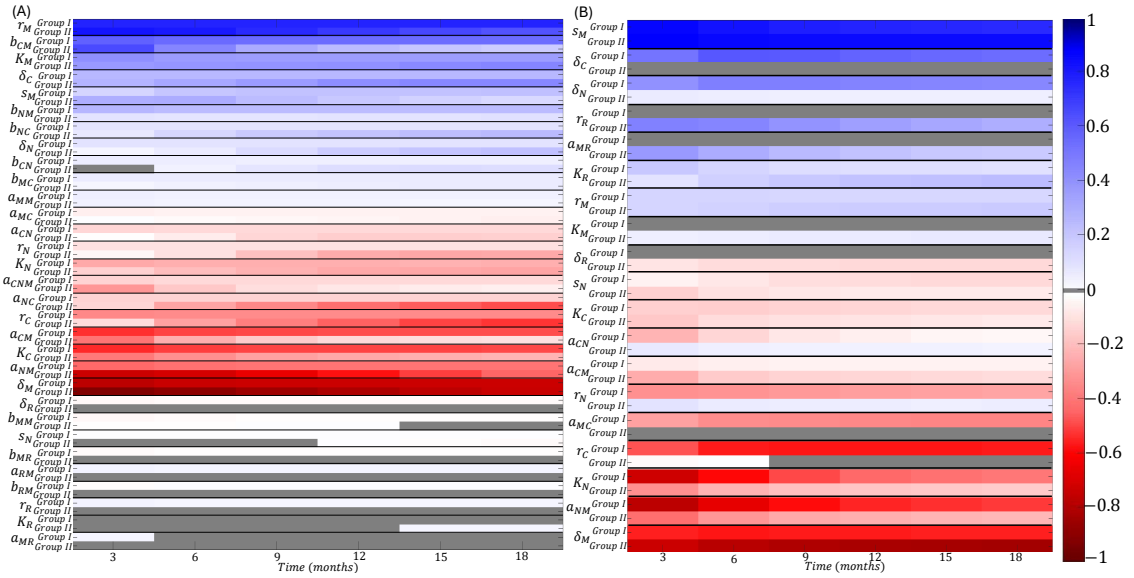

Figure 6.5: **Heatmap of PRCCs for the general model** (2.1.6) **and the simplified model** (2.2.6) **with respect to M protein amount.** (A) (resp. (B)) displays the PRCC values of the parameters of model (2.1.6) (resp. model (2.2.6)) in Table 6.5 for the M protein values at $t = 3,\ 6,\ 9,\ 12,\ 15$, and 18 months, from left to right columns, for model (2.1.6) (resp. model (2.2.6)) under Group I and Group II. The vertical axis represents the parameters, where each pair of rows represents the PRCC of the parameter under Group I and Group II. The horizontal axis displays the time in months. The colour bar represents the PRCC value, with the gray colour representing the parameter with p-value larger than 0.05.

have strong positive effect on both groups, but only the effect strength on Group II changes as time goes on. Notice that r_M and s_M have stronger effect on Group I than on Group II, suggesting increases in r_M or s_M may quickly aggravate the illness for patients in Group I. Additionally, the effect strength of r_M and s_M decreases and the effect strength of $K_M,\ \delta_C,\ b_{NC}$, and δ_N increases as time goes on for Group II. Hence, in Group II, patients with a higher r_M or s_M may have their disease state worsen in a short time period, whereas patients with a higher $K_M,\ \delta_C,\ b_{NC}$ or δ_N may have their disease state worsen in a long time period.

Among the significant parameters mentioned above, only a_{NC} and r_N relate to the treatment parameters, namely, a_{NC} can be changed by F_q and r_N can be changed by F_e. Hence, a stronger anti-PD-1 (i.e., larger F_q) or a stronger elotuzumab (i.e., larger F_e) could mitigate the relapse.

When considering the PRCCs for model (2.2.6) between Groups I and II (shown in Fig. 6.5B), we find the sign of the PRCCs do not change across the time scale $[3, 18]$ months, with the only thing that changing is the magnitude of PRCC across the time interval $[3, 18]$ months. Some parameters affect the M protein level for both Groups I and II the same way (namely, positive or negative correlation) but their effect strengths over time differ. For instance, the parameters s_M, K_R, and r_M have a positive effect on Groups I and II. The effect strengths of s_M and r_M do not change significantly over time but they have a slightly stronger effect on Group II. This indicates that increasing either s_M or r_M can increase the M protein amount for either type of patient, but with more of an effect on a patient in Group II. The parameter K_R has its effect strength, as time goes on, increase for Group II and decrease for Group I. Hence, for a patient in Group I, a higher K_R can worsen their condition, in a short time period, with the opposite time effect seen for a patient in Group II. On the other hand, the parameters δ_M, a_{NM}, K_N, a_{CM}, K_C, and s_N have a negative effect on both Groups I and II, with a_{NM}, K_N, K_C, and s_N having a relatively stronger negative effect on Group I while δ_M and a_{CM} have a relatively stronger negative effect on Group II. This suggests increasing one of a_{NM}, K_N, K_C, s_N, δ_M or a_{CM} can decrease the M protein level, but a_{NM}, K_N, K_C and s_N have a stronger effect on a patient in Group I whereas δ_M and a_{CM} have a stronger effect on a patient in Group II. Additionally, the effect strengths of K_N and K_C decrease, as time goes on, for both Groups I and II. This suggests increasing either K_C or K_N decreases the M protein level of either type of patient for a short period of time.

However, there are parameters that significantly affect only one of the groups. For instance, the parameters δ_C, δ_N, r_C, and a_{MC} significantly affect only Group I, with δ_C and δ_N with a positive effect and r_C and a_{MC} with a negative effect. Furthermore, the effect strengths of δ_C, δ_N, r_C, and a_{MC} increase as time goes on. Hence, increasing r_C or a_{MC} could reduce the M protein level for a patient in Group

I, with the effect lasting for a long time period, while decreasing δ_C or δ_N could reduce the M protein level for a patient in Group I, with the effect working for a long time period. On the other hand, the parameters r_R, a_{MR}, K_M, δ_R significantly affect only Group II, with r_R, K_M, and a_{MR} having a positive effect and δ_R having a negative effect. Furthermore, as time goes on, the effect strengths of r_R and a_{MR} decrease and the effect strengths of K_M and δ_R increase. Thus, decreasing one of r_R, a_{MR}, or K_M could reduce the M protein level and hence reduce the relapse for a patient in Group II, with the effect of r_R and a_{MR} lasting over a short period of time and the effect of K_M working over a long period of time. Additionally, increasing δ_R could reduce the M protein level and reduce relapse in a patient in Group II, with the effect lasting over a long time period.

The parameters r_N and a_{CN} affect Groups I and II differently, namely, r_N and a_{CN} have a negative effect on Group I and a positive effect on Group II, with their effects stronger for Group I compared to Group II. The effect strengths of r_N and a_{CN} for both group decrease as time goes on, indicating that increasing r_N or a_{CN} can reduce the M protein level for a patient in Group I, whereas decreasing r_N or a_{CN} can reduce the M protein level for a patient in Group II, with the effect working in a short time period for both groups.

Among the significant parameters mentioned above, only r_C, a_{MC}, r_N, a_{CN}, r_R, and a_{MR} relate to one of the treatment parameters F_q, F_e, or F_d. In particular, r_C and a_{MC} can be changed by F_q, r_N and a_{CN} can be changed by F_e and r_R and a_{MR} can be changed by F_d. The parameters r_C and a_{MC} have a negative effect on Group I only and hence, an extra treatment of anti-PD-1 (namely, a larger value of F_q) can benefit a patient in Group I (i.e., remission). The parameters r_N and a_{CN} have a negative effect on Group I and a positive effect for Group II. Thus, we can suggest that an extra treatment of elotuzumab (namely, a larger value of F_e) could be beneficial to a patient in Group I but not to a patient in Group II (i.e.,

relapse). Finally, the parameters r_R and a_{MR} have a positive effect on Group II only, indicating that an extra treatment of daratumumab could be effective at reducing the relapse problem seen with patients in Group II.

Thus, a stronger anti-PD-1 (i.e., larger F_q) or a stronger elotuzumab (i.e., larger F_e) could be effective on a patient in Group I, while a stronger daratumumab (i.e., smaller F_d) or a weaker elotuzumab (i.e., smaller F_e) could mitigate the relapse for patients in Group II.

For identifiability analysis, we select parameters that are significant to the M protein level. For model (2.1.6), combining our results and the identifiability done in (19), the parameters r_M, δ_M, a_{NM}, a_{CM}, r_C, δ_C, r_N, and δ_N will be considered for identifiability analysis for both Groups I and II. For model (2.2.6), the parameters s_M, δ_M ,a_{NM}, r_C, δ_C, K_N, a_{CN}, δ_N and r_R will be considered for identifiability analysis for both Groups I and II.

Comparing similar parameters between the general model (2.1.6) and the simplified model (2.2.6), the parameters K_M, r_C, a_{MC}, δ_C, s_N, r_N, a_{CN}, r_R, K_R, a_{MR} and δ_R have different correlation to the M protein level. Thus, these eleven parameters can be used to further identify which model is more plausible.

6.4 Model Prediction and Treatment Design

In this section, we study how the combination therapy between CAR-T cell treatment and one of anti-PD-1, elotuzumab or daratumumab treatment can be used to improve the relapse issue for patients in Group II, namely, $\tilde{P}$ for the general model (2.1.6) and the simplified model (2.2.6) under Group II. Recall that F_d, F_e and F_q represent the treatment effects of daratumumab, elotuzumab and anti-PD-1, respectively. Since the experimental data in (37) was measured after all patients were given CAR-T cells, we set that the CAR-T cell treatment is always there and is only given at the

initial time and then patients were administered an extra treatment from one of the anti-PD-1, elotuzumab or daratumumab in the following treatment schedules:

(S1): Anti-PD-1 with $F_q = 5$, elotuzumab with $F_e = 5$, or daratumumab with $F_d = 0.1$ is only given in [0,1] months.

(S2): Anti-PD-1 with $F_q = 3$, elotuzumab with $F_e = 3$, or daratumumab with $F_d = 0.55$ is only given in [0,2] months.

(S3): Anti-PD-1 with $F_q = 2.3$, elotuzumab with $F_e = 2.3$, or daratumumab with $F_d = 0.7$ is only given in [0,3] months.

(S4): Anti-PD-1 with $F_q = 2$, elotuzumab with $F_e = 2$, or daratumumab with $F_d = 0.775$ is only given in [0,4] months.

(S5): Anti-PD-1 with $F_q = 1.7$, elotuzumab with $F_e = 1.7$, or daratumumab with $F_d = 0.85$ is only given in [0,6] months.

(S6): Anti-PD-1 with $F_q = 5$, elotuzumab with $F_e = 5$, or daratumumab with $F_d = 0.1$ is only given in [0,6] months.

(S7): Anti-PD-1 with $F_q = 3$, elotuzumab with $F_e = 3$, or daratumumab with $F_d = 0.55$ is only given in [0,1] months and [6,7] months.

(S8): Anti-PD-1 with $F_q = 1.7$, elotuzumab with $F_e = 1.7$, or daratumumab with $F_d = 0.85$ is only given in [0,1] months, [2,3] months, [4,5] months, [6,7] months, [8,9] months and [10,11] months.

(S9): Anti-PD-1 with $F_q = 5$, elotuzumab with $F_e = 5$, or daratumumab with $F_d = 0.1$ is only given in [0,1] months, [2,3] months, [4,5] months, [6,7] months, [8,9] months and [10,11] months.

(S10): Anti-PD-1 with $F_q = 2$, elotuzumab with $F_e = 2$, or daratumumab with $F_d = 0.775$ is only given in [0,2] months and [6,8] months.

(S11): Anti-PD-1 with $F_q = 1.7$, elotuzumab with $F_e = 1.7$, or daratumumab with $F_d = 0.85$ is only given in [0,2] months, [4,6] months, and [8,10] months.

(S12): Anti-PD-1 with $F_q = 1.7$, elotuzumab with $F_e = 1.7$, or daratumumab with $F_d = 0.85$ is only given in [0,3] months and [6,9] months.

In the following Figs 6.6, 6.7, 6.9, 6.11, 6.13, and 6.14, we use gray areas to indicate the treatment interval. To compare all schedules fairly, we keep the total effect for all schedules the same, except for (S6) and (S9). We also assume the maximum effect of anti-PD-1, elotuzumab and daratumumab are 5, 5, and 0.1, respectively. Then, we create the following formulas:

$$F_q = 1 + 4/N,\ F_e = 1 + 4/N,\ F_d = 1 - 0.9/N,$$

with N being the whole treatment duration for the extra treatment of anti-PD-1, elotuzumab, or daratumumab treatments, except for schedules (S6) and (S9), where we take $N = 1$ to reach the maximum effect for all treatments. We have schedules (S6) and (S9) as a way to test the same treatment windows in schedule (S5) and (S8) with a higher effect. Furthermore, we can categorize schedules (S1)-(S12) as such:

(i) Schedule (S1) is the extra treatment for an one-month duration.

(ii) Schedules (S2) and (S7) are the extra treatment for a two-month duration.

(iii) Schedule (S3) is the extra treatment for a three-month duration.

(iv) Schedules (S4) and (S10) are the extra treatment for a four-month duration.

(v) Schedules (S5), (S6), (S8), (S9), (S11) and (S12) are the extra treatment for a six-month duration.

The quantity

$$RM(t,P) = \frac{M_{\text{control}}(t,P) - M_{\text{treatment}}(t,P)}{M_0},\ t \in [0,30] \text{ months}, \tag{6.4.1}$$

will be used for measuring how the combination therapy between CAR-T cells and one of anti-PD-1, elotuzumab, or daratumumab with schedules (S1)-(S12) affects the relapse level for patients in Group II. $M_{\text{control}}(t,P)$ represents the solution of $M(t)$ using the parameter set $P \in \tilde{P}$ only treated with CAR-T cells, $M_{\text{treatment}}(t,P)$ displays the solution of $M(t)$ using the parameter set $P \in \tilde{P}$ treated with CAR-T cells and one of anti-PD-1, elotuzumab, or daratumumab, and $M_0 = 1.5\ g/dL$ is the initial condition for M protein as given in Chapter 6.2. Note that a positive $RM(t,P)$ implies the extra treatment further reduces the M protein concentration at time t comparing to the CAR-T cell treatment alone and a negative $RM(t,P)$ implies the opposite. Hence, a schedule with a longer positive duration or larger positive $RM(t,P)$ is recommended to mitigate the relapse issue. First, the combination therapy of anti-PD-1, elotuzumab, or daratumumab with CAR-T cells using schedules (S1)-(S12) will be discussed for the general model (2.1.6) and then a discussion will follow for the simplified model (2.2.6). Finally, a comparison of the conclusions for the general model (2.1.6) and the simplified model (2.2.6) using schedules (S1)-(S12) will be given.

6.4.1 Combination Therapies for Model (2.1.6)

In this subsection, the combination therapies between CAR-T cells and one of anti-PD-1, elotuzumab, or daratumumab, using the parameter sets $P \in \tilde{P}$ for Group II under model (2.1.6), will be analysed using schedules (S1)-(S12).

Fig. 6.6 shows the treatment outcome for schedules (S1)-(S12) for the combination therapy between CAR-T cells and daratumumab and shows that for all

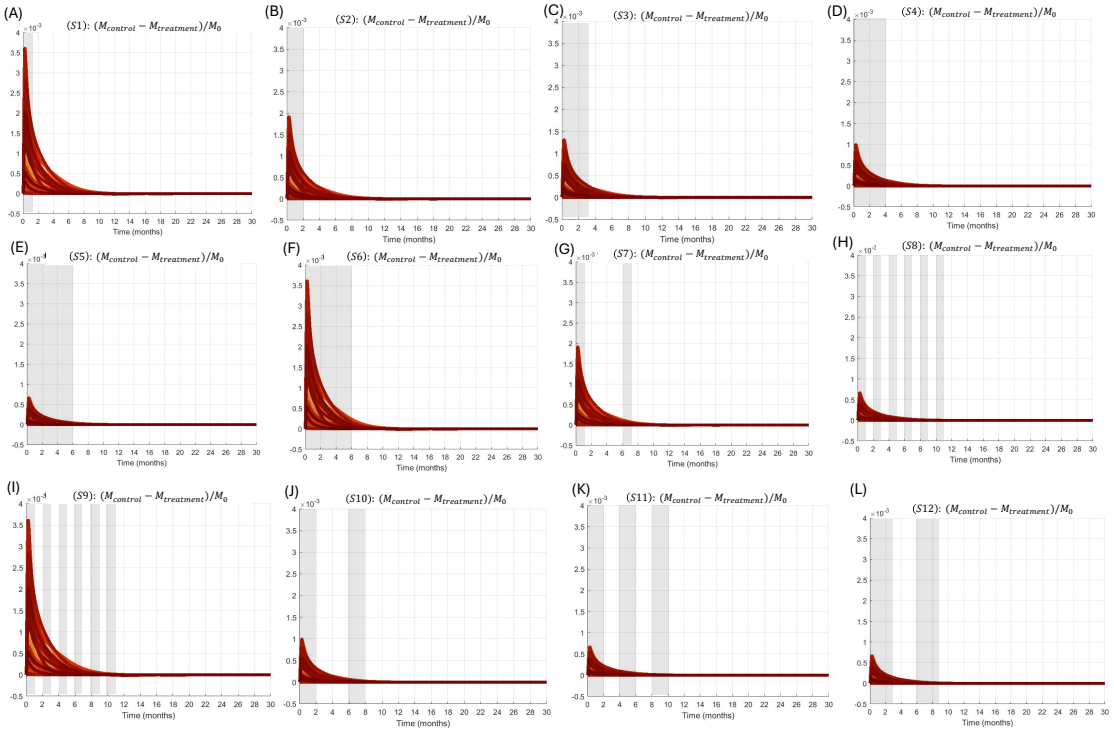

Figure 6.6: **Treatment outcome for combination of daratumumab and CAR-T cells for schedules (S1)-(S12) for model** (2.1.6)**.** (A)-(L) display the treatment outcome for combination of daratumumab and CAR-T cells under schedules (S1)-(S12) respectively. The multi-coloured curves represent the curve $RM(t,P) = (M_{\text{control}}(t,P) - M_{\text{treatment}}(t,P))/M_0$, as defined in Eq. (6.4.1), for $P \in \tilde{P}$, with $M_{\text{treatment}}(t,P)$ for the daratumumab and CAR-T cell treatments. The horizontal and vertical axes represent the time with unit month and the value of $RM(t,P)$. The gray areas represent the treatment period of daratumumab.

parameter sets $P \in \tilde{P}$, $RM(t,P)$ is positive for $t \in [0,30]$ months and the maximum value of $RM(t,P)$ for all $P \in \tilde{P}$ was bounded above by 4×10^{-3} and $RM(t,P)$ is close to 0 by $t = 8$ months, for all schedules. This shows that the effect of daratumumab cannot be maintained after treatment withdrawal and thus, not effective for mitigating the relapse for patients.

Fig. 6.7 displays the treatment outcome for schedules (S1)-(S12) for the combination therapy between CAR-T cells and elotuzumab. We find for every schedule, every patient $P \in \tilde{P}$ has a positive peak at the end of elotuzumab treatment and a positive secondary peak after elotuzumab treatment is withdrawn, indicating that

elotuzumab induces reduction of M protein during and after treatment. It can be seen that all schedules except for (S8), (S9), (S11) and (S12), some of the $RM(t, P)$ are negative for a period of time, indicating the period that elotuzumab actually increases that amount of M protein.

As the total treatment duration increases, the period of negative $RM(t, P)$ narrows down from $[0, 30]$ months to the early period and the magnitude of $RM(t, P)$ increases. When comparing the results for schedules (S2) and (S7), schedules (S4) and (S10), and schedules (S5), (S11) and (S12), it shows that a higher frequency of elotuzumab treatment induces a higher value of $RM(t, P)$ and hence is more effective for mitigating relapse. Additionally, we find, for schedule (S5), the $RM(t, P)$ and the attained maximum for the secondary peak are higher when the treatment effect increases, due to the comparison between (S5) and (S6) and (S8) and (S9). Therefore, elotuzumab administered with a longer duration, a higher frequency or a higher effect can be effective at mitigating relapse in patients.

We define the time to peak, $\hat{t}$, as $max_t RM(t, P) = RM(\hat{t}, P)$ for any time t after the extra treatment is withdrawn, for $P \in \tilde{P}$. We also define the time to control, $\tilde{t}$, if $\tilde{t} \geqslant$ extra treatment withdrawn timing and is the minimal time point such that $RM(\tilde{t}, P) = 0$. Since delaying the time to peak and time to control mitigates the relapse and delays the relapse for patients, respectively, we show the scatterplots of the parameter values in the parameter sets $P \in \tilde{P}$ versus the time to peak and time to control for the combination of elotuzumab and CAR-T cells for schedules (S5) and (S8) shown in Fig. 6.8 and the PRCCs of these parameters for the time to peak and time to control are shown in Table 6.6. We consider only schedules (S5) and (S8) as schedules (S1)-(S3) have $RM(t, P)$ that are always negative, the outcomes of schedules (S4), (S5), (S7), (S10), and (S12) have a similar pattern compared to schedule (S5) and the outcomes of schedules (S9) and (S11) have a similar pattern compared to schedule (S8).

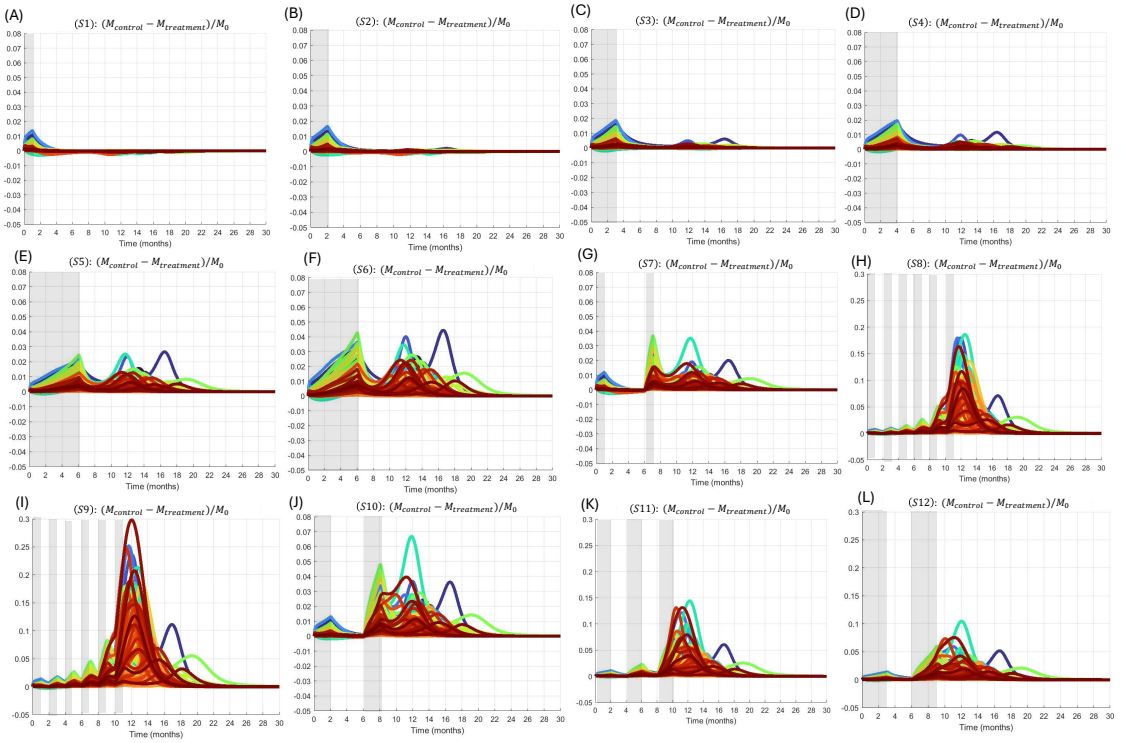

Figure 6.7: **Treatment outcome for combination of elotuzumab and CAR-T cells for schedules (S1)-(S12) for model** (2.1.6)**.** (A)-(L) display the treatment outcome for combination of elotuzumab and CAR-T cells under schedules (S1)-(S12), respectively. The multi-coloured curves represent the curve $RM(t,P) = (M_{\text{control}}(t,P) - M_{\text{treatment}}(t,P))/M_0$, as defined in Eq. (6.4.1), for $P \in \tilde{P}$, with $M_{\text{treatment}}(t,P)$ for the elotuzumab and CAR-T cell treatments. The horizontal and vertical axes represent the time with unit month and the value of $RM(t,P)$. The gray areas represent the treatment period of elotuzumab.

For the time to peak for schedule (S5), we find the parameters δ_C, δ_N, b_{MM}, and b_{NM} were negatively correlated and the parameters r_C, r_N, a_{CN}, a_{NC}, a_{CNM}, a_{MM} and a_{MC} were positively correlated. Moreover, as the treatment frequency increases (i.e., in (S8)), the correlation among the above parameters remain similar, while b_{CM} and a_{RM} become negatively correlated and K_N becomes positively correlated to the time to peak. Based on the correlation strength, increases in r_C or s_N or decreases in δ_C or δ_N efficiently prolong the time to peak, especially r_C and δ_C (namely, the effect on T_C). Moreover, among these parameters, r_N and a_{CN} related to Fe, so elotuzumab is recommended for reducing relapse.

For the time to control for schedule (S5), the parameters r_C, a_{MC}, b_{CN}, b_{MR}, K_M, a_{NC}, and a_{MR} are positively correlated and parameters δ_C, K_N, and r_R are negatively correlated. As the treatment frequency increases, the correlation among the above parameters remain similar, while K_C and b_{MC} become negatively correlated. Increasing r_C or a_{MC} or decreasing δ_C most effectively prolongs the time to control, while reducing r_R is the second most effective way. However, none of these parameters related to elotuzumab, so elotuzumab is insufficient for delaying relapse. However, increasing daratumumab may not always delay due to the opposite effect from a larger a_{MR} or a smaller b_{MR} or a smaller r_R.

Fig. 6.9 displays the results for schedules (S1)-(S12) for the combination therapy between CAR-T cells and anti-PD-1. We find that all treatment schedules do not significantly affect M protein during the treatment period and all schedules induce significant reduction of M protein after the treatment is withdrawn. Moreover, if the treatment is given once, then a shorter treatment duration could include a larger negative $RM(t, P)$ during and after the treatment, which means that the extra anti-PD-1 treatment could aggravate the relapse issue. However, increasing the treatment duration or the treatment frequency could solve this problem that the value of $RM(t, P)$ can be dramatically increased, and hence mitigates the relapse. Additionally, increasing treatment effect amplifies the effect on $RM(t, P)$, namely, the negative values of $RM(t, P)$ are smaller and the positive values of $RM(t, P)$ are larger (see (S5), (S6), (S8), and (S9)).

We also generate scatterplots of parameter values in parameter sets $P \in \tilde{P}$ versus time to peak and time to control for the combination of anti-PD-1 and CAR-T cells for schedule (S5) shown in Fig. 6.10 and their PRCCs to the time to peak and time to control are shown in Table 6.6. We consider only schedule (S5) as schedules (S1)-(S3) can lead to severe relapse in patients and schedules (S4), (S6)-(S12) have a similar pattern compared to schedule (S5). For the time to peak for schedule (S5),

Table 6.6: **PRCCs for the time to peak and time to control for Figs. 6.8 and 6.10.** The first column lists the parameters. The second, fourth, and sixth columns (resp. third, fifth and seventh columns) display their PRCCs to the time to peak (resp. time to control) for the combination therapy between CAR-T cells and elotuzumab (F_e) for schedule (S5), the combination therapy between CAR-T cells and elotuzumab (F_e) for schedule (S8) and the combination therapy between CAR-T cells and anti-PD-1 for schedule (S5), respectively. All PRCCs have p-value less than 0.05, except those marked with a superscript $*$.

Parameter	Peak-F_e (S5)	Control-F_e (S5)	Peak-F_e (S8)	Control-F_e (S8)	Peak-F_q (S5)	Control-F_q (S5)
s_M	-0.09815^*	-0.09308^*	-0.03822^*	-0.1301^*	-0.09153^*	-0.09647^*
r_M	-0.02668^*	-0.00484^*	-0.02959^*	0.03944^*	-0.01556^*	0.05505^*
K_M	0.1361^*	0.2605	0.17^*	0.2881	0.12732^*	0.2257
δ_M	0.05189^*	-0.01399^*	0.05075^*	-0.02351^*	0.04709^*	-0.01721^*
a_{NM}	-0.03246^*	0.0461^*	-0.1461^*	0.00301^*	-0.03199^*	-0.00073^*
b_{NM}	-0.1814	-0.1096^*	-0.127^*	-0.1437^*	-0.1984	-0.2009
a_{CM}	0.1331^*	0.1323^*	0.1726^*	0.07482^*	0.1428^*	0.07329^*
b_{CM}	-0.0579^*	0.001607^*	-0.3148	-0.00249^*	-0.03289^*	-0.01525^*
a_{CNM}	0.2298	0.1265^*	0.3436	0.1016^*	0.2307	0.094^*
a_{MM}	0.2037	0.08955^*	0.3646	0.03087^*	0.1968	0.09867^*
b_{MM}	-0.2357	-0.1121^*	-0.1812	-0.139^*	-0.2208	-0.1296^*
a_{RM}	-0.1542^*	-0.05697^*	-0.3371	0.003492^*	-0.1427^*	-0.07401^*
b_{RM}	0.0598^*	0.07381^*	0.0491^*	0.07338^*	0.0706^*	0.1249^*
r_C	0.4752	0.6437	0.5411	0.6293	0.5091	0.6312
K_C	0.1136^*	-0.1119^*	0.0728^*	-0.2128	0.1296^*	-0.07692^*
δ_C	-0.6447	-0.7749	-0.5983	-0.7911	-0.6118	-0.803
a_{MC}	0.2033	0.2906	0.2076	0.2745	0.1969	0.3455
b_{MC}	-0.04539^*	-0.1410^*	-0.00976^*	-0.1873	-0.05233^*	-0.2066
a_{NC}	0.2752	0.2256	0.4346	0.1837	0.3169	0.09251^*
b_{NC}	-0.02746	0.02677^*	-0.05346^*	-0.00013^*	-0.05993^*	-0.05101^*
s_N	0.09194^*	0.1702^*	0.1111^*	0.1125^*	0.09727^*	0.1428^*
r_N	0.3609	-0.02305^*	0.2595	0.00837^*	0.3348	0.1249^*
K_N	0.1679^*	-0.2736	0.4654	-0.2527	0.1661^*	-0.2553
δ_N	-0.4196	0.1585^*	-0.445	0.1618^*	-0.3831	0.05907^*
a_{CN}	0.2857	-0.04143^*	0.3044	-0.02321^*	0.2904	0.07585^*
b_{CN}	0.03864^*	0.2755	0.1598^*	0.2931	0.07411^*	0.2125
r_R	0.1084^*	-0.2364	0.09313^*	-0.2064	0.09277^*	-0.1288^*
K_R	-0.02757^*	-0.1093^*	-0.1498^*	-0.1187^*	-0.02458^*	-0.09992^*
δ_R	-0.06843^*	0.1409^*	-0.01519^*	0.1162^*	-0.05767^*	0.08771^*
a_{MR}	0.009769^*	0.1804	-0.02061^*	0.2055	-0.03675^*	0.2118
b_{MR}	0.1264^*	0.269	0.06384^*	0.2358	0.1508^*	0.2633

the parameters r_C, r_N, a_{NC}, a_{CN}, a_{CNM}, a_{MM}, and a_{MC} are positively correlated and parameters δ_C, δ_N, b_{MM}, and b_{NM} are negatively correlated. The correlation strength suggests that increasing r_C, r_N, a_{NC}, or a_{CN} or decreasing δ_C or δ_N most effectively prolongs the time to peak. Since r_C and a_{NC} related to F_q, anti-PD-1 is an efficient treatment to reduce relapse. For the time to control for schedule (S5), the parameters r_C, a_{MC}, b_{MR}, K_M, b_{CN}, and a_{MR} are positively correlated and δ_C, K_N, b_{MC}, and b_{NM} are negatively correlated. Similarly, increasing r_C, a_{NC}, r_N, or a_{CN} or decreasing δ_C or δ_N most effectively prolongs the time to control, and hence

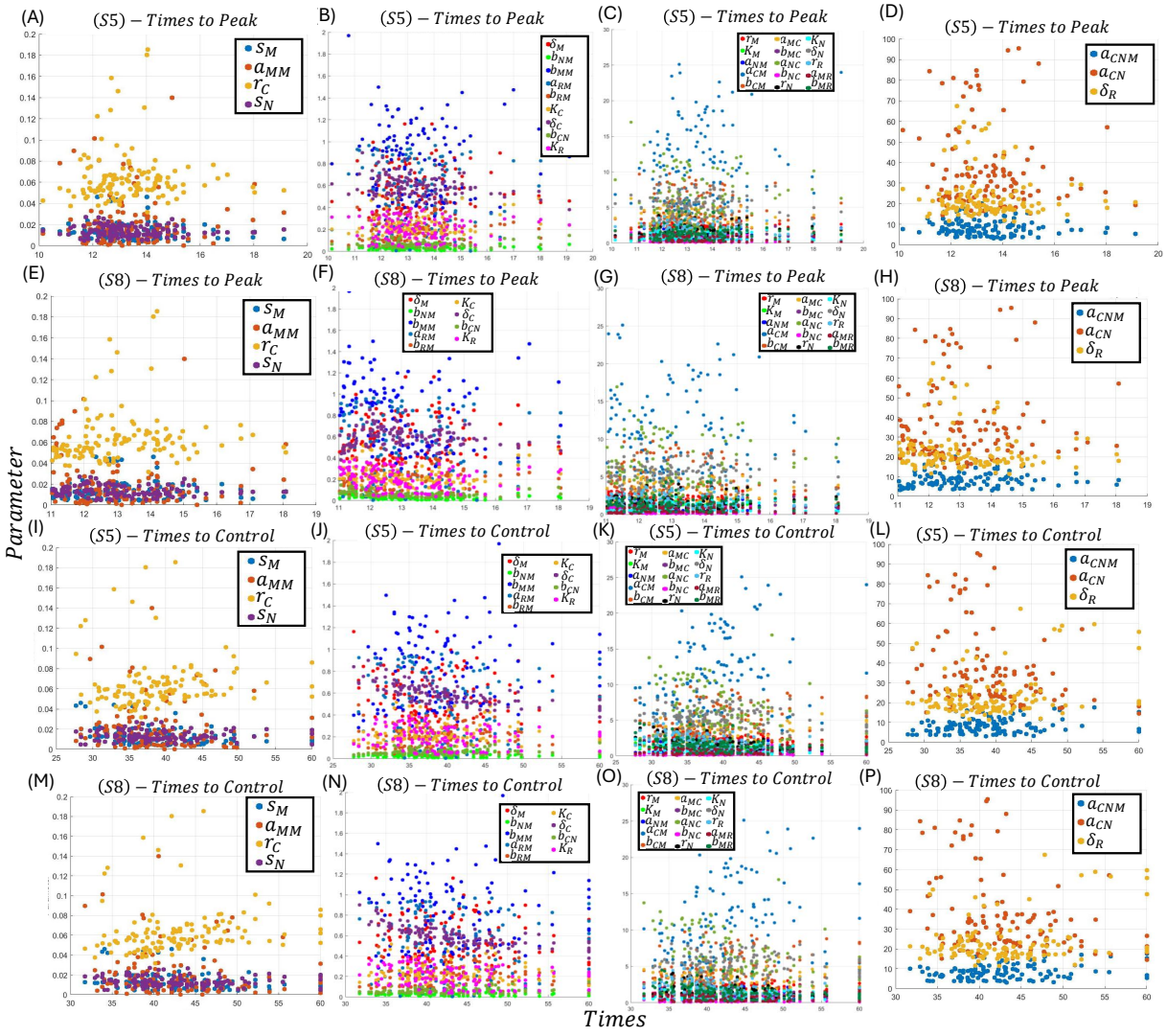

Figure 6.8: **Scatterplots of the time to peak and time to control, for the combination therapy of elotuzumab and CAR-T cells under schedules (S5) and (S8) of model** (2.1.6)**.** The first and second rows (resp. third and fourth rows) display the scatterplots of parameters with respect to the time to the peak (resp. time to control) for model (2.1.6) for schedule (S5) and (S8), respectively. The considered parameters in each subfigure are indicated in the figure legend. The vertical and horizontal axes represent the parameter value and the time with unit month.

anti-PD-1 can also delay relapse.

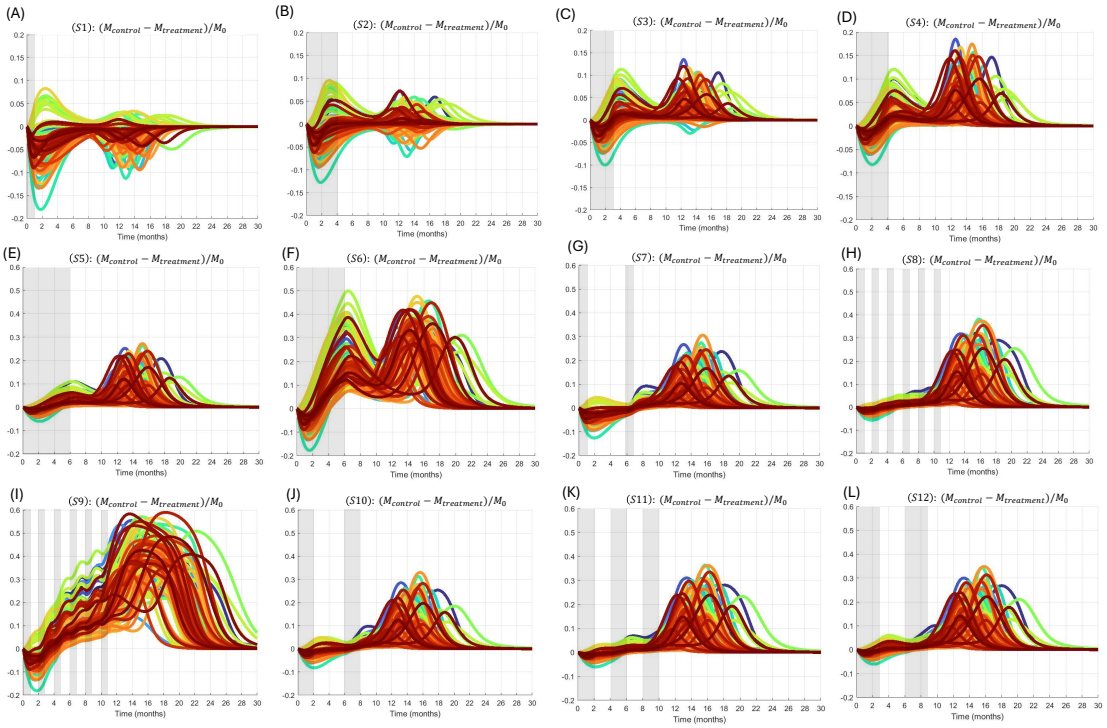

Figure 6.9: **Treatment outcome for combination of anti-PD-1 and CAR-T cells for schedules (S1)-(S12) for model** (2.1.6)**.** (A)-(L) display the treatment outcome for combination of anti-PD-1 and CAR-T cells under schedule (S1)-(S12), respectively. The multi-coloured curves represent the curve $RM(t, P) = (M_{\text{control}}(t, P) - M_{\text{treatment}}(t, P))/M_0$, as defined in Eq. (6.4.1), for $P \in \tilde{P}$, with $M_{\text{treatment}}(t, P)$ for the anti-PD-1 and CAR-T cell treatments. The horizontal and vertical axes represent the time with unit month and the value of $RM(t, P)$. The gray areas represent the treatment period with anti-PD-1.

6.4.2 Combination Therapies by Using Model (2.2.6)

In this subsection, the combination therapies between CAR-T cells and one of anti-PD-1, elotuzumab or daratumumab, using the parameter sets $\tilde{P}$ for Group II under model (2.2.6), will be studied using the schedules (S1)-(S10).

Fig. 6.11 displays the treatment results schedules (S1)-(S12) for the combination therapy between CAR-T cells and daratumumab and we find that $RM(t, P)$ for all $P \in \tilde{P}$ are always positive for $t \in [0, 30]$ months and had a significant reduction in M protein, for all schedules. Moreover, a higher treatment effect further enhances the reduction in M protein. This shows that, no matter the treatment duration and

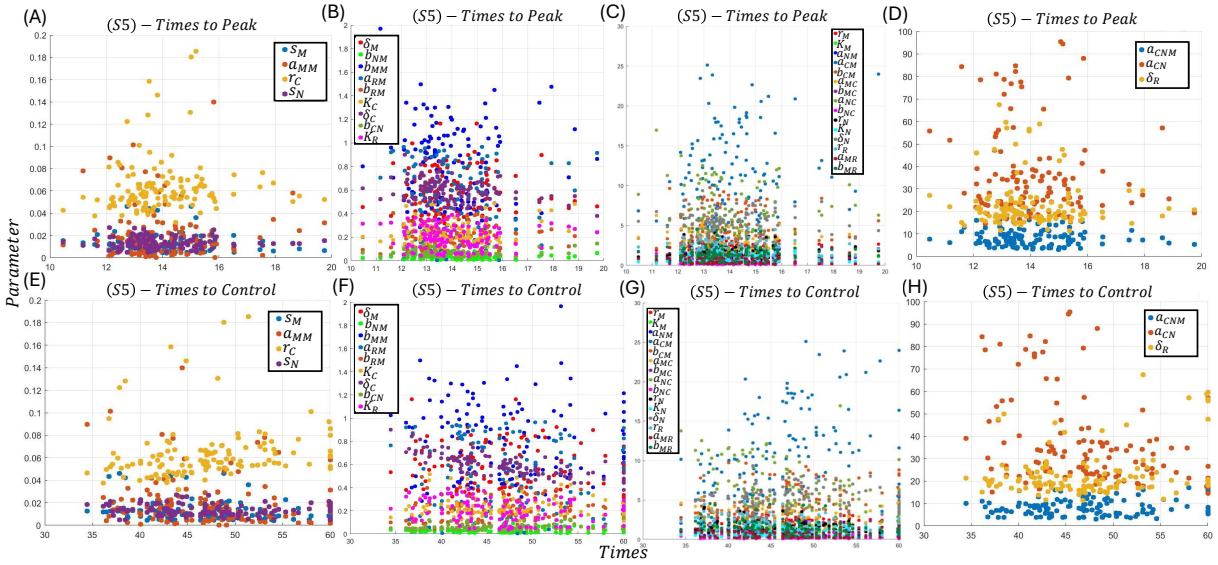

Figure 6.10: **Scatterplots of time to peak and time to control, for the combination therapy of anti-PD-1 and CAR-T cells under schedule (S5) for model** (2.1.6)**.** (A)-(D) (resp. (E)-(H)) display the scatterplots of parameters with respect to the time to the peak (resp. time to control) for model (2.1.6). The considered parameters in each subfigure are indicated in the figure legend. The vertical and horizontal axes represent the parameter value and the time with unit month.

frequency, daratumumab is effective at mitigating relapse in patients and a higher effect of daratumumab induces a better treatment outcome.

We generate scatterplots of $\tilde{P}$ versus the time to peak and time to control for the combination therapy between CAR-T cells and daratumumab for schedule (S1), shown in Fig. 6.12. Their PRCCs to the time to peak and time to control are displayed in Table 6.7. We only consider schedule (S1) as all other schedules have a similar pattern compared to (S1). For the time to peak for (S1), the parameters δ_R, K_R, s_M, K_M, and K_C are positively correlated, while r_R, a_{MR}, δ_M, and r_N are negatively correlated. These parameters also have similar correlations to the time to control, while δ_N and a_{CN} are positively correlated and s_N is negatively correlated to the time to control. Based on the correlation strength, decreasing a_{MR}, r_R, or δ_M or increasing δ_R or s_M most effectively prolongs the time to peak and time to control, namely reduce and delay the relapse. Moreover, r_R and a_{MR} related to F_d, and hence increasing the effect of daratumumab (i.e., reducing F_d) can efficiently

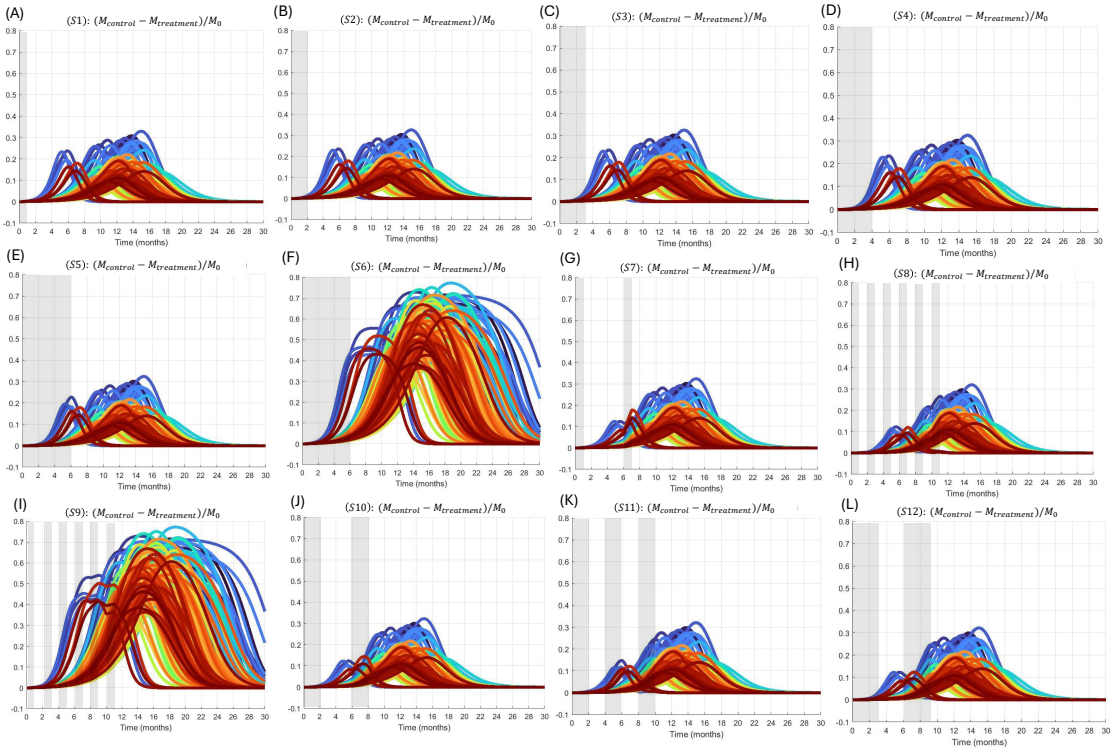

Figure 6.11: **Treatment outcome for combination of daratumumab and CAR-T cells for schedules (S1)-(S12) for model** (2.2.6)**.** (A)-(L) display the treatment outcome for combination of daratumumab and CAR-T cells under schedules (S1)-(S12), respectively. The multi-coloured curves in each plot represent the curve $RM(t, P)$, as defined in Eq. (6.4.1), for $P \in \tilde{P}$, with $M_{\text{treatment}}(t, P)$ for the daratumumab and CAR-T cell treatments. The horizontal and vertical axes represent the time with unit month and the value of $RM(t, P)$. The gray areas represent the treatment period with daratumumab.

mitigate and delay the relapse.

Fig. 6.13 display the treatment outcome for the combination therapy between CAR-T cells and elotuzumab for schedules (S1)-(S12) and we find $RM(t, P)$ was always negative during and after treatment for all schedules, for all $P \in \tilde{P}$ and $t \in [0, 30]$ months. In particular, we find that as the treatment duration increased, $RM(t, P)$ decreased. Thus, elotuzumab should not be considered as a viable way of mitigating relapse.

Fig. 6.14 displays the treatment outcome for the combination therapy between CAR-T cells and anti-PD-1 for schedules (S1)-(S12). For each treatment schedules,

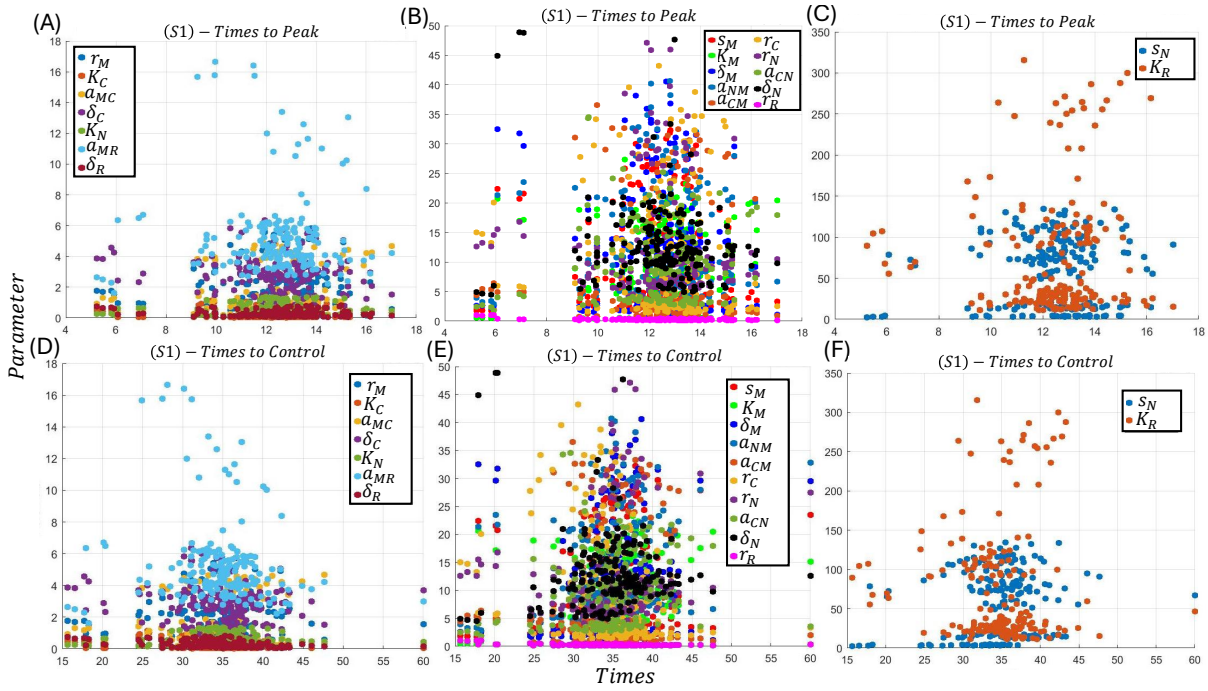

Figure 6.12: **Scatterplots of time to peak and time to control, for the combination therapy of daratumumab and CAR-T cells under schedule (S1) for model** (2.2.6)**.** (A)-(C) (resp. (D)-(F)) display the scatterplots of parameters with respect to the time to the peak (resp. time to control) for model (2.2.6). The considered parameters in each subfigure are indicated in the figure legend. The vertical and horizontal axes represent the parameter value and the time with unit month.

patients (i.e., parameter sets) can be separated into two groups: one has a positive secondary peak for $RM(t, P)$, denoted as $\tilde{P}_{pos}$ and one has a negative secondary peak for $RM(t, P)$ denoted as $\tilde{P}_{neg}$. For the parameter sets $P \in \tilde{P}_{pos}$, all treatment schedules induce significant reduction of M protein during the treatment period, and the reduction decreases after the treatment is withdrawn. Moreover, for the single treatment schedule, increasing treatment duration enhances the maximal reduction of M protein after the treatment is withdraw, but cannot change the ones during the treatment period. Additionally, a higher treatment effect induces a higher M protein reduction during and after the treatment, whereas increasing treatment frequency does not improve the treatment outcome during and after the treatment. Therefore, CAR-T cell combined with a single anti-PD-1 treatment with a longer duration or a stronger effect could mitigate the relapse issue for patients related to the group $\tilde{P}_{pos}$.

Table 6.7: **PRCCs for the time to peak and time to control for Fig. 6.12.** The first column lists the parameter. The second (resp. third) column displays their PRCCs to the time to peak (resp. time to control) for the combination therapy between CAR-T cells and daratumumab for schedule (S1) for patients $P \in \tilde{P}$. All PRCCs have p-value less than 0.05, except those marked with a superscript $*$.

Parameter	Peak-F_d (S1)	Control-F_d (S1)
s_M	0.2731	0.3831
r_M	0.1067*	0.0401*
K_M	0.1957	0.2264
δ_M	-0.4435	-0.4225
a_{NM}	0.0405*	-0.1154*
a_{CM}	0.01431*	0.02217*
r_C	0.1069*	-0.01682*
K_C	0.1669	0.1998
a_{MC}	0.00851*	-0.09906*
δ_C	-0.1178*	-0.0606*
s_N	-0.05243*	-0.2404
r_N	-0.2709	-0.09247*
K_N	0.09087*	-0.08603*
a_{CN}	0.05121*	0.1636
δ_N	0.1315*	0.2708
r_R	-0.5712	-0.5575
K_R	0.3425	0.04858*
a_{MR}	-0.5323	-0.6181
δ_R	0.5387	0.4255

To study the biomarkers that can be used to identify if a patient may response positively to an extra treatment of anti-PD-1, we consider the parameter sets $P \in \tilde{P}_{pos}$ and $P \in \tilde{P}_{neg}$ for schedule (S5), due to its longer treatment duration. Fig. 6.15 displays the boxplots of parameter values in $\tilde{P}_{neg}$ and $\tilde{P}_{pos}$ and we find the distributions of parameters, s_M, K_M, s_N, and K_N, are significantly lower and K_R is significantly higher for $\tilde{P}_{pos}$ comparing to $\tilde{P}_{neg}$. This indicates that combination of CAR-T cells and anti-PD-1 is recommended for a patient with a lower source of M protein or NK cells, or a lower carrying capacity of M protein or NK cells, or a higher carrying capacity of regulatory T cells.

Next, we consider the relationship between the parameter values in $\tilde{P}^{\text{pos}}$ and the time to peak and time to control, shown in Figs. 6.16 and 6.17 respectively, for

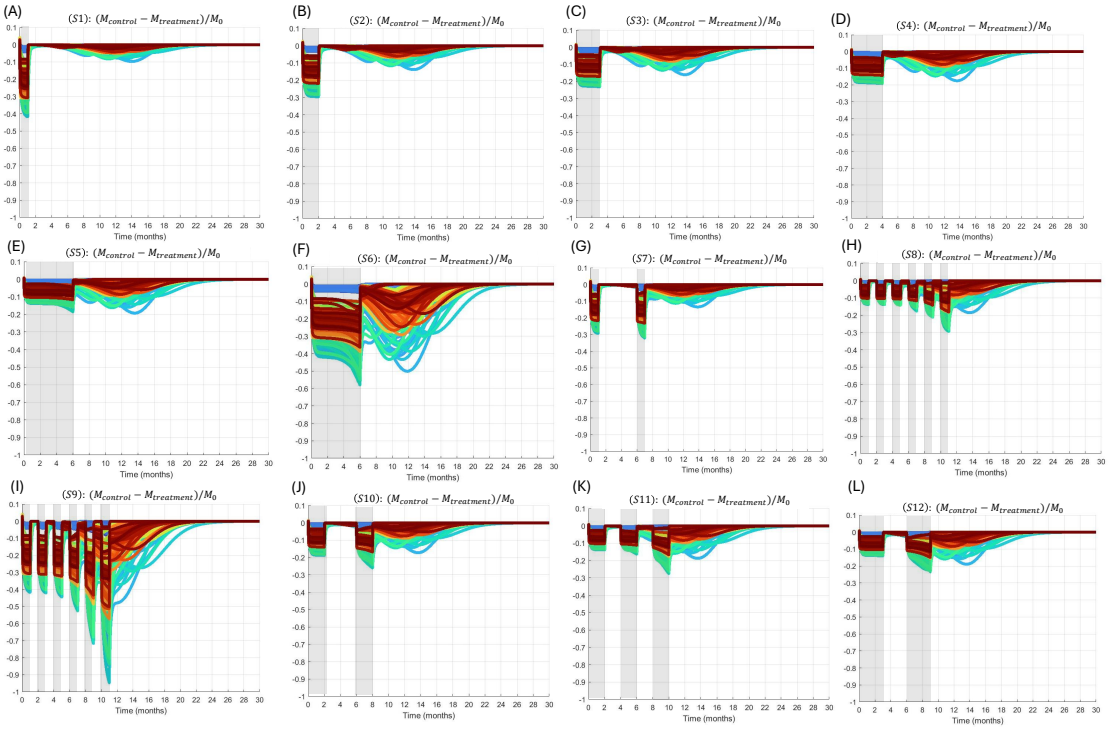

Figure 6.13: **Treatment outcome for combination of elotuzumab and CAR-T cells for schedules (S1)-(S12) for model** (2.2.6)**.** (A)-(L) display the treatment outcome for combination of elotuzumab and CAR-T cells under schedules (S1)-(S12), respectively. The multi-coloured curves in each plot represent the curve $RM(t, P)$, as defined in Eq. (6.4.1), for $P \in \tilde{P}$, with $M_{\text{treatment}}(t, P)$ for the elotuzumab and CAR-T cell treatments. The horizontal and vertical axes represent the time with unit month and the value of $RM(t, P)$. The gray areas represent the treatment period with elotuzumab.

model (2.2.6) under schedules (S1), (S3), (S5), (S6) and (S8). We only consider schedules (S1), (S3), (S5), (S6), and (S8) as the outcomes of schedules (S2) and (S7) are similar to schedule (S1), and the outcomes of schedules (S4) and (S10) are similar to schedule (S3). Additionally, the outcome of schedule (S9) is similar to schedule (S6), and the outcomes of schedules (S11) and (S12) are similar to schedule (S5). Their PRCCs to the time to peak is shown in Table 6.8 and their PRCCs to the time to control is displayed in Table 6.9.

We find that δ_R is positively correlated and a_{MR} and r_R are negative correlated to both time to peak and time to control. Hence, decreasing the amount of T_{reg}s

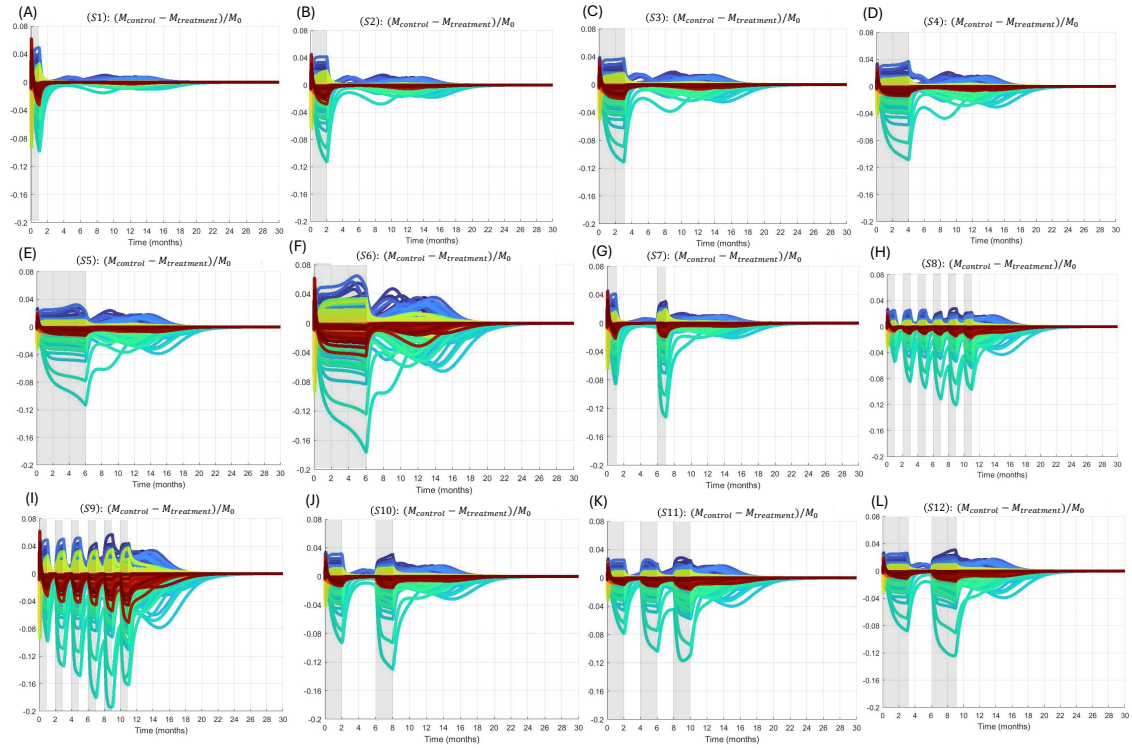

Figure 6.14: **Treatment outcome for combination of anti-PD-1 and CAR-T cells for schedules (S1)-(S12) for model** (2.2.6)**.** (A)-(L) display the treatment outcome for combination of anti-PD-1 and CAR-T cells under schedules (S1)-(S12), respectively. The multi-coloured curves in each plot represent the curve $RM(t, P)$, as defined in Eq. (6.4.1) for $P \in \tilde{P}$, with $M_{\text{treatment}}(t, P)$ for the anti-PD-1 and CAR-T cell treatments. The horizontal and vertical axis represent the time with unit month and the value of $RM(t, P)$. The gray areas represent the treatment period with anti-PD-1.

by reducing the homeostasis or increasing the death rate can efficiently mitigate or delay relapse. However, anti-PD-1 does not affect the amount of T_{reg}s directly, so anti-PD-1 cannot change the relapse issue directly.

6.4.3 Comparison of Treatment Outcomes Between Models (2.1.6) and (2.2.6)

When comparing the results and predictions of Chapters 6.4.1 and 6.4.2, we find different conclusions for the general model (2.1.6) and the simplified model (2.2.6). When considering model (2.1.6), for the combination therapy of CAR-T cells and

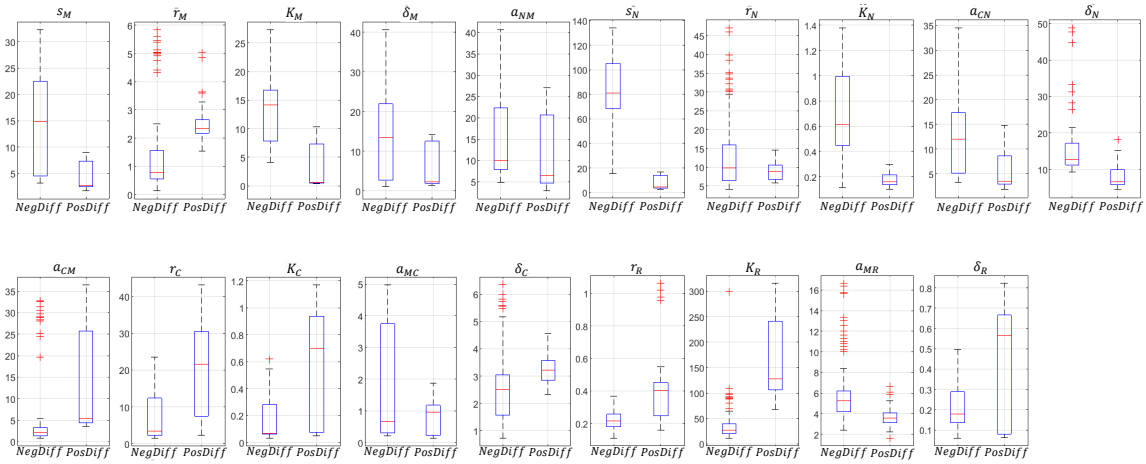

Figure 6.15: **Distributions of $\tilde{P}_{neg}$ and $\tilde{P}_{pos}$ for schedule (S5) using model** (2.2.6) **under CAR-T cell and anti-PD-1 treatments.** The first and second boxplot, indicated by *NegDiff* and *PosDiff* respectively, in each subfigure display the distributions of the corresponding parameter of $\tilde{P}_{neg}$ and $\tilde{P}_{pos}$, respectively.

anti-PD-1, the results of $RM(t, P)$ show that the combination therapy is always effective at mitigating relapse after treatment is withdrawn, with a long enough duration or a high enough frequency. Moreover, a stronger efficacy of anti-PD-1 further improves the treatment outcome during the treatment and mitigates relapse after the treatments are withdrawn. On the other hand, combination of CAR-T cells and elotuzumab also induce effective reduction of M protein during and after the treatment in all schedules. However, the magnitude of the $RM(t, P)$ peak for the combination of CAR-T cells and elotuzumab is smaller than the one for the combination of CAR-T cells and anti-PD-1. This finding suggests that anti-PD-1 could be the best option for mitigating relapse for patients in Group II. Additionally, Figs. 6.8 and 6.10 and Table 6.6 identify which parameters (i.e., reactions) could be the key players, linked to the anti-PD-1 or elotuzumab treatment, to cause the delay (by using time to control) or mitigation (by using time to peak) of relapse. Finally, daratumumab cannot induce significant improvement of the relapse issue.

When considering model (2.2.6), combination of CAR-T cells and anti-PD-1 shows that, for each treatment schedule, patients (i.e., parameter sets) can be sepa-

Table 6.8: **PRCCs for the time to peak for Fig. 6.16.** The first column lists the parameter. The second, third, fourth, fifth and sixth columns display their PRCCs to the time to peak for the combination therapy between CAR-T cells and anti-PD-1 (F_q) for schedules (S1), (S3), (S5), (S6) and (S8) for patients $P \in \tilde{P}^{\text{pos}}$ with a positive secondary peak, respectively. All PRCCs have p-value less than 0.05, except those marked with a superscript $*$.

Parameter	F_q (S1)	F_q (S3)	F_q (S5)	F_q (S6)	F_q (S8)
s_M	-0.2546^*	-0.1088^*	-0.2016^*	-0.2317^*	-0.1412^*
r_M	-0.3241	-0.191^*	-0.2345^*	-0.234^*	-0.4244
K_M	0.1814^*	0.02212^*	-0.07245^*	-0.08655^*	0.4669
δ_M	0.05065^*	-0.0439^*	0.007296^*	0.02938^*	-0.3621^*
a_{NM}	0.2875^*	0.1553^*	0.1158^*	0.1331^*	-0.1249^*
a_{CM}	0.1747^*	0.238^*	0.1976^*	0.1326^*	0.2827^*
r_C	0.3088	0.43	0.209^*	0.2189^*	0.2829^*
K_C	0.1864^*	0.1587^*	-0.00113^*	-0.0101^*	0.03983^*
a_{MC}	0.1772^*	0.261^*	0.1173^*	0.1016^*	0.07113^*
δ_C	0.1098^*	-0.1547^*	-0.03704^*	-0.04682^*	-0.00993^*
s_N	0.2698^*	0.168^*	0.08704^*	0.07471^*	0.097^*
r_N	-0.3322	-0.06067^*	0.06731^*	0.06877^*	0.1407^*
K_N	0.1559^*	-0.045^*	0.2134^*	0.2283^*	-0.0352^*
a_{CN}	-0.02084^*	0.1156^*	-0.05107^*	-0.07282^*	0.4905
δ_N	0.1336^*	-0.1221^*	-0.2641^*	-0.2329^*	-0.1928^*
r_R	-0.5652	-0.6566	-0.6818	-0.7235	-0.6274
K_R	0.1614^*	0.1021^*	0.0185^*	0.04662^*	-0.09808^*
a_{MR}	-0.5216	-0.5811	-0.6346	-0.6907	-0.2513^*
δ_R	0.6327	0.6717	0.6708	0.6758	0.6595

rated into two groups: one has a positive secondary peak for $RM(t, P)$ and one has a negative secondary peak for $RM(t, P)$. For the parameter sets having a positive secondary peak for $RM(t, P)$, all treatment schedules induce significant reduction of M protein during the treatment period, and the reduction decreases after the treatment is withdrawn. This property is quite different to the finding of anti-PD-1 from model (2.1.6) that all treatment schedules do not significantly affect M protein during the treatment period and all schedules induce significant reduction of M protein after the treatment is withdrawn.

For the combination of CAR-T cells and elotuzumab of model (2.2.6), all treatment schedules generate negative $RM(t, P)$, indicating promotion of M protein dur-

Table 6.9: **PRCCs for the time to control for Fig. 6.17.** The first column lists the parameter. The second, third, fourth, fifth and sixth columns display their PRCCs to the time to control for the combination therapy between CAR-T cells and anti-PD-1 (F_q) for schedules (S1), (S3), (S5), (S6) and (S8) for patients $P \in \tilde{P}^{\text{pos}}$ with a positive secondary peak, respectively. All PRCCs have p-value less than 0.05, except those marked with a superscript $*$.

Parameter	F_q (S1)	F_q (S3)	F_q (S5)	F_q (S6)	F_q (S8)
s_M	-0.1887^*	-0.1803^*	-0.1686^*	-0.06108^*	-0.1673^*
r_M	-0.1272^*	0.06291^*	0.1182^*	0.204^*	0.1565^*
K_M	-0.08853^*	-0.1842^*	-0.177^*	-0.1914^*	-0.1365^*
δ_M	0.07401^*	0.007394^*	-0.0501^*	-0.04922^*	-0.1019^*
a_{NM}	0.1389^*	0.04413^*	-0.00821^*	-0.08295^*	-0.06913^*
a_{CM}	0.04404^*	0.17839^*	0.2038^*	0.09321^*	0.2237^*
r_C	0.09179^*	0.2471^*	0.264	0.1641^*	0.3155
K_C	-0.00793^*	0.2604^*	0.27	0.336	0.2922
a_{MC}	0.02989^*	0.1716^*	0.1497^*	0.0814^*	0.1704^*
δ_C	0.04574^*	-0.1287^*	-0.1502^*	-0.3111	-0.2466^*
s_N	0.2621^*	0.1869^*	0.1694^*	0.01719^*	0.2304^*
r_N	-0.1517^*	0.03994^*	0.08813^*	0.09358^*	0.1618^*
K_N	0.02664^*	-0.1576^*	-0.1887^*	-0.2468^*	-0.2523^*
a_{CN}	0.1451^*	0.1543^*	0.164^*	0.1897^*	0.183^*
δ_N	0.04115^*	0.0056^*	-0.02321^*	0.01415^*	-0.05634^*
r_R	-0.4466	-0.6343	-0.6416	-0.6228	-0.6704
K_R	-0.03647^*	0.02276^*	0.06074^*	0.2741	0.02246^*
a_{MR}	-0.283^*	-0.606	-0.6108	-0.653	-0.6425
δ_R	0.4393	0.5884	0.5795	0.5477	0.6058

ing and after the treatment. Hence, the elotuzumab treatment should not be considered, which is very different to the finding of elotuzumab from model (2.1.6) that all schedules efficiently reduce M protein level during and after the treatments and hence mitigate relapse.

For the combination of CAR-T cells and daratumumab for model (2.2.6), all treatment schedules have similar results that they efficiently reduce M protein during and after the treatment, and hence mitigate relapse, which is very different to the finding of daratumumab from model (2.1.6) that daratumumab can only induce insufficient reduction of M protein. Notice that the treatment schedule and total effect cannot significantly change $RM(t, P)$, so the most simplified schedule (S1) is

recommended to patients.

For model (2.1.6), the significant parameters have similar PRCCs between the combination of CAR-T cells and elotuzumab and the combination of CAR-T cells and anti-PD-1 when considering the time to peak and time to control. More precisely, the parameters r_C, r_N, a_{CN}, a_{CNM}, a_{MM}, and a_{MC} are positively correlated and δ_C, δ_N, b_{MM}, and b_{NM} are negatively correlated to the time to peak for CAR-T cells combined with elotuzumab or anti-PD-1. On the other hand, the parameters r_C, a_{MC}, b_{MR}, K_M, and a_{MR} are positively correlated and δ_C and K_N are negatively correlated to the time to control for CAR-T cells combined with elotuzumab or anti-PD-1. Moreover, among these significant parameters, only r_C and a_{MC} related to anti-PD-1 and r_N and a_{CN} related to elotuzumab, so enhancing the treatment effect of elotuzumab or anti-PD-1 could efficiently mitigate and delay the relapse when combining with CAR-T cells.

For model (2.2.6), the significant parameters have similar PRCCs between time to peak and time to control when considering CAR-T cells combining with daratumumab or anti-PD-1. More precisely, parameters δ_R, s_M, K_M, and K_C are positively correlated and a_{MR}, r_R, and δ_M are negatively correlated to the time to peak and time to control for the combination of CAR-T cells and daratumumab. On the other hand, parameters δ_R is positively correlated and a_{MR} and r_R are negatively correlated to the time to peak and time to control for the combination of CAR-T cells and anti-PD-1. Moreover, among the significant parameters, only r_R and a_{MR} directly related to the corresponding treatment daratumumab, so enhancing the treatment effect of daratumumab could efficiently mitigate and delay the relapse when combining with CAR-T cells, which is oppositive to the finding from model (2.1.6).

Therefore, model (2.1.6) suggests that either anti-PD-1 or daratumumab combined with CAR-T cells can mitigate the relapse issue, and anti-PD-1 is the most efficient treatment under long treatment duration or high treatment efficacy, whereas

daratumumab should not be used due to its insufficient treatment efficacy. On the other hand, model (2.2.6) suggests that either anti-PD-1 or daratumumab combined with CAR-T cells can mitigate the relapse issue, but the combination with anti-PD-1 may not be effective for all patients and the combination with daratumumab is efficient for any treatment duration and treatment frequency.

6.5 Identifiability Analysis

In (19), the authors perform both structural and practical identifiability analysis on model (2.1.6), under the control case (i.e., $F_q = F_e = F_d = 1$). The authors used the matlab package *GenSSI* to identify eight structurally identifiable parameters: r_M, δ_M, a_{NM}, a_{CM}, r_C, δ_C, r_N, and δ_N, assuming noise-free data for M protein, CTLs, NK cells and T_{reg}s. Next, the authors used the Markov Chain Monte Carlo method with Metropolis-Hastings sampling to evaluate the practical identifiability on the same eight parameters, using steady state data from (44), and found that the eight parameters were practically non-identifiable. Due to the lack of experimental data, in (19), the authors calibrated the model outcomes to the steady states of four variables with mean and relatively large standard derivations. The selected eight parameters show broad distributions and hence are practical non-identifiable to the data of steady state. The possible reason of the practical non-identifiability could be the large standard derivations.

In this section, we perform the identifiability analysis on the general model (2.1.6) and the simplified model (2.2.6), under the control case (i.e., $F_q = F_e = F_d = 1$), using the profile likelihood mentioned in Chapter 3.4. For model (2.1.6), we analyse the structural and practical identifiability of the eight parameters, r_M, δ_M, a_{NM}, a_{CM}, r_C, δ_C, r_N, and δ_N, selected from (19), for Groups I and II datasets. For model (2.2.6), based on the PRCCs and Fig. 6.5 in Chapter 6.3, we focus on the parameters

s_M, δ_M, a_{NM}, r_C, δ_C, K_N, a_{CN}, δ_N and r_R for both Group I and Group II data.

We apply the profile likelihood method outlined in Chapter 3.4 for the identifiability analysis. We use the parameter values P_{best} from Tables 6.1 and 6.2 for the general model (2.1.6) and the simplified model (2.2.6), respectively, to obtain the value of $F_{ls}(\hat{P})$ in Eq. (3.4.4), namely, the RSS values listed in Tables 6.1 and 6.2. We consider the confidence level $\alpha = 0.9$ and set degrees of freedom (df) to be 31 for model (2.1.6) and 19 for model (2.2.6) to generate the $\chi^2(\alpha, df)$ for both datasets. Then, for each considered parameter, we perform the processes (i)-(ii) in Chapter 3.4 calibrating to the Group I and Group II datasets to find the finite sample confidence interval for the considered parameter defined in Definition 3.4.2. For simplicity, we use the following condition

$$\{P_i : F_{ls}(P_i) < F_{ls}(\hat{P}) + \chi^2(\alpha, df)\}$$

to identify the finite sample confidence intervals, instead of Eq. (3.4.4). We generate the figures for the profile likelihood curves in similar figures as shown in Fig. 3.1. The results are displayed in Fig. 6.18 for model (2.1.6) and in Fig. 6.19 for model (2.2.6). Since the curves in Fig. 6.19B look flat compared to the curves in Figs. 6.18 and 6.19A, Table 6.10 is provided for clarity.

For model (2.1.6), the profile likelihoods of these eight parameters all have a unique global minimum (which is at P_{best} highlighted by the star mark in Fig. 6.18) for Groups I and II indicating that these eight parameters are structurally identifiable to the M protein data (similar to Fig. 3.1F). This finding agrees with the conclusion made in (19) by using the matlab package *GenSSI*. Moreover, none of these profile likelihoods have intersections with the threshold $F_{ls}(\hat{P}) + \chi^2(\alpha, df)$ indicating that these eight parameters are practically non-identifiable to M protein data for both Group I and Group II data (similar to Fig. 3.1F). Therefore, the model calibration of model (2.1.6) by using the M protein data (with noise) from Group I and Group

Table 6.10: $F_{ls}(P_i)$ **for the profile likelihood for model** (2.2.6) **calibrating to Group II data.** Each pair of rows display the $F_{ls}(P_i)$ versus the values of the corresponding parameter P_i on a logarithmic scale. The $F_{ls}(P_i)$ value coloured in red represents the global minimum of $F_{ls}(P_i)$ for the corresponding parameter P_i.

$log(s_M)$	-4	-1.928	0.479	0.603	0.7	0.955	1.146	2.017	3.002	4
$F_{ls}(P_i)$	1.808	1.775	1.93	1.8994	1.9053	1.9107	1.9004	4.2436	4.2435	4.2435
$log(\delta_M)$	-4	-0.0835	0.122	0.261	0.451	0.834	1.072	2.008	3.001	4
$F_{ls}(P_i)$	1.8166	1.81	1.7751	1.8994	1.764	2.0303	1.7774	4.2436	4.2436	4.2435
$log(a_{NM})$	-2.959	-0.157	0.756	0.826	0.886	1.068	1.223	2.028	3.003	4
$F_{ls}(P_i)$	1.9727	1.8367	1.7804	1.8994	1.9317	1.8845	1.8882	1.9367	4.2438	4.2435
$log(r_C)$	-4	-0.303	0.175	0.398	0.544	0.875	1.097	2.011	3.001	4
$F_{ls}(P_i)$	1.777	1.756	1.8392	1.8994	2.0354	1.9395	1.989	1.9562	1.9044	1.9227
$log(\delta_C)$	-4	-0.496	0.12	0.365	0.521	0.864	1.091	2.01	3.001	4
$F_{ls}(P_i)$	1.9087	1.9283	2.0464	1.8994	1.7825	1.8968	2.2433	4.2435	4.2435	4.2435
$log(K_N)$	-4	-1.606	-0.372	-0.28	0.183	0.742	1.022	2.002	3	4
$F_{ls}(P_i)$	1.7239	1.7346	1.9361	1.8994	1.9049	1.9203	1.7435	4.2435	4.2435	
$log(a_{CN})$	-4	0.209	1.026	1.065	1.101	1.221	1.335	2.048	3.005	4.001
$F_{ls}(P_i)$	1.8921	1.754	1.8088	1.8994	1.7803	1.7896	1.7837	1.8083	1.7376	1.8383
$log(\delta_N)$	-4	-0.0765	0.993	1.034	1.073	1.2	1.319	2.045	3.005	4
$F_{ls}(P_i)$	2.0407	1.6802	1.7697	1.8994	1.7236	1.7981	1.7877	1.7544	1.7662	1.7242
$log(r_R)$	-4	-1.254	-0.976	-0.808	0.0628	0.712	1.007	2.001	3	4
$F_{ls}(P_i)$	1.77	1.785	1.7462	1.8994	1.715	1.697	1.7798	1.7906	1.7829	

II cannot uniquely determine the values of these eight parameters: r_M, δ_M, a_{NM}, a_{CM}, r_C, δ_C, r_N, and δ_N. Notice that the practical identifiability analysis in (19) focuses on the steady state data, whereas our analysis focuses on the M protein data over time for patients with remission and relapse pattern. Both findings suggest that these eight parameters are practically non-identifiable to the steady state of four variables and M protein variation data.

Similarly, for the nine selected parameters of model (2.2.6), all profile likelihoods have a unique global minimum (highlighted by the star mark in Fig. 6.19) and none of these profile likelihoods have intersections with the threshold $F_{ls}(\hat{P}) + \chi^2(\alpha, df)$, for Groups I and II. Thus, these nine parameters of model (2.2.6) are structurally identifiable but practically non-identifiable to M protein data for both Group I and Group II data (similar to Fig. 3.1F). Hence, the model calibration of model (2.2.6) to noise-free M protein data can uniquely determine the values of these nine parameters, s_M, δ_M, a_{NM}, r_C, δ_C, K_N, a_{CN}, δ_N, and r_R, but we lose this property when

calibrating to M protein data with noise.

Table 6.11: $F_{ls}(P_i)$ **for simultaneous perturbation in the practically non-identifable parameters for model** (2.1.6)**, calibrating to Group I and Group II data.** The first row displays the perturbation size on all practically non-identifiable parameters. The second row (resp. third row) displays the corresponding $F_{ls}(P_i)$ of model (2.1.6) calibrating to Group I (resp. Group II) data.

Change	-0.15	-0.1	-0.05	-0.001	-0.0001	0	0.0001	0.001	0.05	0.1	0.15
Group I	4.5364	4.537	4.5415			4.101			4.1203	4.07	4.5741
Group II	1.764	1.7321	1.7135	1.7087	1.5452	1.5339	1.5904	1.6485	1.7289	1.7269	1.7119

Table 6.12: $F_{ls}(P_i)$ **for simultaneous perturbation in the practically non-identifable parameters for model** (2.2.6)**, calibrating to Group I and Group II data.** The first row displays the perturbation size on all practically non-identifiable parameters. The second row (resp. third row) displays the corresponding $F_{ls}(P_i)$ of model (2.2.6) calibrating to Group I (resp. Group II) data.

Change	-0.15	-0.1	-0.05	0	0.05	0.1	0.15
Group I	4.0766	4.0512	4.0552	4.0522	4.0493	4.0495	4.0631
Group II	2.0851	1.7281	1.7446	1.8994	1.7538	1.7292	1.7432

To improve the practical non-identifiability of the selected parameters for the general model (2.1.6) and the simplified model (2.2.6), we further study how these practically non-identifiable parameters affect the model outputs in model calibration and then suggest extra data points to reduce the variation of model outputs. For each model, we tie all practically non-identifiable parameters together and simultaneously add a small perturbation on them to find the corresponding $F_{ls}(P_1, \cdots, P_k)$ ($P_1, \cdots, P_k$ are the practically non-identifiable parameters) by performing the processes (i)-(ii) in Chapter 3.4 calibrating to the Group I and Group II datasets. Here, we only consider the cases when $F_{ls}(P_1, \cdots, P_k) \approx F_{ls}(\hat{P})$, instead of searching for the finite sample confidence intervals. The values of $F_{ls}(P_1, \cdots, P_k)$ are displayed in Tables 6.11 and 6.12 for the general model (2.1.6) and the simplified model (2.2.6), respectively. Among these cases, we only select the cases with $F_{ls}(P_1, \cdots, P_k) \approx F_{ls}(\hat{P})$ and then use the whole parameter set producing the $F_{ls}(P_1, \cdots, P_k)$ to generate the model solution over the period $[0, 18]$ months used in the data fitting. The model

solutions are shown in Figs. 6.20 and 6.21 for the general model (2.1.6) and the simplified model (2.2.6), respectively.

We then discuss the variations of all variables as follows:

(i) For model (2.1.6) using Group I data (i.e., second row in Table 6.11 and Fig. 6.20 (A)-(D)), we only consider the cases with perturbation sizes 0, 0.05 and 0.1. Among these three cases, there is a small variation in M protein after six months, and negligible variations in CTLs, NK cells, and T_{reg}s and the levels of these three variables remain nearly constant throughout the entire period. Thus, adding several data points of M protein after six months, or one data point for any of CTLs, NK cells, or T_{reg}s could improve the practical non-identifiability for model (2.1.6) calibrating to Group I data.

(ii) For model (2.1.6) using Group II data (i.e., third row in Table 6.11 and Fig. 6.20 (E)-(H)), we only consider the cases with perturbation sizes 0, 0.0001 and -0.0001. Among these three cases, there is a small variation in M protein after six months and a small variation in CTLs before six months, whereas a large variation in NK cells before 12 months for the case with perturbation size -0.0001 and a large variation in T_{reg}s after 2 months for the case with perturbation size 0.0001. Thus, adding several data points of M protein after six months, or CTLs before six months, or one data point for NK cells before 12 months or T_{reg}s after 2 months could improve the practical non-identifiability for model (2.1.6) calibrating to Group II data.

(iii) For model (2.2.6) using Group I data (i.e., second row in Table 6.12 and Fig. 6.21 (A)-(D)), we consider all cases since all $F_{ls}(P_1, \cdots, P_k) \approx F_{ls}(\hat{P})$. Among these seven cases, there is a small variation in M protein after six months, negligible variations in CTLs, a large variation in NK cells after two months, and a large variation in T_{reg}s and the levels remain nearly constant throughout

the entire period. Hence, adding several data points of M protein after six months or NK cells after two months, or one data point for T_{reg}s could improve the practical non-identifiability for model (2.2.6) calibrating to Group I data.

(iv) For model (2.2.6) using Group II data (i.e., third row in Table 6.12 and Fig. 6.21 (E)-(H)), we only consider the cases with perturbation sizes $-0.1, -0.05, 0.1$, and 0.15. Among these four cases, there is a small variation in M protein during 8 months to 14 months for the case with perturbation size -0.05, a large variation in CTLs for the whole period (especially the cases with perturbation size -0.05 and 0.1), a large variation in NK cells with the level remaining nearly constant throughout the entire period, and a large variation in T_{reg}s after 12 months. Therefore, adding several data points of M protein during 8 months to 14 months, or CTLs throughout the whole period, or T_{reg}s after 12 months, or one data point for NK cells could improve the practical non-identifiability for model (2.2.6) calibrating to Group II data.

In summary, because the M protein is the only data used in the model calibration, its variation is relatively smaller than that of the other variables in both models and datasets. Moreover, when calibrating to Group I data, the model predictions for the other three variables differ considerably. Model (2.1.6) shows that different parameter sets with similar RSS values can still produce significantly different levels of CTLs, NK cells, and T_{reg}s. In addition, these levels remain nearly constant over time, indicating that the populations of these three cell types do not change. On the other hand, model (2.2.6) shows that different parameter sets with similar RSS values can yield similar behaviours for CTLs and NK cells but markedly different levels of T_{reg}s. Moreover, only the T_{reg}s display a flat pattern. Therefore, we may need additional data for CTLs, NK cells, and regulatory T cells to improve the practical non-identifiability of the general model (2.1.6), whereas additional data for regulatory T cells alone may be sufficient to improve the practical non-identifiability

of the simplified model (2.2.6). When calibrating to Group II data, both models show large variations and non-flat patterns in CTLs, NK cells, and T_{reg}s. Thus, additional data for CTLs, NK cells, and T_{reg}s at both short- and long-term time points are needed to improve the practical non-identifiability in both models.

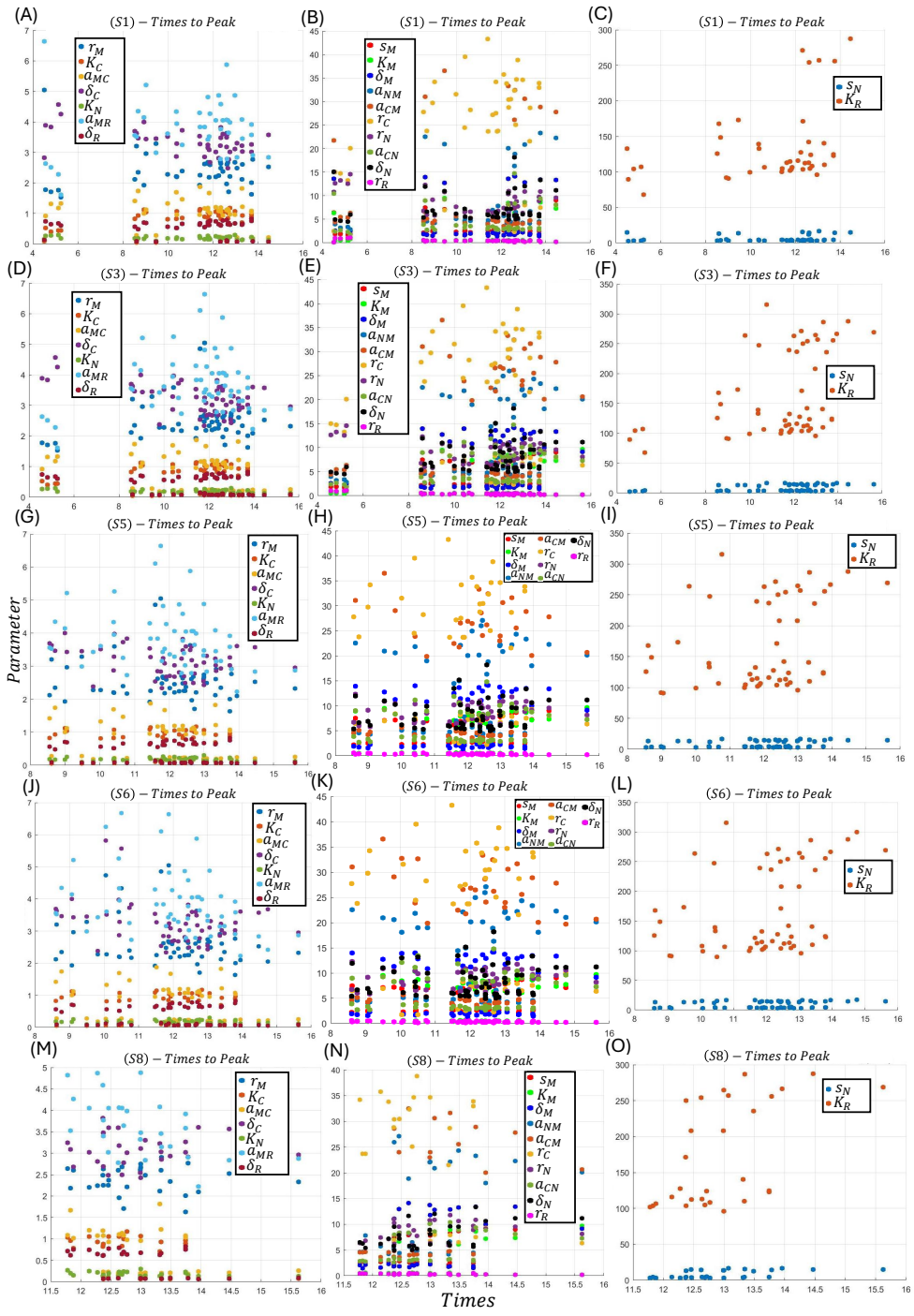

Figure 6.16: **Scatterplots of time to peak, for the combination therapy of anti-PD-1 and CAR-T cells under schedules (S1), (S3), (S5), (S6) and (S8) for model** (2.2.6)**.** From top to bottom, the rows display the scatterplots for schedules (S1), (S3), (S5), (S6), and (S8), respectively, for the parameters with respect to the time to peak for model (2.2.6) under CAR-T cell and anti-PD-1 treatments. The considered parameters in each subfigure are indicated in the figure legend. The vertical and horizontal axes represent the parameter value and the time with unit month.

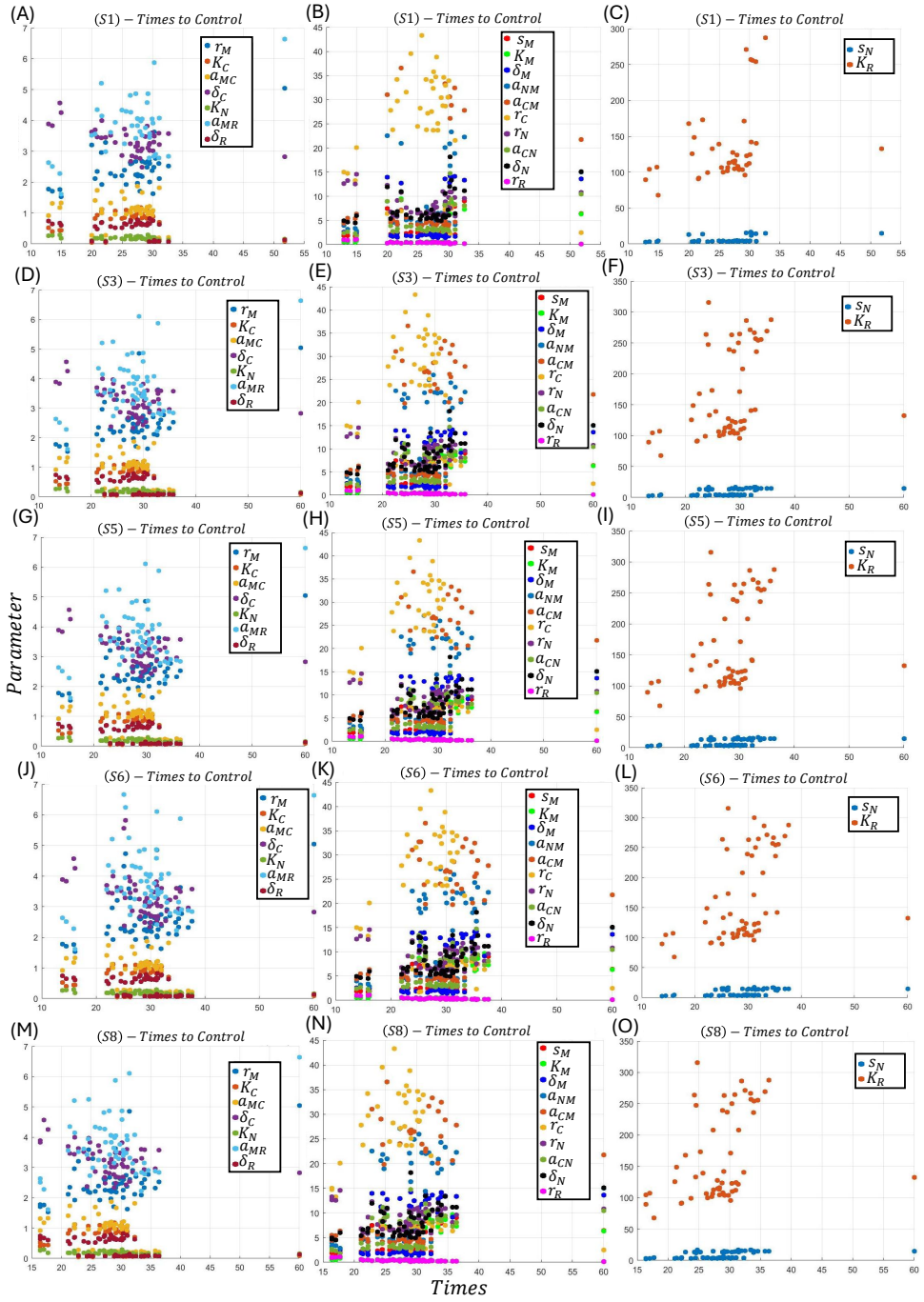

Figure 6.17: **Scatterplots of time to control, for the combination therapy of anti-PD-1 and CAR-T cells under schedules (S1), (S3), (S5), (S6) and (S8) for model** (2.2.6)**.** From top to bottom, the rows display the scatterplots for schedules (S1), (S3), (S5), (S6), and (S8), respectively, for the parameters with respect to the time to control for model (2.2.6). The considered parameters in each subfigure are indicated in the figure legend. The vertical and horizontal axes represent the parameter value and the time with unit month.

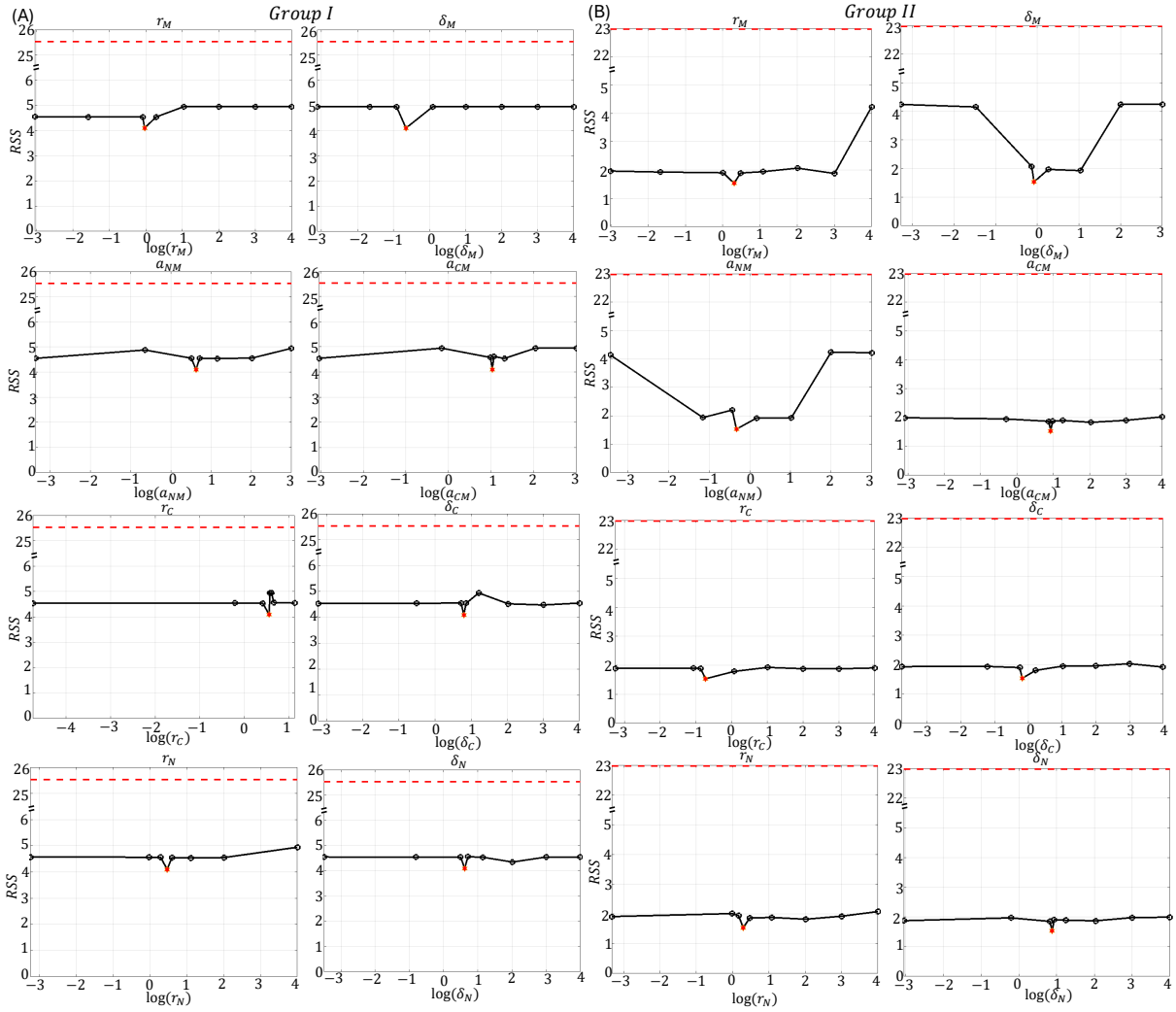

Figure 6.18: **Profile likelihoods for model** (2.1.6)**.** (A) and (B) show the profile likelihoods when calibrating model (2.1.6) to Group I and Group II data, respectively. The horizontal axis represents the logarithm range of the considered parameter and the vertical axis shows the $F_{ls}(P_i)$ where P_i is the considered parameter. The black curve displays the profile likelihood $\mathcal{L}^*(P_i)$, where the circled marks represent the minimal RSS of tested parameter values and the red star indicates the minimum $\mathcal{L}^*(P_i)$ of the considered parameter. The red dashed line represents the threshold $\chi^2(0.9, 31) + F_{ls}(\hat{P})$.

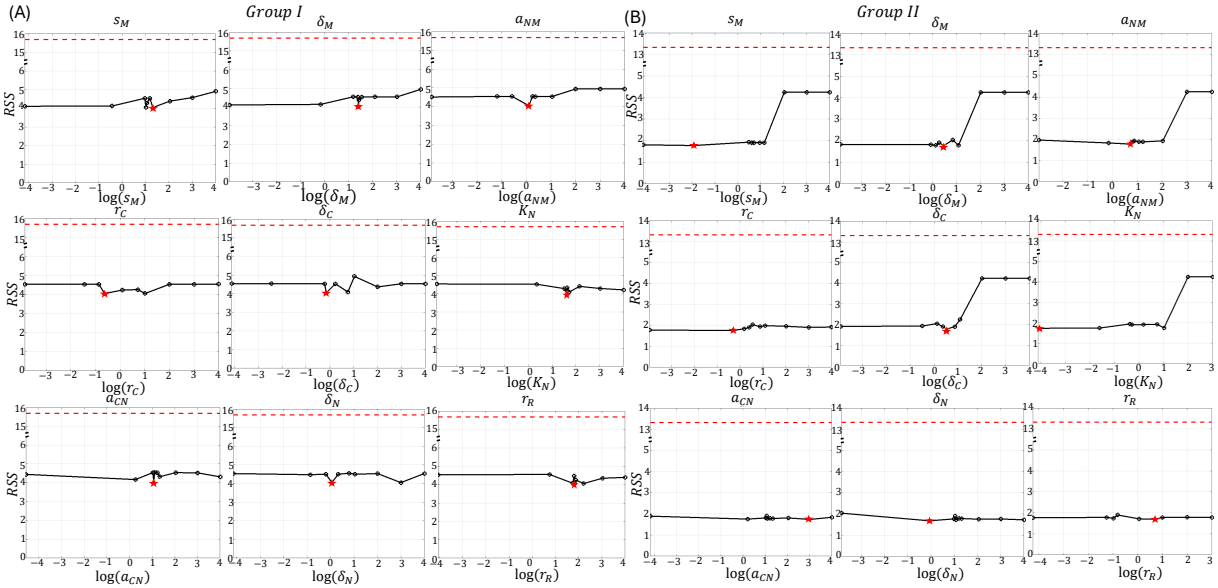

Figure 6.19: **Profile likelihoods for model** (2.2.6)**.** (A) and (B) show the profile likelihoods when calibrating model (2.2.6) to Group I and Group II data, respectively. The horizontal axis represents the logarithm range of the considered parameter and the vertical axis shows the $F_{ls}(P_i)$ where P_i is the considered parameter. The black curve displays the profile likelihood $\mathcal{L}^*(P_i)$, where the circled marks represent the minimal RSS of tested parameter values and the red star indicates the minimum $\mathcal{L}^*(P_i)$ of the considered parameter. The red dashed line represents the threshold $\chi^2(0.9, 19) + F_{ls}(\hat{P})$.

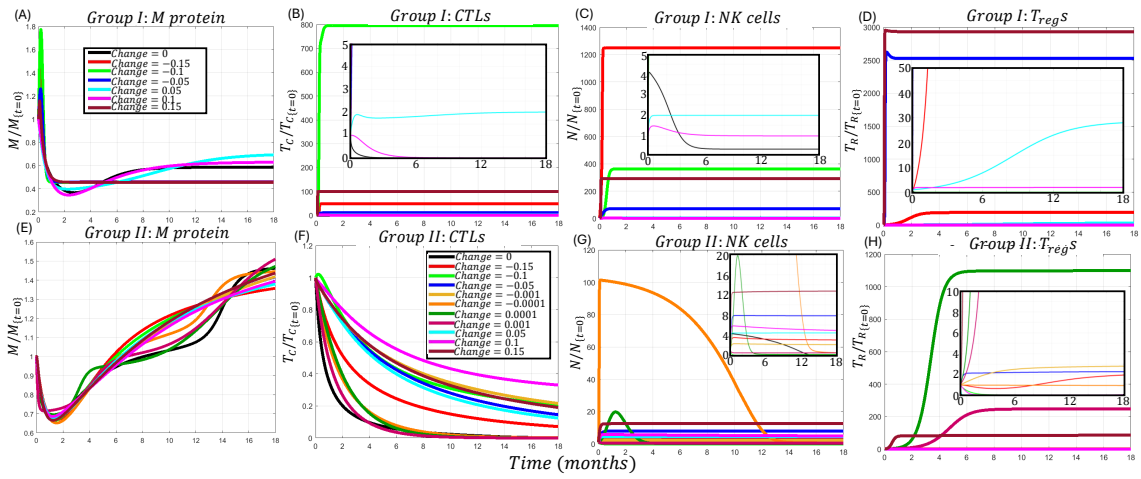

Figure 6.20: **Solutions of** M**,** T_C**,** N**,** T_R **of model** (2.1.6)**.** (A)-(D) (resp. (E)-(H)) display the solutions of M, T_C, N, T_R, respectively, along the profile likelihoods of all eight practically non-identifiable parameters of model (2.1.6) calibrating to Group I (resp. Group II). The horizontal and vertical axes represent the time with unit month and the model variable divided by its initial condition, respectively. The legend for (A)-(D) (resp. (E)-(H)) is displayed in (A) (resp. (F)). (B)-(D),(G), and (H) display a zoomed-in region for clarity.

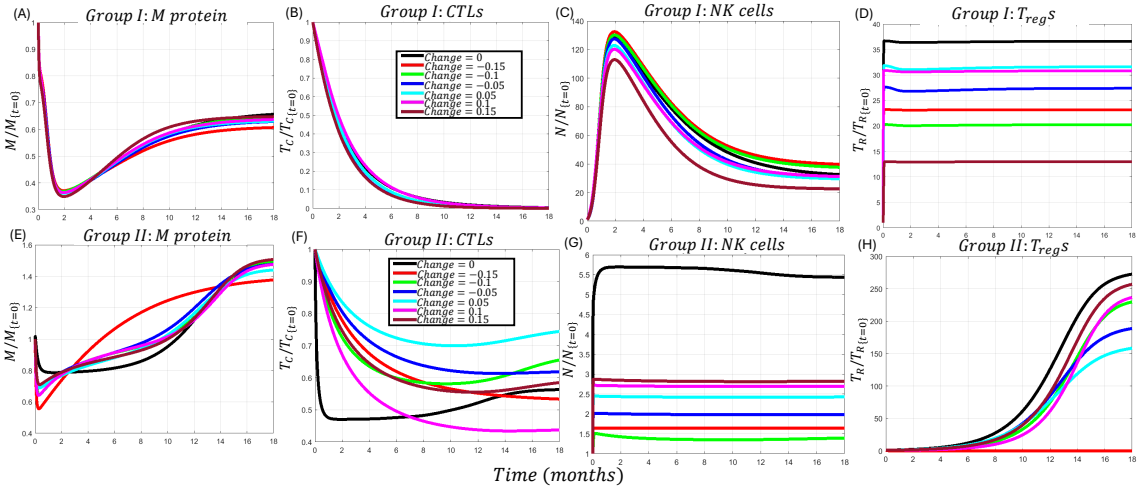

Figure 6.21: **Solutions of M, T_C, N, T_R of model** (2.2.6)**.** (A)-(D) (resp. (E)-(H)) display the solutions of M, T_C, N, T_R, respectively, along the profile likelihoods of all nine practically non-identifiable parameters of model (2.2.6) calibrating to Group I (resp. Group II). The horizontal and vertical axes represent the time with unit month and the model variable divided by its initial condition, respectively. The legend for (A)-(D) (resp. (E)-(H)) is displayed in (B) (resp. (F)).

7

Discussion

In this work, we modified the ODE model in (19) to construct two models, a general model (2.1.6) and a simplified model (2.2.5) with its non-dimensional version model (2.2.6), with both models including the effects of the anti-PD-1 (F_q), elotuzumab (F_e) and daratumumab (F_d) treatments. Our goals are to compare the properties of the general model (2.1.6) and the simplified model (2.2.5), and to use these two models to investigate how monotherapies of anti-PD-1, elotuzumab, and daratumumab affect the long-term behaviour of M protein in patients.

In (19), the authors randomly generated parameter sets and used numerical computation to find the corresponding steady states evaluated from random initial condition, then studied the distributions of these steady states and time to steady state. Next, they applied global sensitivity analysis to identify significant parameters to the model outcome, then performed identifiability analysis on these significant parameters. Next, in (18), the authors performed mathematical analysis on model (2.1.6), under the control case (i.e., $F_q = F_e = F_d = 1$). They reduced the model from four variables (i.e., $M(t)$, $T_C(t), N(t)$, and $T_R(t)$) to two variables (i.e., $M(t)$ and $T_C(t)$) using the experimental data in (44) to assume $N(t)$ and $T_R(t)$ were constants. The authors found that the reduced model had two types of non-negative equilibria,

$E_1^* := (M^*, 0)$ and $E_2^* := (M^*, T_C^*)$ and established conditions for their existence and local stability. For the trivial equilibrium E_1^*, their analysis demonstrated that based on the level of M^*, the model has a unique equilibrium which is locally asymptotically stable, or has three equilibria: a stable one with a low level of M^*, a stable one with a high level of M^*, and an unstable one with an intermediate level of M^*. For the positive equilibrium E_2^*, their numerical test displayed that increasing the value of a_{CNM} induces bistability. More precisely, a small a_{CNM} could induce a E_2^* with a relatively high level of M protein representing high tumour burden. As a_{CNM} increases, the model generates three E_2^* that a stable one with a low level of M protein, a stable one with a high level of M protein, and an unstable one with an intermediate level of M protein. If we further increase a_{CNM}, then the model only possesses a stable E_2^* with a low level of M protein.

However, there was not enough evidence in (44) to support $N(t)$ and $T_R(t)$ were constants and hence we still focused model (2.2.5), keeping all model variables in our study. First, our numerical study showed that, when comparing the distribution of the steady states and the time to steady state (TTSS) for models (2.1.6) and (2.2.5) using one of the monotherapies, both models had similar conclusions from random or specific initial conditions of M protein. We also found that increasing the effect of anti-PD-1 boosts CTL and NK cell responses and reduces M protein and $\mathrm{T_{reg}}$ responses. Moreover, increasing the effect of daratumumab only decreases the median of $\mathrm{T_{reg}}$s, and increasing the effect of elotuzumab only slightly increases the median of the NK cells. Additionally, the median of TTSS decreases as the effect of anti-PD-1 increases and the median of TTSS increases as the effect of daratumumab increases, whereas the effect of elotuzumab does not significantly change the median of TTSS.

Second, in analysis, we found four types of non-negative equilibria for model (2.2.5): $X_1^* = (M^*, 0, N^*, 0)$ representing the second best case for patients, $X_2^* =$

$(M^*, 0, N^*, T_R^*)$ representing the worst case for patients, $X_3^* = (M^*, T_C^*, N^*, 0)$ representing the best case for patients, and $X_4^* = (M^*, T_C^*, N^*, T_R^*)$ representing the uncertain case for patients, where X_1^* always exists and the other three equilibria exist under certain conditions. We established conditions for their local stability and found properties of parameters which can induce an asymptotically stable X_i^* with low M protein level, representing the remission of patients.

Our numerical examples showed that the homeostasis rate of $\mathrm{T_{reg}}$s, r_R, and the homeostasis rate of CTLs, r_C, are potential bifurcation parameters for model (2.2.5), because varying one of these values can change the number and stability of equilibria X_i^*. Different to the bistability property of model (2.1.6) shown in (18), the numerical examples of our model (2.2.5) for the equilibrium with low or high M protein level displayed that the dynamics shifts from a unique asymptotically stable equilibrium, then to a stable oscillation pattern due to Hopf bifurcation, as r_C increases.

In (19), due to the lack of experimental data, the authors can only use the distribution of steady states and sensitivity analysis for the solutions from random initial conditions, without providing model calibration to support the accuracy of their numerical findings. Different to this limitation in (19), we found clinical data of M protein level over 18 months for MM patients after CAR-T cell treatment in (37), so we were able to perform model calibration to the data in (37) on the general model (2.1.6) and the simplified model (2.2.6), which filled in the gaps in the work from (19), and then compared the properties between these two models. We categorized the data in (37) into two groups, Group I for remission and Group II for relapse, based on the trend of M protein over time. We calibrated the general model (2.1.6) and the simplified model (2.2.6), under the control case (i.e., $F_q = F_e = F_d = 1$), to find appropriate parameter sets representing the virtual cohort patients for both groups. Our AIC result showed that model (2.2.6) is more plausible for both Groups I and II, even though model (2.1.6) has a smaller minimal RSS for Group II.

For the selected appropriate parameter sets of the general model (2.1.6) and the simplified model (2.2.6) (i.e., the virtual cohort patients), we first identified potential biomarkers to predict patients' status, based on the distribution of parameter values between Groups I and II. We found that the parameters K_C, a_{MC}, and r_R have similar distribution between the general model (2.1.6) and the simplified model (2.2.6), so the prediction of patients' status from these three parameters is independent of model selection. However, parameters K_M, δ_M, a_{NM}, r_C, δ_C, r_N, and K_N have opposite distributions between these two models, so the accuracy of patient status prediction based on these seven parameters relies on the model selection, namely, which model is more plausible.

We also performed sensitivity analysis on these appropriate parameter sets of both groups and both models to calculate their PRCCs to the M protein level over time. For the significant parameters of model (2.1.6), the signs of their PRCCs do not change over time and between groups, and the only thing changes is the magnitudes of the PRCCs. Hence, these parameters affect the level of M protein in the same way for all time and between Groups I and II. Moreover, some parameters have stronger effect on Group I (e.g. r_M and s_M) or Group II (e.g. δ_M, a_{NM}, a_{NC}, and r_N), or stronger effect in short duration (e.g. r_M, s_M) or long duration (e.g. a_{NC}, r_N, K_M, δ_C, b_{NC}, and δ_N). This observation indicates which parameters are potential treatment target to reduce M protein level for patients in Groups I or II, or the treatments have a better reduction of M protein in a short or long duration. On the other hand, the variation of PRCCs of the simplified model (2.2.6) is richer than the ones of the general model (2.1.6). Similarly, the signs of PRCCs for the significant parameters of model (2.2.6) remain unchanged and the magnitudes change over time. However, some parameters only affect one group (namely, δ_C, δ_N, a_{MC}, and r_C only affect Group I, whereas r_R, a_{MR}, K_M, and δ_R only affect Group II) and these parameters can only use to affect M protein level for the corresponding

group. Additionally, the parameters a_{CN} and r_N have different signs of PRCCs between groups, and hence targeting these parameters in treatment induce oppositive outcomes for patients in Groups I and II.

Next, for both models, we considered the combination therapy between CAR-T cell treatment and one of anti-PD-1 (F_q), elotuzumab (F_e), or daratumumab (F_d) under different treatment schedules on Group II to control the relapse issue. For model (2.1.6), it suggested that elotuzumab or anti-PD-1 administered with a longer duration, a higher frequency, or a higher effect can be effective at mitigating relapse in patients. Notice that, for anti-PD-1 treatment, a single short administration should be avoided because it could aggravate the relapse issue, and a high effect administration could amplify the relapse level at the early stage. On the other hand, an extra treatment of daratumumab cannot improve the relapse issue, so daratumumab is not recommended. For model (2.2.6), it indicated that all treatment schedules of daratumumab have similar results for all patients in Group II that they efficiently reduce M protein during and after the treatment. However, anti-PD-1 only works for certain patients. When anti-PD-1 works, a single treatment with a longer duration improves the reduction of M protein after the treatment is withdrawn. Moreover, a higher treatment effect improves the reduction of M protein, whereas increasing treatment frequency does not improve the treatment outcome, during and after the treatment. On the other hand, elotuzumab always aggravated the relapse issue, so it should be avoided. Therefore, the predictions from model (2.2.6) indicate that a single short administration of daratumumab is recommended to all patients with relapse, but a single longer anti-PD-1 with strong effect is only recommended to certain patients.

Finally, for both models, we used the method of profile likelihoods to perform the identifiability analysis of the parameters r_M, δ_M, a_{NM}, a_{CM}, r_C, δ_C, r_N, and δ_N for the general model (2.1.6) and the parameters s_M, δ_M, a_{NM}, r_C, δ_C, K_N, a_{CN},

δ_N and r_R for the simplified model (2.2.6). We found that the selected parameters for each model were structurally identifiable but practically non-identifiable when calibrating to M protein data in (37). We then use the variations of model solutions along the profile likelihoods of the practically non-identifiable parameters to suggest extra experimental data for improving the practically non-identifiable parameters.

Notice that the minimal RSS for both models are close to each other, so the reason that the AIC suggested model (2.2.6) is more plausible could be simply due to the number of parameters. Our numerical predictions showed several different outcomes between these two models, so we offer the following approaches to further evaluate which model is more plausible:

(i) Based on the parameter distribution: we need extra experimental data to indicate one of the distributions for K_M, δ_M, r_C, δ_C, s_N, r_N, and K_N for patients in Groups I and II. If K_M, δ_M, and K_N have relatively higher distribution and r_C, δ_C, and r_N have relatively lower distribution for patients in Group I, then the simplified model (2.2.6) is more plausible, otherwise the general model (2.1.6) is more plausible.

(ii) Based on the PRCCs: Because only model (2.2.6) has parameters that only affects one group of patients or have different signs of PRCCs between groups, we need extra experimental data to determine the effect on M protein between Groups I and II from one of the parameters: δ_C, δ_N, a_{MC}, r_C, r_R, a_{MR}, K_M, δ_R, a_{CN}, and r_N. If one of δ_C, δ_N, a_{MC}, r_C, r_R, a_{MR}, and K_M can only affect one group of patients, or one of r_N and a_{CN} has oppositive effect between Groups I and II, then the simplified model (2.2.6) is more plausible, otherwise the general model (2.1.6) is more plausible.

(iii) Based on the combination treatment: Because daratumumab is the only insufficient treatment from model (2.1.6) and elotuzumab is the only treatment

could aggravate the relapse issue from model (2.2.6), we need extra experimental data to measure the treatment outcomes of combination of CAR-T cells and daratumumab and combination of CAR-T cells and elotuzumab. If the combination of CAR-T cells and daratumumab cannot induce significant reduction of M protein, then the general model (2.1.6) is more plausible. On the other hand, if the combination of CAR-T cells and elotuzumab could aggravate the relapse level, then the simplified model (2.2.6) is more plausible.

(iv) Based on the identifiability analysis: When calibrating to Group I data, the general model (2.1.6) shows constant levels and significantly variations in CTLs, NK cells, and regulatory T cells, whereas the simplified model (2.2.6) only shows constant levels and significantly variations in regulatory T cells. Thus, if extra experimental data of CTLs or NK cells from patients in Group I does not maintain at a constant level over time, then the simplified model (2.2.6) is more plausible, otherwise the general model (2.1.6) is more plausible.

Thus, as more experimental data pertaining to parameter values and more time series data become available, we could use that to verify our conclusions, find better fitting parameter values, and determine the more plausible model with more confidence.

Bibliography

[1] Boyman, O., Sprent, J., The role of interleukin-2 during homeostasis and activation of the immune system, Nat. Rev. Immunol., 2012, 12(3), 180.

[2] Brouwer, A.F, Meza, R, Eisenberg, M.C., Parameter estimation for multistage clonal expansion models from cancer incidence data: A practical identifiability analysis, PLoS Comput Biol., 2017 Mar 13, 13(3):e1005431.

[3] Brown, R., Pope, B., Yuen, E., Bibson, J., Joshua, D., The expression of T cell related costimulatory molecules in multiple myeloma. Leukemia Lymphoma, 1998, 31(3–4), 379–384.

[4] Carbone, E., Neri, P., Mesuraca, M., Fulciniti, M.T., Otsuki, T., Pende, D., Groh, V., Spies, T., Pollio, G., Cosman, D., Catalano, L., Tassone, P., Rotoli, B., Venuta, S., HLA class I, NKG2D, and natural cytotoxicity receptors regulate multiple myeloma cell recognition by natural killer cells, Immunobiology, 2005, 105(1), 251–258.

[5] Cerwenka, A., Baron, J., Lanier, L., Ectopic expression of retinoic acid early inducible-1 gene (RAE-1) permits natural killer cell-mediated rejection of a MHC class I-bearing tumor in vivo., Proc. Natl. Acad. Sci., 2001, 98(20), 11521–11526 .

[6] Chen, M.-L., Pittet, M.J., Gorelik, L., Flavell, R.A., Weissleder, R., von Boehme, H., Khazaie, K., Regulatory T cells suppress tumor-specific CD8 T cell cyto-

toxicity through TGF-β signals in vivo., Proc. Natl. Acad. Sci., 2005, 102(2), 419–424.

[7] Conlon, K.C., Miljkovic M.D., Waldmann T.A., Cytokines in the Treatment of Cancer. Journal of Interferon & Cytokine Research, 2019, 39(1), 6-21. doi: 10.1089/jir.2018.0019.

[8] D'Arena, G., Rossi, G., Laurenti, L., Statuto, T., D'Auria, F., Valvano, L., Simeon, V., Giudice, A., Innocenti, I., Feo, V.D., Filosa, R., Musto, P., Circulating regulatory T-cells in monoclonal gammopathies of uncertain significance and multiple myeloma: In search of a role, J. Immunol. Res., 2016, Article ID 9271469.

[9] Dhodapkar, M.V., Geller, M.D., Chang, D.H., Shimizu, K., Fujii, S.-I., Dhodapkar, K.M., Krasovsky, J., A reversible defect in natural killer T cell function characterizes the progression of premalignant to malignant multiple myeloma, J. Exp. Med., 2003, 197 (12), 1667–1676.

[10] Diefenbach, A., Jensen, E.R., Jamieson, A.M., Raulet, D.H., Rae1 and H60 ligands of the NKG2D receptor stimulate tumor immunity. Nature, 2001, 413(6852), 165.

[11] Dimopoulos, M., Kyle, R., Fermand, J.-P., Rajkumar, S.V., Miguel, J.S., Chanan-Khan, A., Ludwig, H., Joshua, D., Mehta, J., Gertz, M., Avet-Loiseau, H., Beksaç, M., Anderson, K.C., Moreau, P., Singhal, S., Goldschmidt, H., Boccadoro, M., Kumar, S., Giralt, S., Munshi, N.C., Consensus recommendations for standard investigative workup: report of the International Myeloma Workshop Consensus Panel 3, Blood, 2011, 117(18), 4701–4705. doi: 10.1182/blood-2010-10-299529.

[12] Durie, B.G., Salmon, S.E., A clinical staging system for multiple myeloma:

correlation of measured myeloma cell mass with presenting clinical features, response to treatment, and survival. Cancer, 1975, 36, 842-854. doi: 10.1002/1097-0142(197509)36:3<842::aid-cncr2820360303>3.0.co;2-u.

[13] Eisenberg, M.C., Robertson, S.L., Tien, J.H., Identifiability and estimation of multiple transmission pathways in cholera and waterborne disease, Journal of Theoretical Biology, 2013, 324, 84-102.

[14] Favaloro, J., Brown, R., Aklilu, E., Yang, S., Suen, H., Hart, D., Fromm, P., Gibson, J., Khoo, L., Ho, P.J., Joshua, D., Myeloma skews regulatory T and pro-inflammatory T helper 17 cell balance in favor of a suppressive state, Leukemia Lymphoma, 2014, 55(5), 1090–1098.

[15] Feyler, S., von Lilienfeld-Toal, M., Jarmin, S., Marles, L., Rawstron, A., Ashcroft, A., Owen, R.G., Selby, P.J., Cook, G., , CD4+CD25+FoxP3+ regulatory T cells are increased whilst CD3+CDCD8abTCR+ double negative T cells are decreased in the peripheral blood of patients with multiple myeloma which correlates with disease burden, Br. J. Haematol., 2009, 144, 686–695.

[16] Feyler, S., Scott, G.B., Parrish, C., Jarmin, S., Evans, P., Short, M., McKinley, K., Selby, P.J., Cook, G., Tumour cell generation of inducible regulatory T-cells in multiple myeloma is contact-dependent and antigen-presenting cell-independent, PLoS ONE, 2012, 7(5), e35981.

[17] Fu, Y., Lim, S., Urano, D., Tunc-Ozdemir, M., Phan, N.G., Elston, T.C., Jones, A.M., Reciprocal encoding of signal intensity and duration in a glucose-sensing circuit, Cell, 2014, 156, 1084-1095. doi:10.1016/j.cell.2014.01.013.

[18] Gallaher, J., Larripa, K., Ledzewicz, U., Renardy, M., Shtylla, B., Tania, N., et al, A mathematical model for tumor-immune dynamics in multiple myeloma, Understanding Complex Biol. Syst. Math. AWMS, 2018, 14, 89-122.

[19] Gallaher, J., Larripa, K., Renardy, M., Shtylla, B., Tania, N., White, D., et al, Methods for determining key components in a mathematical model for tumor-immune dynamics in multiple myeloma, J. Theor. Biol., 2018, 458, 31-46.

[20] Gao, M., Gao, L., Yang, G., Tao, Y., Hou, J., Xu, H., Hu, X., Han, Y., Zhang, Q., Zhan, F., Wu, X., Shi, J., Myeloma cells resistance to NK cell lysis mainly involves an HLA class I-dependent mechanism, Acta Biochimica et Biophysica Sinica (Shang- hai), 2014, 46(7), 597–604.

[21] Gerecke, C., Fuhrmann, S., Strifler, S., Schmidt-Hieber, M., Einsele, E., Knop, S., The Diagnosis and Treatment of Multiple Myeloma, Dtsch. Arztebl. Int., 2016 113(27-28), 470-476. doi: 10.3238/arztebl.2016.0470.

[22] Ghiringhelli, F., Ménard, C., Terme, M., Flament, C., Taieb, J., Chaput, N., Puig, P.E., Novault, S., Escudier, B., Vivier, E., et al., CD4+ CD25+ regulatory T cells inhibit natural killer cell functions in a transforming growth factor- β-dependent manner, J. Exp. Med., 2005, 202(8), 1075–1085.

[23] Greipp, P.R., Miguel, J.S., Durie, B.G.M., Crowley, J.J., Barlogie, B., Bladé, J., Boccadoro, M., Anthony Child, J., Avet-Loiseau, H., Kyle, R.A., Lahuerta, J.J., Ludwig, H., Morgan, G., Powles, R., Shimizu, K., Shustik, C., Sonneveld, P., Tosi, P., Turesson, I., Westin, J., International staging system for multiple myeloma, Journal of Clinical Oncology, 2005, 23(15), 3415-3420. doi: 10.1200/JCO.2005.04.242.

[24] Huntington, N.D., Vosshenrich, C.A.J., Di Santo, J.P., Developmental pathways that generate natural-killer-cell diversity in mice and humans, Nat. Rev. Immunol., 2007, 703-714. doi: 10.1038/nri2154.

[25] Joshua, D.E., Bryant, C., Dix, C., Gibson, J., Ho, J., Biology and

therapy of multiple myeloma, Med. J. Aust., 2019, 210(8), 375-380. doi: 10.5694/mja2.50129.

[26] Kaufman, H.L., Kohlhapp, F.J., Zloza, A., Oncolytic viruses: a new class of immunotherapy drugs, Nature Review Drug Discovery, 2015, 14, 642-662.

[27] Kawarada, Y., Ganss, R., Garbi, N., Sacher, T., Arnold, B., Hämmerling, G.J., NK- and CD8+ T cell-mediated eradication of established tumors by peritumoral injection of CpG-containing oligodeoxynucleotides, J. Immunol., 2001, 167(9), 5247–5253.

[28] Kumar, S.K., Rajkumar, V., Kyle, R.A., van Duin, M., Sonneveld, P., Mateos, M.-V., Gay, F., Anderson, K.C., Multiple Myeloma, Nat. Rev. Dis. Primers, 2017, 3, 17046. doi: 10.1038/nrdp.2017.46.

[29] Kyle, R.A., Isbuadi, F., Rajkumar, S.V., Management of monoclonal gammopathy of undetermined significance (MGUS) and smoldering multiple myeloma (SMM), Oncology, 2011 25(7), 578-586.

[30] Kyle, R.A., Therneau, T.M., Rajkumar, S.V., Offord, J.R., Larson, D.R., Plevak, M.F., Melton III, L.M., A long-term study of prognosis in monoclonal gammopathy of undetermined significance, N. Engl. J. Med., 2002, 346(8), 564-569. doi: 10.1056/NEJMoa01133202.

[31] Lehman, C., Zeis, M., Uharek, L., Activation of natural killer cells with interleukin 2 (IL-2) and IL-12 increases perforin binding and subsequent lysis of tumour cells, Br. J. Haematol., 2001, 114(3), 660–665.

[32] Li, A.M., Hucks, G.E., Dinofia, A.M., Seif, A.E., Teachey, D.T., Baniewicz, D., et al, Checkpoint Inhibitors Augment CD19-Directed Chimeric Antigen Receptor (CAR) T Cell Therapy in Relapsed B-cell Lymphoblastic Leukemia, Blood, 2018, 132, 556. doi:10.1182/blood-2018-99-112572.

[33] Liu, J., Chen, Z., Li, Y., Zhao, W., Wu, J., Zhang, Z., PD-1/PD-L1 Checkpoint Inhibitors in Tumor Immunotherapy, Front. Pharmcol., 2021, 12, 731798. doi: 10.3389/fphar.2021.731798.

[34] Lütja, S., de Rooy, J.W.J., Croockewit, S., Koedam, E., Oyen, W.J.G., Raymakers, R.A., Role of radiography, MRI and FDG-PET/CT in diagnosing, staging and therapeutical evaluation of patients with multiple myeloma, Ann. Hematol., 2009, 88, 1161-1168. doi: 10.1007/s00277-009-0829-0.

[35] Marino, S., Hogue, I.B., Ray, C.J., Kirschner, D.E., A methodology for performing global uncertaintly and sensitivity analysis in systems biology, J. Theor. Biol., 2008, 254(1), 178-196. doi: 10.1016/j.jtbi.2008.04.011.

[36] Mehrabadi, A.Z., Ranjbar, R., Farzanehpour, M., Shahriary, A., Dorostkar, R., Hamidinejad, M.A., Ghaleh, H.E.G., Therapeutic potential of CAR T cell in malignancies: A scoping review, Biomedicine & Pharmacotherapy, 2022, 146, 112512.

[37] Mei, H., Li, C., Jiang, H., Zhao, X., Huang, Z., Jim, D., Guo, T., Kou, H., Liu, L., Tang, L., Yin, P., Wang, Z., Ai, L., Ke, S., Xia, Y., Deng, J., Chen, L., Cai, L., Sun, C., Xia, L., Hua, G., Hu, Y., A bispecific CAR-T cell therapy targeting BCMA and CD38 in relapsed or refractory multiple myeloma, J. Hematol. Oncol., 2021, 14, 161. doi: 10.1186/s13045-021-01170-7.

[38] Mempel, T.R., Pittet, M.J., Khazaie, K., Weninger, W., Weissleder, R., von Boehmer, H., von Andrian, U.H., Regulatory T cells reversibly suppress cytotoxic T cell function independent of effector differentiation, Immunity, 2006, 25(1), 129–141.

[39] Michels, T.C., Petersen, K.E., Multiple Myeloma: Diagnosis and Treatment, Am. Fam. Physician, 2017, 95(6), 373-383.

[40] Mihara, K., Bhattacharyya, J., Kitanaka, A., Yanagihara, K., Kubo, T., Takei, Y., Asaoku, H., Takihara, Y., Kimura, A., T-cell immunotherapy with a chimeric receptor against CD38 is effective in eliminating myeloma cells, Leukemia, 2012, 26, 365-367. doi: 10.1038/leu.2011.205.

[41] Mikkilineni, L., Kochenderfer, J.N., CAR T cell therapies for patients with multiple myeloma, Nat. Rev. Clin. Oncol., 2021, 8, 71-84. doi: 10.1038/s41571-020-0427-6.

[42] Nooka, A.K., Kaufman, J.L., Hofmeister, C.C., Joseph, N.S., Heffner, T.L., Gupta, V.A., et al., Daratumumab in Multiple Myeloma, Cancer, 2019, 125(14), 2364-2382. doi: 10.1002/cncr.32065.

[43] Pallmer, K., Oxenius, A., Recognition and regulation of T cells by NK cells, Front. Immunol., 2016, 7, 215. doi: 10.3389/fimmu.2016.00251.

[44] Pessoa de Magalhães, R.J., Vidriales, M.-B., Paiva, B., Fernandez-Gimenez, C., García-Sanz, R., Mateos, M.-V., et al., Analysis of the immune system of multiple myeloma patients achieving long-term disease control by multidimensional flow cytometry, Haematologica, 2013, 98(1), 79-86. doi: 10.3324/haematol.2012.067272.

[45] Portet, S., A primer on model selection using the Akaike Information Criterion, Infectious Disease Modelling, 2020, 5, 111-128. doi:10.1016/j.idm.2019.12.010.

[46] Raitakari, M., Brown, R., Gibson, J., Joshua, D., T cells in myeloma, Hematol. Oncol., 2003, 21(1), 33–42.

[47] Raue, A., Kreutz, C., Maiwald, T., Bachmann, J., Schilling, M., Klingmüller, U., Timmer, J., Structural and practical identifiability analysis of partially observed dynamical models by exploiting the profile likelihood, Bioinformatics, 2009, 25(15), 1923–1929.

[48] Schroeder, H.W., Cavacini, L., Structure and function of immunoglobulins, J Allergy Clin Immunol., 2010, 125, S41-52. doi: 10.1016/j.jaci.2009.09.046.

[49] Shanker, A., Buferne, M., Schmitt-Verhulst, A.-M., Cooperative action of CD8 T lymphocytes and natural killer cells controls tumour growth under conditions of restricted T-cell receptor diversity. Immunology, 2010, 129(1), 41–54.

[50] Shanker, A., Verdeil, G., Buferne, M., Inderberg-Suso, E.-M., Puthier, D., Joly, F. , Nguyen, C. , Leserman, L. , Auphan-Anezin, N., Schmitt-Verhulst, A.-M., CD8 T cell help for innate antitumor immunity. J. Immunol., 2007, 179(10), 6651–6662.

[51] Smyth, M.J., Teng, M.W., Swann, J., Kyparissoudis, K., Godfrey, D.I., Hayakawa, Y., CD4+ CD25+ T regulatory cells suppress NK cell-mediated immunotherapy of cancer. J. Immunol., 2006, 176(3), 1582–1587.

[52] Sterner, R.C., Sterner, R.M., CAR-T cell therapy: current limitations and potential strategies, Blood Cancer Journal, 2021, 11(4), 69. doi:10.1038/s41408-021-00459-7.

[53] Townsend, C.L., Laffy, J.M.J., Wu, Y.-C.B., Silva O'Hare, J., Martin, V., Kipling, D., Fraternali, F., Dunn-Walters, D.K., Significant differences in physicochemical properties of human immunoglobulin kappa and lambda CDR3 Regions, Front. Immunol., 2016, 7, 388. doi: 10.3389/fimmu.2016.00388.

[54] Wang, Y., Sanchez, L., Siegel, D.S., Wang, M.L., Elotuzumab for the treatment of multiple myeloma, Journal of Hematology and Oncology, 2016, 9, 55. doi:10.1186/s13045-016-0284-z.

[55] Wen, Y.-J., Min, R., Tricot, G., Barlogie, B., Yi, Q., Tumor lysate-specific cytotoxic t lymphocytes in multiple myeloma: promising effector cells for immunotherapy, Blood, 2002, 99(9), 3280–3285.

[56] https://www.mayoclinic.org/diseases-conditions/multiple-myeloma/diagnosis-treatment/drc-20353383

[57] https://www.moffitt.org/cancers/multiple-myeloma-plasma-cell-tumor/treatment/immunotherapy/